Contract Report 2016-03

Detection and Predictability of Spatial and Temporal Patterns and Trends of Riverine Nutrient Loads in the Midwest

Momcilo Markus, Alena Bartosova, Siddhartha Verma

February 2016

Illinois State Water Survey
Prairie Research Institute
University of Illinois at Urbana-Champaign

Champaign, Illinois

Detection and Predictability of Spatial and Temporal Patterns and Trends of Riverine Nutrient Loads in the Midwest

Principal Investigators:

Momcilo Markus and Alena Bartosova

Illinois State Water Survey

Graduate Research Assistant:

Siddhartha Verma

Department of Agricultural and Biological Engineering

Illinois State Water Survey

2204 Griffith Dr.

Champaign, IL 61820

ILLINOIS STATE WATER SURVEY

PRAIRIE RESEARCH INSTITUTE

EXECUTIVE SUMMARY

The deleterious effects of multiple stressors on global water resources have become more significant over the past few decades. Anthropogenic activities such as industrialization, urbanization, deforestation, and increased application of agricultural nutrients have led to a decline in overall quality of our aquatic environment. Additionally, these activities have increased greenhouse gas concentrations globally, warming the earth's atmosphere and eventually having a detrimental effect on global water and energy balances. The global water cycle has been altered, leading to its overall intensification and an increase in frequency of extreme floods and droughts. Addressing increasing water demands coupled with declining water quality and a depletion of water resources requires new approaches in water management. In determining optimum management actions, it is critical to understand the spatial and temporal variability and trends in water quantity and quality.

This research aims to improve our knowledge of anthropogenic and natural impacts on water resources by evaluating and refining the science of predicting pollutant (nutrient and sediment) loadings from medium- to large-scale watersheds. To enable these goals, this research is centered on large watersheds in the Midwestern United States, which have been some of the primary sources of nutrient and sediment loadings to downstream water bodies such as the Gulf of Mexico and Lake Erie. In total, 14 watersheds in Illinois, Indiana, Ohio, and Michigan, with extensive water quality datasets, are analyzed in different stages of this research. Most of these watersheds are predominantly agricultural with intensive row-cropped farmlands and have a network of sub-surface tile drainage systems.

Pollutant loadings and associated hydrological processes have been simulated using four major modeling approaches: statistical modeling, empirical modeling, physically based modeling, and data mining methods. This report includes eight chapters. The first three chapters describe the problem and research objectives, study area, and data preparation and processing. Next, the impacts of available water quality data on concentration and load predictions and trend calculations are assessed based on traditional statistical methods and several new, improved, and modified approaches (Chapter 4). This segment emphasizes the difficulties in predicting nutrient load and concentration trends under changing climatic conditions, highlighting the importance of continuous nutrient monitoring.

Next, two data mining techniques (the nearest-neighbor method and decision trees), scarcely used in hydrology, were applied to predict the missing Nitrate Nitrogen (NO3-N) concentrations for two extensively monitored watersheds in the Lake Erie basin. These predictions (Chapter 5) are important in load estimations and demonstrate the potential of data mining to produce results comparable with statistical and empirical methods presented in the previous chapter.

In Chapter 6, statistical regression techniques are used to assess the role of large load events in predicting Total Suspended Solids (SS), Total Phosphorus (TP), and NO3-N annual loads. A novel constituent-specific baseflow separation technique based on mechanistic differences in nutrient and sediment loadings is proposed and applied. As a result, regression relationships between the largest annual loads and total annual loads were developed for all three constituents. An Analysis of Covariance (ANCOVA) indicated that these relationships are often statistically indistinguishable from each other when applied to watersheds with a similar land use.

Then, in Chapter 7, the temporal patterns of pollutant loadings from large Midwestern watersheds are analyzed using circular statistics. Critical periods of high loadings, precipitation, and river flow were identified. While river flows and pollutant loadings are highest in late winter and early spring (e.g., March and April), rainfall totals are highest during late spring and early summer (e.g., May through August).

Finally, Chapter 8 shows the results based on the physically based SWAT model. The model is calibrated for river discharge and water quality in the largest watershed in the Lake Erie basin, the Maumee River watershed. The calibrated model is used to gauge the impacts of future projected climate

change from the mid-century and late-century time periods on the hydrology and water quality in the watershed. The results indicate that climate change could have a significant impact on sediment and nutrient loads, and that more detailed studies are needed to more accurately assess this impact and its confidence limits.

ACKNOWLEDGEMENTS

Research support was provided by the United States Environmental Protection Agency (Grant EPA GL-00E00683-0) and the Great Lakes Water Quality Consortium. We would like to thank Brian Miller and Lisa Merrifield from Illinois-Indiana Sea Grant at the University of Illinois for their role in research design and administration, and for serving as a liaison with the EPA.

Partial support was also provided by the Agricultural and Biological Engineering Department in the Graduate College of the University of Illinois at Urbana-Champaign. In addition, part of this research was supported by the Illinois River Conservation Reserve Enhancement Program (CREP), funded by the Illinois Department of Natural Resources with Debbie Bruce and Rick Mollahan as project managers.

We would also like to thank Greg McIsaac from the University of Illinois for valuable discussions in early stages of this research, and Peter Richards from Heidelberg University, who provided useful explanations and suggestions regarding the NCWQR data used in this study. Dr. Robert Hirsch (USGS) kindly provided us with the WRTDS software and manual. Finally, we would like to acknowledge the contribution of the Illinois State Water Survey (ISWS) staff, including Amy Russell, Michael Machesky, Jason Zhang, Daeryong Park, and Yanqing Lian for helpful review comments, Lisa Sheppard for editorial assistance, and Sara Olson for assistance with figure preparation.

TABLE OF CONTENTS

List of Figures

List of Tables

1. Problem and Research Objectives

1.1 Introduction

We live in an era in which the impacts of human activities on earth have never been greater. There is growing scientific evidence of enormous anthropogenic disruption of water, energy, and climate cycles over the past several decades. A growing group of scientists around the world are even pushing to define this period as the "Anthropocene," a new geological epoch in which humans are the primary drivers for change in environmental systems and processes (Balter, 2013). Among all environmental changes that are attributed to humans, the alteration of the water cycle is perhaps the most detrimental for the sustainable existence of life. Globally, rapid industrialization, intensification of agriculture, and the growing demands of an increasing population have led to severe water stresses and degradation of water resources. Our activities have altered the intensities of the water cycle, changed patterns of precipitation and river flow, increased sediment and nutrient pollution, drained wetlands, depleted groundwater resources, and increased non-natural sedimentation by dams (Postel, 2013). Moreover, the impacts of these changes have led to a loss in aquatic ecosystem biodiversity, a rise of eutrophic water bodies, and an overall decline of aquatic environment aesthetics.

Water is critical for the future growth of humanity, but at the same time it can be its biggest limiting factor. The human population is projected to reach nine billion by the year 2050, with the majority of growth occurring in regions that are already water stressed. The fulfilling of water needs of the additional two billion people while maintaining the life-support functions of freshwater systems is possibly one of the biggest challenges of the 21st century. To address these challenges in the coming future, it will be vital to meet the additional water quantity requirements with an increased emphasis on higher water quality. However, given the current nature of water management and the existing pressures on water resources, it might not be sustainably possible to meet the demand for high quality water in the future. It will require new ways and approaches in water management and improvement in efficiency of water use. Large-scale advances in water management and gains in efficiencies of water utilization may enable us to meet the demands of a growing global population and economy. However, there is a large degree of uncertainty associated with the amount of improvements needed, the efficiency levels that can be achieved, and whether there is enough time to make significant and relevant gains.

The answers to these questions lie in assessing the current status of our water resources as well as in determining the direction in which they are headed. A key step in these assessments is comprehensive water quality monitoring of our aquatic environments. As stated by Jackson et al. (2001), better monitoring and forecasting of water resources will help to improve allocation of water for competing demands. Water quality monitoring is essential to verify the suitability of water resources for their intended purposes, both locally and on bigger spatial scales, and for characterizing any changes and trends in water quality over time. It helps in quantifying existing or newly emerging water quality problems. Additionally, monitoring is also critical to gauge compliance of water bodies with existing pollution regulations.

Increased pollutant loading from non-point sources around the world has been one of the foremost factors in degrading water quality in receiving streams, rivers, lakes, and estuaries (Howarth, 1998; Kronvang et al., 2005). In the US, increased pollutant loading, specifically nitrogen and phosphorus from the intensively cropped and tile-drained Midwestern watersheds, has been a major cause of severe ecological damage in the Gulf of Mexico (Goolsby et al., 2001; Rabalais et al., 2002) and Great Lakes (Smith et al., 2008). The adverse effects of increased pollutant loading range from eutrophication, hypoxia, and consequently reduced biodiversity, to human health issues such as methemoglobinemia (Camargo and Alonso, 2006). Nutrient and sediment loadings from agricultural watersheds have been identified as a major cause of eutrophication and hypoxia throughout the world. Around the United States,

the Gulf of Mexico and Lake Erie have been known as areas most highly affected by eutrophication caused by anthropogenic activities over the past few decades (Goolsby et al., 2001; Rabalais et al., 2002; Dolan, 1993).

Lake Erie's drainage basin is the most populated and has the most amount of agricultural land among the five Laurentian Great Lake basins. Moreover, it is the shallowest and the southernmost of the five lakes. The extensive application of phosphorus as fertilizer in the 1960-70s within the agricultural farmlands in the Lake Erie basin led to large algal blooms in the lake (Michalak et al., 2013). Consequently, the US and Canadian governments implemented the Great Lakes Water Quality Agreement in the late 1970s and early 1980s, which brought down excessive phosphorus loading from point and non-point sources into Lake Erie (GLWQA, 1978; De Pinto et al., 1986). After a few years with low nutrient loading to the lake and smaller algal blooms, the mid-1990s saw their reemergence which has further increased drastically over the past few years. Hawley et al. (2006) reported one of the largest hypoxic zones over the past few decades which extended to approximately 10,000 square kilometers (km^2) within the lake in 2005. Recently Michalak et al. (2013) reported that the western and central basins of Lake Erie experienced the largest algal bloom in its recorded history with peak intensities over three times greater than the previously largest bloom recorded in 2008. Studies have suggested changes in land use, agricultural practices, water levels, and temperatures, and a rise in severe meteorological conditions contributed to the occurrence of these huge blooms (Hawley et al., 2006; Michalak et al., 2013).

Over the past few decades, water quality monitoring studies have increasingly been carried out to estimate sediment and nutrient loads delivered to rivers and by rivers to receiving lakes and oceans. Nutrients such as nitrogen and phosphorus are the engines of agriculture. Globally, more than a hundred million tons of nutrients are applied each year to agricultural farms to enhance crop yields. This has enabled human civilization to survive by increasing global food production to meet the ever increasing demands. Yet, this modern miracle has come with a price of its own. More than 50 percent of the nutrients applied each year are not used up by crops and are lost to the environment by leaching, erosion, and emissions. Excess nutrients have been primarily responsible for accelerated degradation of river and lake water quality, loss of wildlife habitat, groundwater pollution, and an overall decline in usability of water resources. It has become critical to accurately quantify these losses to help design pollution abatement programs and agricultural best management practices, and to evaluate their effectiveness.

The overall goal of this study is to improve the understanding of anthropogenic and natural impacts on climate-watershed-stream-lake processes in the hydrologic cycle by focusing primarily on sediment and nutrient loadings from large Midwestern watersheds. The research presented in this report addresses three aspects of load estimation. First, the traditional load estimation approach is evaluated, comparing accuracies of several techniques including data mining and the impact of selected techniques on determination of trends. Traditional load estimation approaches rely on having a complete (daily) series of stream flows and concentrations. Concentrations are estimated for days without water quality data using statistical or data mining techniques. Second, an alternative approach was developed in this study. The load is estimated for a limited number of large storm events, eliminating the need to obtain a complete series of concentrations. Regression relationships then relate the load during large storm events to the annual load. Third, a physically based model was used to simulate the impact of projected climate change on flows, nutrient loads, and sediment loads. Specific objectives of this study are summarized as follows:

(i) Evaluate modified and improved statistical approaches to estimate nutrient concentrations, loads, and corresponding trends (Chapter 4);
(ii) Apply new data mining methods in hydrology to predict nutrient loads (Chapter 5);
(iii) Characterize statistical relationships between large load events and total annual pollutant loads (Chapter 6);
(iv) Analyze spatio-temporal patterns of pollutant loadings (Chapter 7) ; and

(v) Quantify the impacts of projected future climate change on hydrology and pollutant loadings using physically based hydrologic modeling (Chapter 8).

1.2 Advances in Load Estimation Approach

In quantifying sediment and nutrient loads delivered by rivers to lakes and oceans, the main concern for water resource managers is to accurately estimate loading rates while minimizing associated uncertainties. However, resource constraints such as manpower and financial limitations often prohibit intensive water quality monitoring needed to achieve accurate load estimates (Yaksich and Verhoff, 1983). Increasing water quality pollution of historically pristine resources warrants the need to monitor more water resources than ever before (Meybeck and Helmer, 1989). Thus limited resources coupled with more monitoring require more efficient approaches to obtain accurate and reliable load estimates.

The majority of pollutant concentration and load estimation is conducted using traditional empirical and statistical approaches. Observed pollutant concentrations are typically related to streamflow and other parameters. A complete series of daily data is then created, using the relationships to estimate concentrations during days without water quality data. Various approaches to predict water quality data for days without observations have been explored and developed from sparse time-series datasets. These approaches have ranged from simple empirical averaging and interpolation to statistical modeling, and even neural networks.

These approaches include the widely applied seven-parameter regression model (Cohn et al., 1992) and simple ratio and averaging estimators which have been tested and evaluated in numerous studies globally. Recently, these approaches have been modified and improved by various residual correction techniques (Aulenbach and Hooper, 2006; Verma et al., 2012) using weighted regressions (Hirsch et al., 2010). As these techniques have been improved fairly recently, they have not yet been applied and evaluated independently on newer datasets. Therefore, the first part of this study features quantifying the variability in selection of these new improved techniques by calculating average annual nitrate concentrations and loads and their respective trends for the Lower Illinois River and its tributaries for an extensive monitoring period from 1975 to 2010. Grimvall et al. (2000) reported that inertia impacted the aquatic and terrestrial systems that control nutrient exporting to reduced application rates and regulatory changes. Temporal analysis of nutrient loadings might also highlight any changes in nutrient loading patterns due to inertia in watershed response.

A variety of data mining techniques are frequently used in other scientific and economic fields. However, only neural networks have been applied in hydrological sciences to estimate concentrations for load calculations. Hence, the second part of this study aims at evaluating data mining techniques such as nearest-neighbor methods and decision trees to predict missing NO_3-N concentrations for two extensively monitored watersheds in the Lake Erie basin. The streamflow and time of the year (Julian day) were the only parameters used to predict missing concentrations after calibrating the data mining models using cross validation and percentage split techniques. If effective, these data mining methods may help monitoring networks to estimate missing sediment and nutrient concentrations in sparse datasets for watersheds with limited or even no water quality monitoring data.

1.3 Load Estimation Approach Based on Large Storm Events

Some research studies have evaluated alternative approaches to estimate annual pollutant loads such as developing regression relationships between a few critical storm (high flow event) loads and annual loads. Richards and Holloway (1987), Preston et al. (1989), Lewis (1996), Robertson and Roerish (1999), Cooper and Watts (2002), Markus and Demissie (2006) and Salles et al. (2008) have reported that a few high flow events carry significant amounts of nutrients exported over a year. Yaksich and Verhoff (1983)

analyzed high flow event-based sampling strategies for watersheds in the Lake Erie basin and recommended intensively sampling two to three of the largest events in a year to obtain annual loading estimates with small errors. Thus, development of robust statistical relationships between observed loads during a few critical high flow events and observed total annual loads could provide an alternative approach to estimate annual pollutant loads for a certain watershed. If successful, such an approach will provide watershed managers and sampling programs with an option of estimating annual pollutant loadings simply by sampling a few high flow events in a year, thereby leading to a significant reduction in monitoring costs over a year.

A comprehensive analysis hasn't been done in previous studies to validate this hypothesis for a wide range of watershed sizes, locations, land uses, and pollutants. Specifically, there is a lack of such studies examining the predictability of annual nutrient loads from a few large load events in large agricultural Midwestern watersheds, particularly when they are the principal sources of nutrient and sediment loadings delivered to the Gulf of Mexico and Lake Erie. Multiyear water quality data consisting of Total Suspended Solids (SS), Total Phosphorus (TP) and Nitrate Nitrogen (NO_3-N) concentrations from 10 large Midwestern watersheds were used in this study to statistically evaluate the relationships between nutrient and sediment loads exported through a few large events (the biggest load events) and total annual loads. Most of the watersheds analyzed in the study are typical agricultural Midwestern watersheds, draining into the Lake Erie and the Mississippi River basins. A hypothesis that a watershed-specific correlation between the few biggest load events and total annual load exists and can be used to precisely and efficiently predict annual loads was tested. Spatial transferability of the relationships was confirmed to ensure applicability to streams with similar watershed characteristics.

One of the challenges of the practical application of this approach is a need for the *a priori* prediction of a large load event that might be critical to predict total annual loads, and that should be monitored. It may be virtually impossible to precisely forecast the occurrence of an event that will be important to predict annual loads. However, monitoring streams with strong temporal patterns in load exporting can be redefined by intensively focusing on periods of high load exporting.

Eutrophic conditions in Lake Erie have generally been observed in late summer-early fall periods, when low flow conditions exist in the streams draining into these water bodies. Low flow conditions favor nutrient uptake and extensive algae growth, eventually leading to hypoxic conditions. Eutrophication in such water bodies is largely driven by nutrient loadings from agricultural lands (Royer et al., 2006). The loadings of nutrients are largely dependent on the landscape characteristics, geological and climatological factors, along with agricultural management practices and their influences on hydrological processes (Mourad and van der Perk, 2009).

Streams in the Midwestern United States typically have higher flows in late winter and early spring. This coincides with the fallow period in the agricultural watersheds contributing to these streams. This period of high flow is usually accompanied by large nutrient loadings from these watersheds. Agricultural management practices such as no cover crops, fall fertilizer application, and broadcasting of fertilizers rather than soil injection contribute to a higher nutrient export during such high flows. Additionally, the Midwestern watersheds are characterized by intensive installation of sub-surface tile drain systems. The installation of these tile drain systems modifies the natural landscape characteristics and affects the natural nutrient transport processes by expediting the export of dissolved nutrients by bypassing the preferential groundwater flow paths. This nutrient-rich water is delivered to downstream lakes and estuaries, eventually causing algal blooms and eutrophic conditions.

Typically, nutrient concentrations in agricultural rivers have some seasonal variability which needs to be characterized to quantify annual loadings from the system (Lampman et al., 1999). Zhang et al. (1995) concluded that if this seasonal variability is not characterized, it may contribute to the difficulty in determining long-term changes in nutrient concentrations and loadings. Additionally, the seasonal variability in nutrient loadings may influence the impact of these nutrients in the receiving water bodies

and also give an insight into the nature of the nutrient sources contributing to the river systems (Lampman et al., 1999). Quantifying the temporal patterns in nutrient loadings is critical in developing efficient nutrient criteria, numeric standards, and total maximum daily loads (TMDLs) for impaired receiving streams, rivers, and lakes (Royer et al., 2006).

Despite the widely acknowledged seasonality in load export patterns from large agricultural Midwestern watersheds and the importance of a few large load events in total annual loads, few comprehensive efforts have been made to quantify these patterns on large spatio-temporal scales. The few studies that exist simply analyzed pollutant export patterns from very small experimental watersheds limited to a smaller geographical area. Therefore, another part of this study analyzed spatio-temporal patterns in nutrient and sediment load export from eight large Midwestern watersheds over long monitoring durations (8-32 years).

The spatio-temporal analysis was conducted in two phases. The first phase focused on the temporal occurrence of the top load events for TSS, TP, and NO_3-N. The second phase of the analysis focused on examining the timing of average annual flow, pollutant concentrations, and corresponding loads over the complete monitoring duration for each watershed. These analyses reveal the temporal patterns of pollutant load export that can then be further used to design more efficient monitoring programs. Identification of temporal patterns in load export would also help in designing targeted regulatory programs and policies for reducing riverine pollutant loads.

1.4 Nutrient and Sediment Loadings in the Changing Climate

Water managers will face an increasing host of challenges such as population growth, land use changes, economic development, changing social values, and climate change in the future. Climate change is one of the biggest and most dynamic challenges expected. There is growing scientific and observational evidence that climate change is caused by the rise in greenhouse gas concentrations in the earth's atmosphere and its overall warming. It is likely to affect the fundamental drivers of the hydrological cycle and influence outcomes such as water quantity, water quality, floods, droughts, navigation, and hydropower. There are knowledge gaps in observational data and an understanding of the complex dynamics of climate change and its impacts on a wide range of watersheds in different global regions. Current water management practices might not be robust enough to cope with climate change and its impacts on water resources.

It has become ever more crucial for water managers and environmental scientists to propose newer water management approaches by tracking and anticipating, and responding to climate change (Brekke et al., 2009). Specifically, it is vital to estimate the impacts of projected climate change on water resources and hydrological processes on both global and local scales (Jackson et al., 2001). This would enable water managers to determine the necessary adaptation options and mitigating measures that might reduce the impacts of climate change on water resources. Rivers, lakes, and oceans are key components of the global hydrological cycle. It is critical to understand the impacts of impending climate change on the functionality of these water bodies due to increasing pressures on water resources with potentially increasing nutrient and sediment loading.

The effects of climate change can be estimated using physically based hydrologic models coupled with future climate data from General Circulation Models (GCMs). These hydrologic models utilize commonly measured hydro-climatic parameters along with spatial watershed data to recreate the hydrological processes in a watershed. Once calibrated, future GCM projections can be input to the model to simulate new sets of outputs in a changing climate. Comparing the outputs for current and projected future climate change can help to understand the sensitivity of the watershed processes to climate change. The last part of this research uses the Soil and Water Assessment Tool (SWAT) to evaluate the impacts of projected change in temperature and precipitation for the mid-century (2045-2055) and late-century

(2089-2099) periods on the flow and sediment and nutrient loading in a large watershed in the Lake Erie basin. The Maumee watershed typifies a Midwestern agricultural watershed with intensive row-crop agriculture and a high density of sub-surface tile drainage systems. It is also the largest contributor of nutrient and sediment loads to Lake Erie.

2. Study Area

This research utilized a multiyear daily time series of water quality data from 10 watersheds in northern and central Ohio, southeastern Michigan, northeastern Indiana, and central Illinois. Six of the watersheds analyzed in this study, Cuyahoga, Grand, Maumee, Raisin, Sandusky, and Vermilion (OH), drain into Lake Erie. Two watersheds, Great Miami and Muskingum, drain southwards into the Ohio River basin. In this study, these eight watersheds are referred to as the Ohio watersheds. The remaining two watersheds are in Illinois. The Vermilion (IL) and Upper Sangamon drain into the Upper Mississippi River basin (Figure 2.1). These two watersheds are referred to as the Illinois watersheds. Agriculture was the predominant land-use in the study watersheds, although some had significant areas of wooded forests and/or urbanization (Table 2.1). A detailed description of the watersheds is provided in subsequent sections.

Data from all 10 watersheds were processed consistently. The eight Ohio watersheds were analyzed i) to identify relationships between annual loads and loads carried during large events, and ii) to determine temporal patterns of large events. The two Illinois watersheds were then used to test the spatial transferability of the relationships. Maumee was selected as a case study to simulate impacts of climate change on load exporting. The applicability of data mining techniques was explored using two Ohio watersheds with different land uses; Maumee (agricultural watershed) and Cuyahoga (urbanized watershed). In addition to the above listed sites, data from four water quality monitoring sites in Illinois (one on the Sangamon River, one on the La Moine River, and two on the Illinois River, Figure 2.3) were used in the last part of this research to evaluate i) the performance of several methods for annual load estimation and ii) long-term changes in average annual nitrate concentrations and total annual loads at four stations in the watershed.

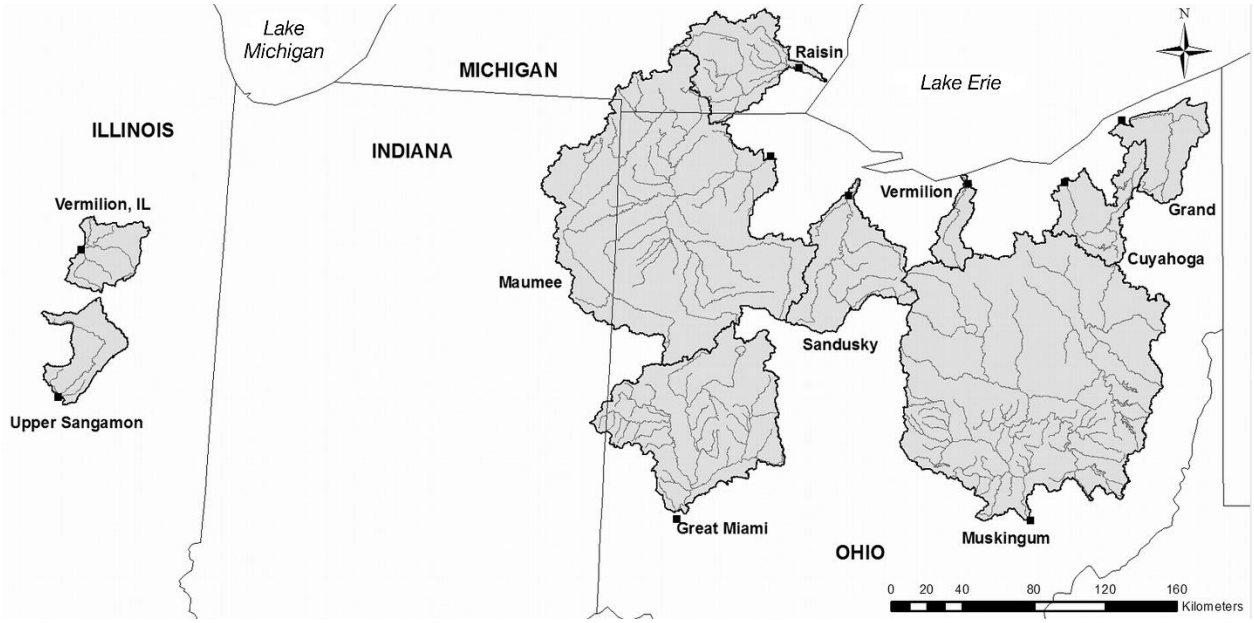

Figure 2.1: Locations of watersheds and gaging stations

Table 2.1: Characteristics of studied watersheds (upstream of the indicated USGS gaging station)

	USGS Station Number	Monitoring Period	*Watershed size (km²)*	*Land-use (%)**		
				Agriculture	*Urban*	*Wooded*
OHIO WATERSHEDS - Lake Erie basin						
Cuyahoga	04208000	1982-2009	1,843	17	47	35
Grand	04212100	1989-2006	1,758	37	10	52
Maumee	04193500	1975-2009	16,427	81	11	8
Raisin	04176500	1982-2007	2,755	72	11	16
Sandusky	04198000	1975-2005	3,285	83	9	8
Vermilion, OH	04199500	2001-2008	697	71	1	26
Ohio River basin						
Great Miami	03271601	1996-2009	6,953	82	5	10
Muskingum	03150000	1995-2009	19,208	52	2	43
ILLINOIS WATERSHEDS - Upper Mississippi River basin						
Upper Sangamon	05572000	1993-1999	1,406	90	5	1
Vermilion, IL	05554500	1988-1999	1,492	95	3	2

Notes: *Land-use data for Cuyahoga, Grand, Maumee, Raisin, and Sandusky as reported by Bosch et al., 2011

2.1 Ohio Watersheds

All watersheds except Cuyahoga and Grand are primarily agricultural (Table 2.1) with most of their land area under row-crop agriculture with corn-soybean annual rotations. The Cuyahoga watershed is predominantly an urbanized watershed (47 percent urban land use) with the Greater Cleveland urban area covering most of the northern half of the watershed. The Grand watershed is the only one that is mostly forested with about 52 percent of its land area occupied by wooded forests. The Raisin watershed is the northernmost watershed with virtually all its land area in Michigan. It is a typical Midwestern watershed which is predominantly agricultural; however, it is different from other watersheds due to the higher degree of impoundment in the middle and lower sections. The Raisin watershed has about 14 impoundments with a surface area of at least 10 hectares (24.7 acres), including artificial reservoirs, natural lakes, and small ponds (Bosch, 2008).

Soils in these watersheds, especially in northern Ohio, eastern Indiana, and southern Michigan, are composed of fine glacial till. They are generally very fertile but poorly drained, leading to extensive adoption of tile-drainage in these areas. Soils in central and northeastern Ohio are also of glacial origin but are coarser and less fertile. The most common soils in the Sandusky, the northern reaches of Maumee, and Raisin watersheds were formed in lake and beach sediments and glacial till associated with the glacial lakes. These soils are characterized by clayey topsoils with 3 percent or greater organic matter content in the upper 25 cm of the soil profile (Ohio Department of Natural Resources Division of Soil and Water Resources-Soil Regions). The central part of Maumee, most of Great Miami, and the southern part of Sandusky watersheds are characterized by coarse-textured soils formed by glacial deposits. These soils are better drained than soils formed by lake and beach sediments but are relatively older and thereby more

weathered and less fertile for agricultural production. The Muskingum watershed is characterized by clayey soils with high slopes and little organic matter content. These soils are well drained and have heavily wooded areas. Soils in the Grand and Cuyahoga watersheds were also formed by glacial deposits and range from coarse to fine-textured with better drained soils seen in the southern parts of these watersheds. Most of the land in northwestern Ohio, eastern Indiana, and Southern Michigan is characterized by low slopes and fertile but poorly drained soils; therefore, large parts are artificially drained using sub-surface tile drain systems. The Vermilion and the Upper Sangamon watersheds in Illinois are characterized by highly fertile but poorly drained prairie soils formed by the loamy glacial drifts. These Illinois watersheds are also extensively drained using subsurface drainage systems.

Muskingum is the largest watershed analyzed in this study with a drainage area of about 19,200 km^2 upstream of the sampling station sampling gage. Among the watersheds draining into the Lake Erie basin, Maumee is the largest with about 16,400 km^2 of watershed area upstream of the sampling station. Vermilion (OH) is the smallest watershed analyzed in this study with a drainage area of about 700 km^2. Cuyahoga and Grand watersheds experience slightly higher annual precipitations compared with the western watersheds, which is attributed to more lake-effect precipitation (Bosch et al., 2011).

Maumee is one of the largest watersheds in Ohio contributing to the Great Lakes basins. The Maumee River watershed extends from 40° 23' to 42° 5' N latitude, and from 83° 20' to 85° 15' W longitude. It covers a large part of northwest Ohio along with small portions of Indiana and Michigan (Figure 2.2). Although the river drains out to Lake Erie near the city of Toledo, this study focuses on the river basin draining up to the U.S. Geological Survey (USGS) gaging station at Waterville, Ohio (Station #04193500) with a total drainage area of 16,395 km^2. Meteorological data from the watershed indicate that the mean annual precipitation for the Maumee River watershed ranges from 840 to 940 mm. Similarly, the mean monthly temperature in the watershed ranges from -3.6°C (in December) to 23.1°C (in July). The watershed elevation varies from 150 to 470 m above mean sea level. Figure 2.2 also shows the river network in the Maumee River basin.

The Maumee River basin is predominantly agricultural. Agricultural land covers 73 percent (cropland 71 percent and pastureland 2 percent) of the watershed area. Other significant land uses in the basin are urban (10 percent of the watershed) and forested land (8 percent) (Natural Resources Conservation Service, 2005). Most soils in the basin are formed from the weathering of glacial till. Most of the soils in the basin are poorly drained, rich in organic matter, and have a high clay content. So, subsurface drains and surface ditches are common in the basin as they drain over 90 percent of agricultural area (Natural Resources Conservation Service, 2005). The Maumee River is not only the largest tributary but also the largest contributor of nutrient and suspended sediment loading to Lake Erie (Myers et al., 2000; Richards et al., 2002). According to the 1997 National Resource Inventory data, the rate of soil erosion in the basin was estimated to be 4,958,700 tons/year (Natural Resources Conservation Service, 2005).

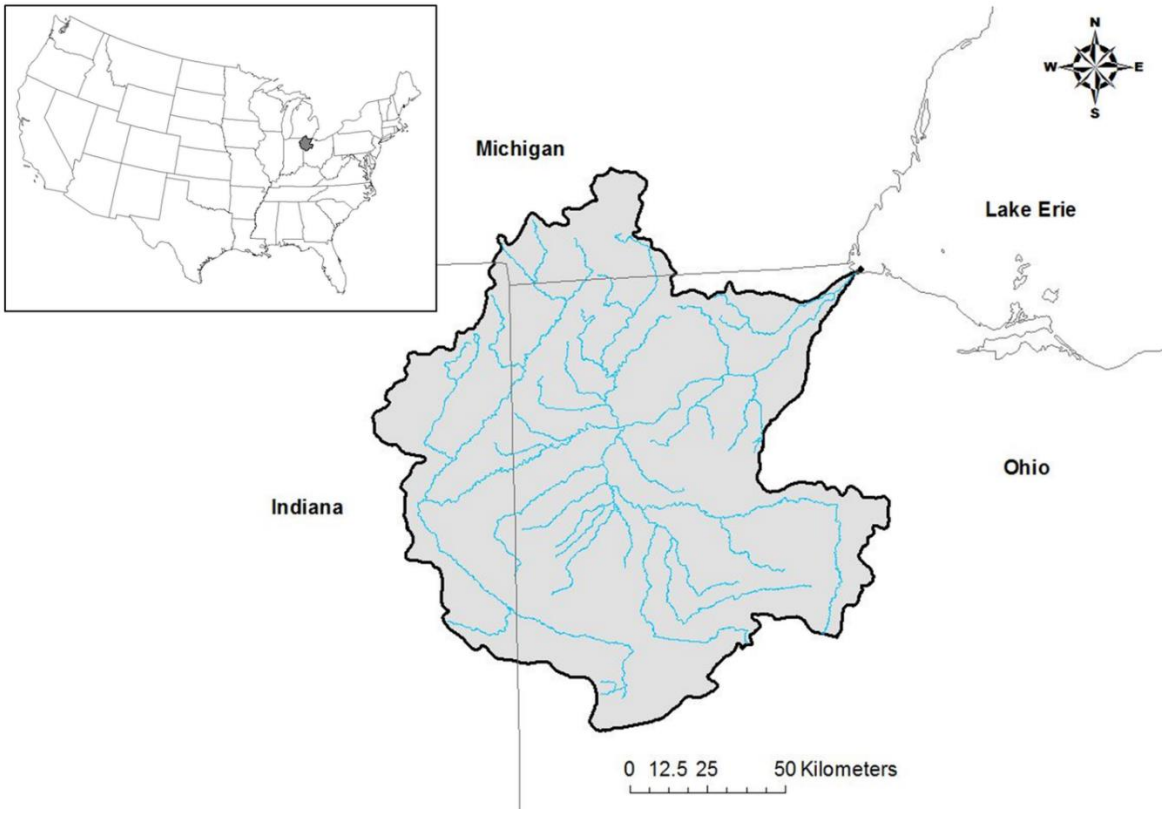

Figure 2.2: The Maumee River watershed with its stream network

2.2 Illinois Watersheds

The Illinois River drains over 74,000 km^2 primarily in Illinois and portions of Indiana, Wisconsin, and Michigan. Land use is predominantly agricultural, but the watershed also receives discharge and runoff from the Chicago metropolitan as well as other urban areas along its length. The river has been further altered by navigation dams and a diversion of water from Lake Michigan. The study area is located in the Lower Illinois River basin (Figure 2.3), which stretches from the Fox River to the Illinois River's confluence at the Mississippi River.

Four water quality monitoring stations operated by the Illinois Environmental Protection Agency (IEPA) as part of their statewide ambient network were selected (Wallin and Schafer, 1979; IEPA, 2007). The stations include two sites on the Illinois River (Havana and Valley City), one site on the Sangamon River at Oakford, and one site on the La Moine River at Ripley (Table 2.2 and Figure 2.3). The Sangamon River is the largest tributary to the Illinois River. It comprises 19 percent of the total drainage area at Valley City. The Upper Sangamon River at Monticello has a drainage area of 1,406 km^2. Agriculture is the dominant land use within the Upper Sangamon watershed. Row crops (corn and soybeans) cover approximately 87 percent of the total watershed area. The Vermilion River at Pontiac (IL) has a drainage area of 1,570 km^2. This watershed is also predominantly agricultural. The Sangamon River at Oakford and the La Moine River at Ripley account for 60.3 percent and 15.3 percent of the drainage area between Havana and Valley City, respectively.

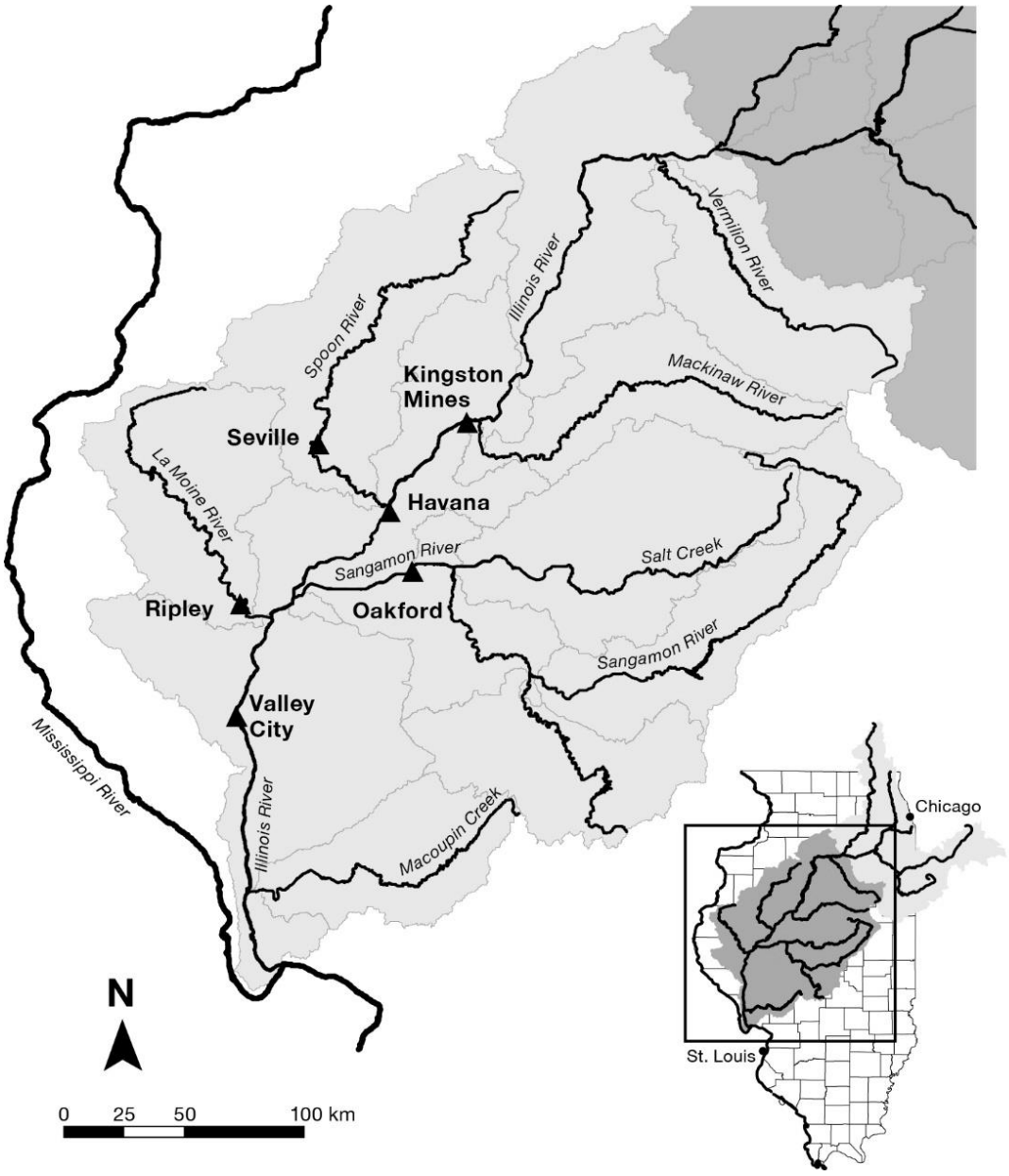

Figure 2.3: Map of the main channel and tributaries in the Lower Illinois River basin

Table 2.2: Streamgages for nitrate concentration and discharge (1975-2010)

USGS station	*EPA station*	*Streamgage*	*Drainage Area (km2)*	*Number of samples*	*Mean discharge (m3/s)*	*Mean NO_3-N conc.*
05570500	D-31	Illinois River at Havana*	46,845	269	568.3*	4.16
05586100	D-32	Illinois River at Valley City	68,465	344	707.3	3.99
05583000	E-25	Sangamon River at Oakford	13,038	261	132.2	4.52
05585000	DG-01	La Moine River at Ripley	3,310	407	30.3	2.93

Notes: *Flows calculated via hydrologic modeling (Lian et al. 2010) for 1978-2007

3. Data Preparation and Processing

3.1 Precipitation

Precipitation is the main driver of water movement from the agricultural fields to the drainage ditches. It is thus essential to calculate the daily mean precipitation across these watersheds over the monitoring period. Daily precipitation data from all the available weather stations that are within these watersheds were acquired from the Midwestern Regional Climate Center (MRCC) database. Daily mean areal precipitation across a watershed was computed by using Thiessen weighted precipitation (Thiessen, 1911) from all weather stations in and around a watershed.

Figure 3.1 shows the location of all watersheds analyzed in this study and the weather stations used to calculate the Thiessen weighted daily precipitation values across the watersheds. The watershed areas ranged from approximately 700 to 19,000 square kilometers with the total number of weather stations ranging from 2 to 19 for the calculation of Thiessen weighted daily precipitation. Table 3.1 shows the total number of weather stations used to calculate the Thiessen weighted daily mean areal precipitation across the watersheds.

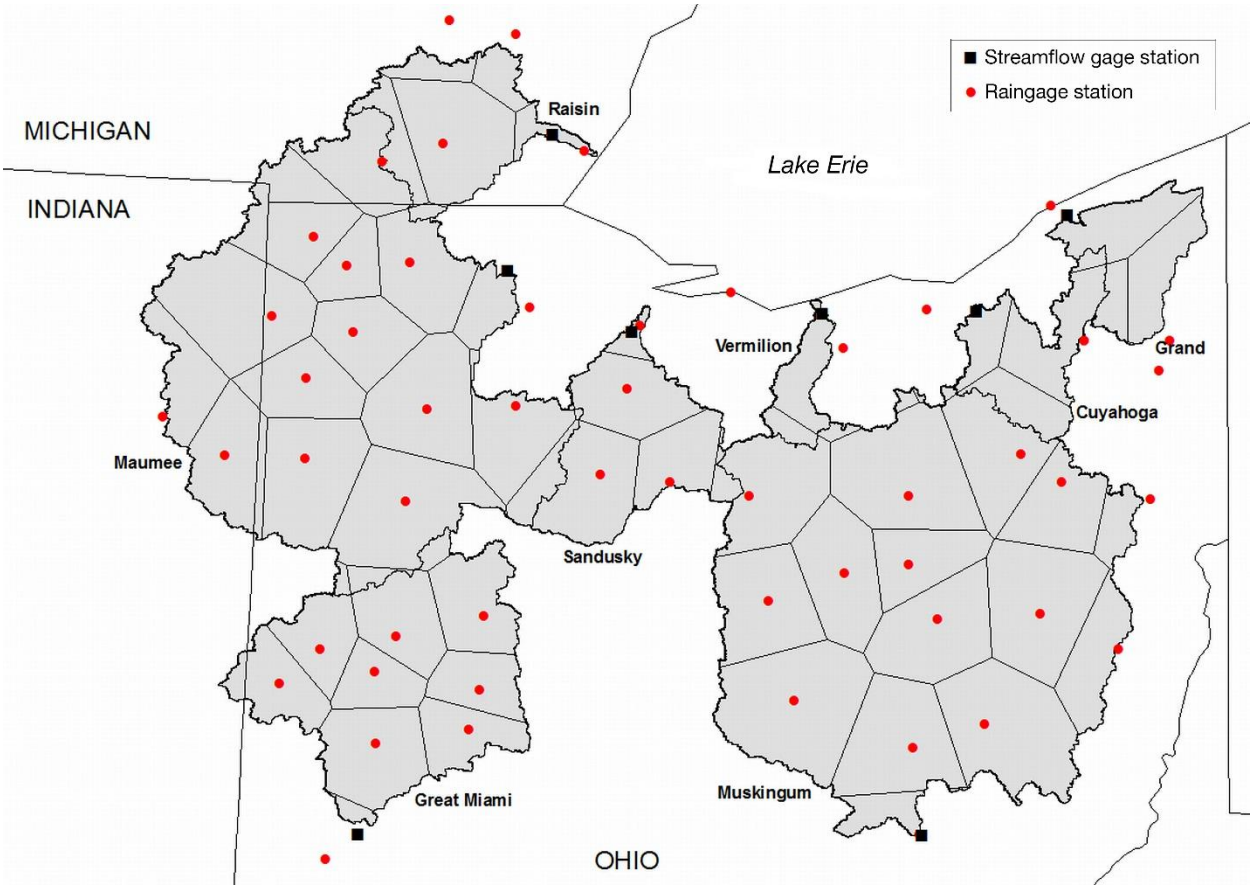

Figure 3.1: Location of watersheds with their respective gaging stations and weather stations along with Thiessen polygons for calculating daily mean areal precipitation

Table 3.1: Number of weather stations per watershed

Watershed	*Number of weather stations*
Cuyahoga	5
Grand	4
Great Miami	10
Maumee	19
Muskingum	17
Raisin	6
Sandusky	6
Vermilion (OH)	2

3.2 Water Quality Data

3.2.1 Ohio Watersheds

The Water Quality Lab (WQL) at the National Center for Water Quality Research at Heidelberg College intensively sampled the Ohio watersheds for monitoring periods ranging from 8 to 32 years for different watersheds. This sampling program was designed to characterize annual pollutant loads, thus daily samples were collected during low flows with additional samples collected during storm events. The sampling stations were coupled with existing USGS gaging stations. Simple grab samples using an auto-sampler were collected at the sampling stations as opposed to depth and width-integrated samples, but were comparable as stations were located in regions where water was well mixed (Richards et al., 2001). In-depth details about the sampling program and chemical analyses are described in Baker (1985), Richards and Baker (1993), and Richards et al. (2001). Three pollutants, Suspended Solids (SS), Total Phosphorus as P (TP), and Nitrate plus Nitrite Nitrogen (NO_2-N+NO_3-N, indicated as NO_3-N from here on), were analyzed in this study.

The WQL datasets reported laboratory-analyzed pollutant concentrations along with the corresponding 15-minute flow measurements at the sampling stations corresponding to the USGS gage. Yaksich and Verhoff (1983) reported that if water quality measurements are not made during high flow events, the annual pollutant loads can be underestimated significantly. As one of the primary objectives of this study was to assess the role of large load events on annual loads, data preprocessing was conducted to eliminate water years with considerable missing concentration and flow data. Missing flow volumes attributed to a lack of sampling coverage in a water year were computed by comparing the water year flow volumes from WQL datasets and water year flow volumes from daily flows reported by the USGS.

Figure 3.2 shows sample hydrographs from the Sandusky watershed for water years 1988 and 1989. In this figure, the continuous curve indicates the mean daily flows which are derived from the 15-minute measurements as reported by the USGS. The points on the figure indicate the 15-minute flows from the USGS gages as reported by the WQL datasets which correspond to the time of water sample collection for pollutant concentration analysis. In the water year 1988, the WQL did not report any pollutant concentrations until late January, and therefore, it was excluded from this study to avoid underestimation of total annual pollutant loads and probable overestimation of the contributions of high flow loads to annual loads. On the other hand, the water year 1989 was included in the study as the WQL covered the whole year with consistent daily sampling coupled with multiple samples during high flow events.

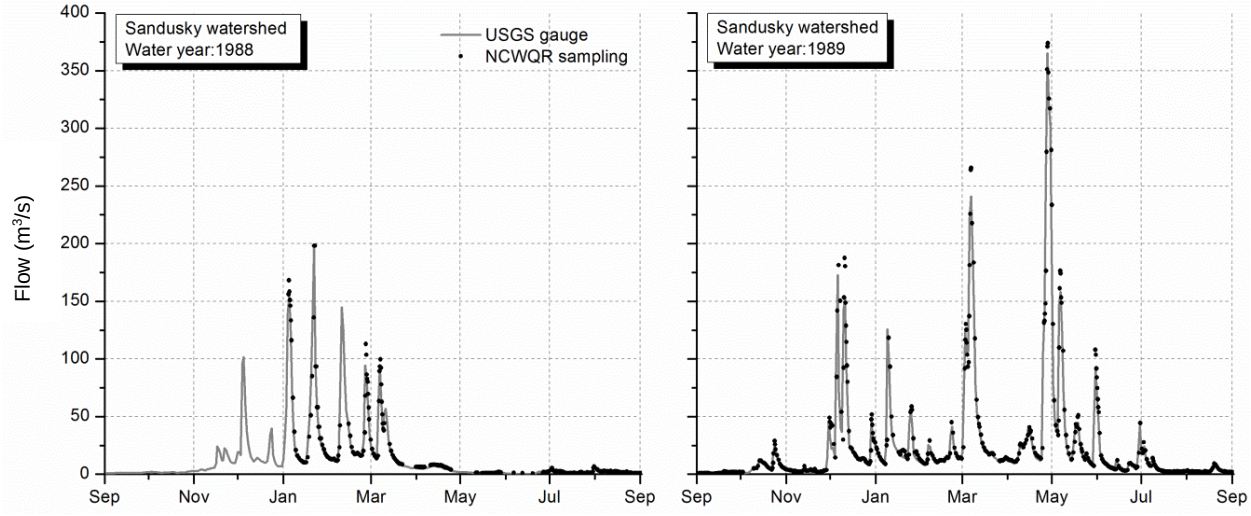

Figure 3.2: Hydrographs from the Sandusky watershed for water years 1988 and 1989 showing the example years excluded (1988) and included (1989) from this study based on completeness of flow measurement sampling

3.2.2 Illinois Watersheds

NO_3-N data for Vermilion watersheds in Illinois were obtained directly from the Illinois-American Water Company at Pontiac. NO_3-N data for the Upper Sangamon were prepared using weekly observed data collected by the Illinois State Water Survey (ISWS) (Demissie and Keefer, 1996; Keefer and Demissie, 2000).

Pre-1999 NO_3-N data for the remaining sites were available from Legacy STORET (USEPA, 2011), while newer data are housed in multiple internal IEPA databases. Sample size ranged from 261 to 407 (Table 2.2). Although each station is part of an ambient network routinely sampled over its history on 4- to 6-week intervals, data from other IEPA monitoring projects were included in the analysis when available. The date range for this analysis, 1975 to 2010, was selected to take advantage of the longest timeline available for nitrate data. Only the Havana site had a period of record 1978-2007. Daily flow data were available from USGS gages at Valley City, Oakford, and Ripley. Daily flow data for the Havana water quality site were determined using a hydrologic model by Lian et al. (2010), which simulated flows for the entire Illinois River using the Hydrologic Simulation Program-FORTRAN (HSPF).

3.3 Identifying Water Years with Complete Datasets

Data preprocessing was conducted to identify and remove water years with a significant portion of missing flow data and to keep only those years with more complete data. This was done to avoid underestimation of annual pollutant loads and possible incorrect estimation of the event loads. From exploratory runs it was found that annual loads were highly underestimated for years when more than 20 percent flow volume did not have observed water quality data. Typically, one to two major load events were not sampled during the identified years. Thus, any water year with more than 20 percent of flow data without corresponding water quality data was excluded from the analysis.

Table 3.2 shows the percentage of missing flow volumes along with missing water quality data for each year, which were then used to identify years excluded from the analysis for the Cuyahoga and Maumee watersheds. For a few years, the numerical integration of WQL flows reported higher annual

flow volumes than that computed using average daily flows as reported by the USGS. The WQL reported 15-minute flows corresponding to sample collection time-stamps. During the intensively sampled high flow events, there were a few reported flows which were much higher than the average flow for that day. Also, the WQL sampling wasn't at uniform time intervals. Numerical integration to compute daily flow volumes thus resulted in higher volumes than from USGS daily flows. As the authors compared total annual flow volumes, higher volumes over a few days resulted in higher annual volumes overall. Such years are indicated by a negative missing flow volume in Table 3.2. The maximum number of years excluded was 6 from the 32-year monitoring record from the Sandusky watershed. Just one out of the eight years of monitoring record was excluded for the Vermilion (OH) watershed (Table 3.3).

Table 3.2: Percent flow and days without observed water quality data: Cuyahoga and Maumee

Watershed	*Cuyahoga*		*Maumee*	
Year	*Missing flow*	*Missing days*	*Missing flow*	*Missing days*
1982	21.2%	19.3%	10.4%	13.3%
1983	5.0%	2.8%	-0.4%	0.0%
1984	4.3%	4.4%	-1.7%	0.5%
1985	5.5%	1.8%	0.8%	3.5%
1986	1.6%	1.9%	0.1%	2.2%
1987	1.8%	6.5%	1.7%	2.1%
1988	24.3%	23.6%	7.4%	4.5%
1989	13.4%	17.6%	0.8%	2.0%
1990	36.1%	40.1%	-0.2%	0.2%
1991	9.3%	10.9%	4.9%	4.6%
1992	55.1%	34.6%	27.1%	10.3%
1993	9.8%	8.0%	17.7%	12.1%
1994	8.5%	6.0%	8.2%	6.3%
1995	14.6%	10.6%	0.3%	5.6%
1996	15.6%	8.5%	7.8%	8.0%
1997	10.9%	12.8%	-4.6%	3.1%
1998	-0.7%	2.0%	-1.1%	0.3%
1999	1.2%	0.7%	-2.8%	0.6%
2000	7.1%	7.2%	0.5%	3.6%
2001	3.3%	3.1%	19.7%	8.6%
2002	9.2%	7.1%	17.3%	7.1%
2003	0.9%	8.1%	-10.0%	1.3%
2004	4.9%	10.4%	10.6%	13.9%
2005	46.3%	24.1%	43.6%	14.2%
2006	10.0%	7.1%	23.2%	14.9%
2007	-2.1%	2.7%	4.6%	2.6%

Watershed	*Cuyahoga*		*Maumee*	
Year	*Missing flow*	*Missing days*	*Missing flow*	*Missing days*
2008	4.5%	3.8%	-2.6%	1.3%
2009	8.3%	4.1%	-9.7%	4.5%

Notes: * Years with more than 20 percent flow volume missing (excluded from further analyses) are highlighted.

Table 3.3: Monitoring periods, years of record, and number of years included in analysis for all watersheds

	Monitoring period	*Years of record*	*Years selected in this study*
Lake Erie basin			
Cuyahoga	1982-2009	28	24
Grand	1989-2006	18	13
Maumee	1975-2009	32	29
Raisin	1982-2007	26	23
Sandusky	1975-2005	31	25
Vermilion (OH)	2001-2008	8	7
Ohio River basin			
Great Miami	1996-2009	14	10
Muskingum	1995-2009	15	14

3.4 High Flow Event Separation

To assess the role of large load events on annual pollutant loads, it is essential to identify and separate high flow events in a water year. Identifying the beginning of high flow events in hydrographs isn't very complicated since a precipitation event is usually followed by a steep rise in the hydrograph. Identifying the exact end of a high flow event is more complicated since the receding limb of the hydrograph was generally more gradual. Additionally, after a high flow event, the flow stabilized at a higher value as compared to the beginning of the event. There was some overlapping of closely occurring events with two or more hydrograph peaks separated by a flow value that was lower than peak flows but could not be considered low flow. Similar to Richards et al. (2001), snowmelt-driven events were treated similarly to precipitation events as flow volumes for both kinds of events were similar.

In this study, a new approach to identify high flow events was developed and tested. This approach used two baseflow separation filters from the Web-based Hydrograph Analysis Tool (WHAT) (Kyoung et al., 2005) and compared them to identify the beginning and end of high flow events. The first method, a

local minimum filter, linearly connects local minima to separate out the baseflow from a hydrograph. The second method, a recursive digital filter, separates baseflow and direct runoff similarly to separating high frequency and low frequency signals in signal processing. The Baseflow Index value (BFI_{max}=0.80) used in the recursive digital filter was selected based on a recommendation by Kyoung et al. (2005) for perennial streams with porous aquifers to minimize the subjective influence of different BFI_{max}. The results from both methods were compared. The points of intersection of baseflow curves from both these filters defined the beginning and end of a high flow event (Figure 3.3).

The high flow event begins where the flow starts to increase above the baseflow, i.e., when the first non-zero value is encountered for direct runoff. When the last non-zero value appeared on the receding limb of the hydrograph, the end point was selected as the first local minimum encountered after the last non-zero value for direct runoff. Markus and Demissie (2006) reported that in loading analysis, the uncertainty in identification of the beginning and end of high flow events results in insignificant errors due to negligible loads exported during low flows. Similarly, in this study small errors in identifying the correct endings of high flow events were neglected.

In the watersheds analyzed in this study, the SS concentration peaks coincided with or just preceded the hydrograph peaks. This relationship is typical since SS is generally transported through overland surface flow. The pollutograph for SS indicated a much steeper rise in concentration compared to the hydrograph (Figure 3.3). Similarly, TP is also exported through overland flow (Royer et al., 2006; Richards et al., 2001). TP concentration peaks also closely align with hydrograph peaks because TP is generally bound to sediment particles. It was observed that NO_3-N concentrations decreased as flow increased at the beginning of an event, mainly due to dilution as most of the large stream flow increases were caused by surface flow. Later, when the surface flow contributions to stream flow decreased, NO_3-N concentrations increased and reached their peaks later than the hydrograph peaks, showing that NO_3-N is exported mainly through subsurface flow (Richards et al., 2001; Schilling and Zhang, 2004; Royer et al., 2006; Zhang et al., 2010; and Zhu et al., 2011) that is slower than the surface flow export. Also, during a few large precipitation events the subsurface tile drain outlets might get submerged, backing up the tile, which eventually starts flowing once the water levels in drainage ditches subside, further delaying the NO_3-N concentration peaks.

Given the mechanistic differences in the export of SS, TP, and NO_3-N from watersheds and the criticality of defining high flow events adequately to determine loads associated with the events, hydrographs were separated differently for different pollutants. This was done using a new index called the Baseflow Filter Ratio (BFR), which for any local minima was defined as the ratio of the local minimum filter baseflow value and the digital recursive filter baseflow value. The intersection of both baseflow filter curves identified the beginning and ending of high flow events. The BFR was used to further split these events into smaller individual events based on the pollutants being evaluated. If the BFR exceeded a set threshold at any local minima point in an identified high flow event, the event was further split at that point into two smaller events. Setting a high threshold for the BFR resulted in a larger number of events when multiple peaks occurred in close proximity to each other (Figure 3.4).

For fast-response pollutants such as SS and TP for which pollutographs closely follow or just precede hydrographs, a high BFR of 1.75 was used, which very closely identified individual high flow events when each prominent peak in the hydrograph was separated and accounted as a different event. For slow-response pollutants such as NO_3-N for which pollutographs recede more gradually than hydrographs and concentration peaks tends to lag hydrograph peaks, a lower BFR of 1.25, which identified individual high flow events when events occurring very closely (two or more close peaks) were accounted as one. This is necessary to capture the full NO_3-N load associated with the flow event. Figure 3.4 shows the impact of BFRs in separating hydrographs into high flow events based on the pollutant being evaluated.

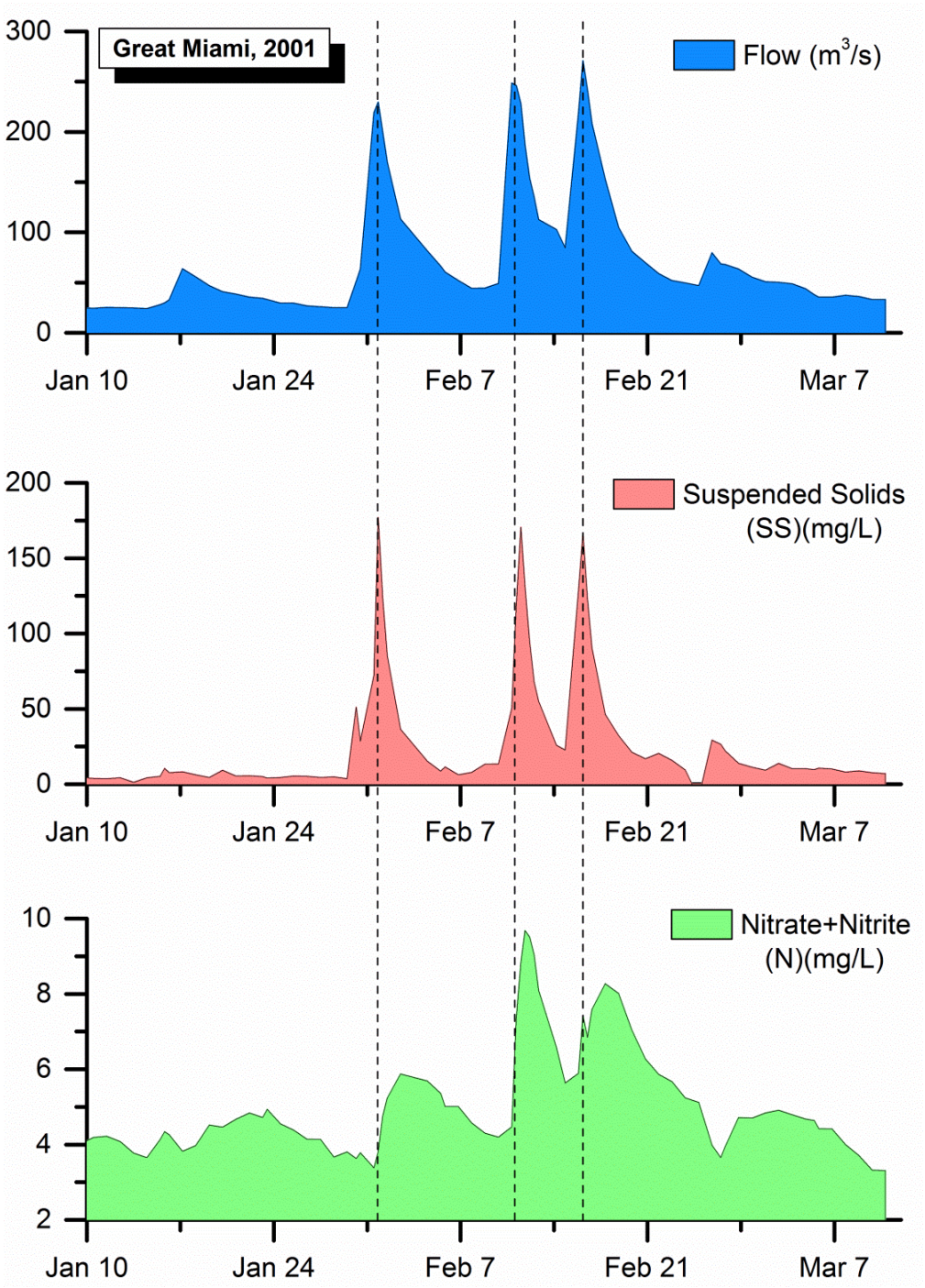

Figure 3.3: Sample hydrograph and SS and NO_3-N pollutographs: Great Miami watershed

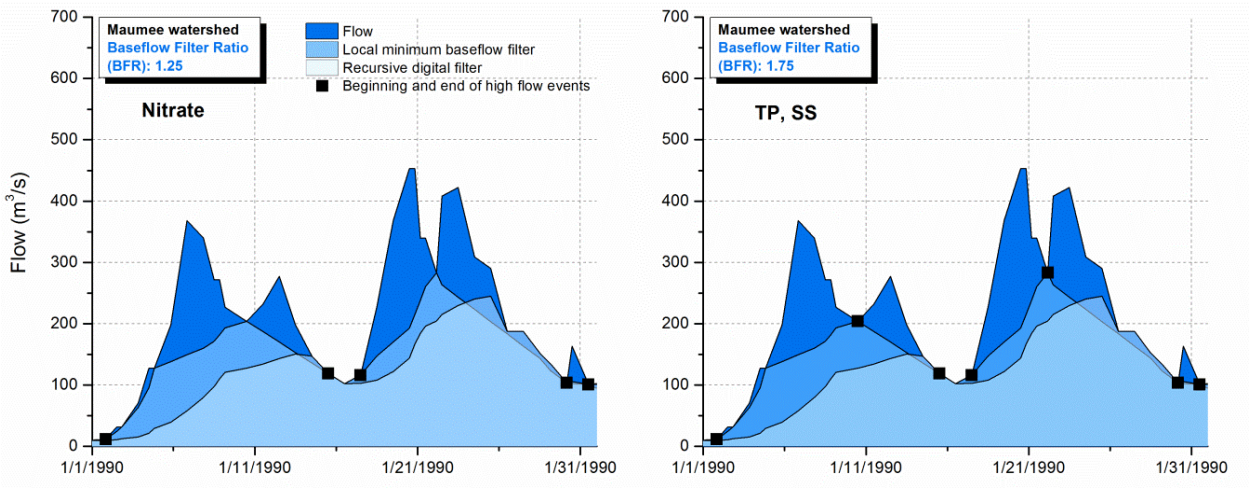

Figure 3.4: Example of different high flow event definitions based on the Baseflow Filter Ratio (BFR): a) BFR = 1.25 with 3 events and 1 period between events, b) BFR = 1.75 with 5 events and 1 period between events

3.5 High Flow Loads and Annual Loads

The WQL databases reported observed pollutant concentrations and flow data for each of the eight watersheds on a daily or sub-daily basis. Given the high number of observations for each water year, annual water year loads were computed for SS, TP, and NO_3-N using a simple numeric integration approach (El-Shaarawi et al., 1986; Preston et al., 1989; Richards et al., 2001; Guo et al., 2002, Aulenbach and Hooper, 2006; Toor et al., 2008; Verma et al., 2012). In cases in which nearly continuous data are available, a numeric integration approach is the most desirable as it is free from statistical assumptions of normality and is simple to implement (Richards et al., 2001). Annual loads were computed as:

$$\text{Load} = \int C(t)Q(t)dt \qquad (3.1)$$

where C is the pollutant concentration, Q is the flow, and *dt* is the duration represented by the sample. The duration associated with each sample collected comprised half the time between the preceding and current samples plus half the time between the current and following samples.

Similarly, pollutant loads were also computed for all high flow events separately for each water year and watershed. These high flow events for each pollutant, water year, and watershed were then ranked based on loads exported during these events. From now on, these high flow events will be referred to as *load events*. Further analysis was performed to check whether top load events were also the events with the highest peak flows. Figure 3.5 shows the average percentage of common top events based on total loads exported and on peak flows for all the Ohio watersheds over their complete monitoring durations. The size of the circles in Figure 3.5 is relatively proportional to the watershed sizes (not to scale). The analysis was performed for both BFR values used in this study (1.25 for NO_3-N and 1.75 for SS and TP). For example, the hollow circle in the left chart in Fig. 3-5 for the Muskingum watershed for the BFR=1.25 case shows that 80 percent of the top 5 events based on NO_3-N loading and peak flows were common over the 15 years of monitoring, i.e., four of the top five on average. For most of the agricultural

watersheds roughly more than 75 percent of the top 5 load events were common with the top 5 events based on peak flows.

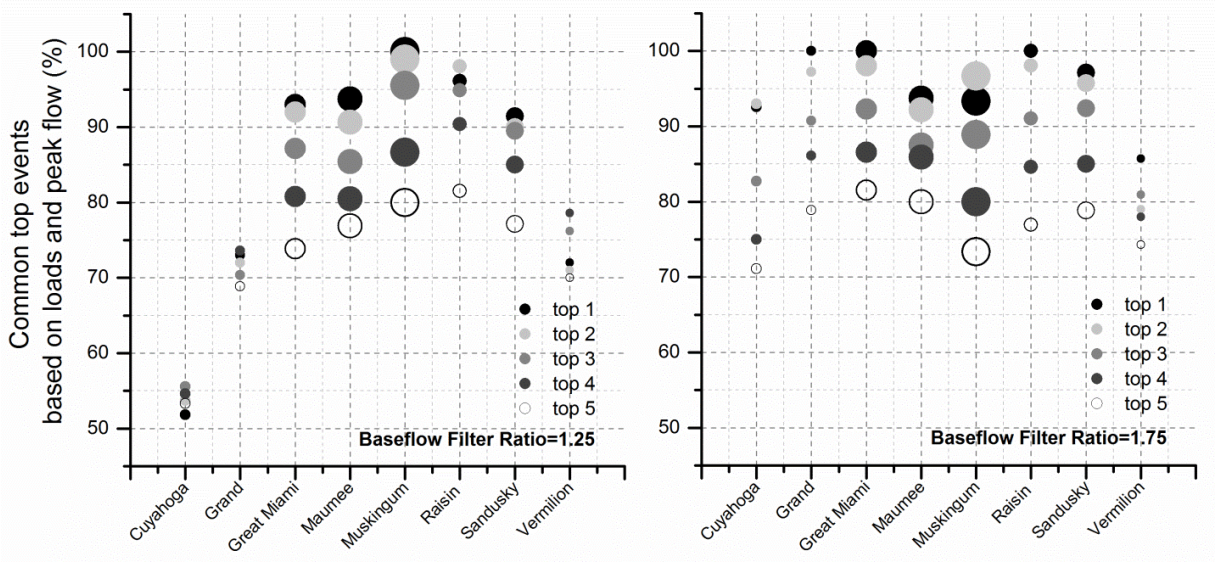

Figure 3.5: Percentage of common top events based on loads exported and peak flows for BFR=1.25 (NO_3-N) and BFR=1.75 (SS, TP). The size of points shows relative watershed sizes.

Figure 3.6 shows the cumulative contributions of up to the top 25 load events to annual loads for an agricultural watershed, i.e., Maumee and an urbanized watershed, i.e., Cuyahoga. The top 5 load events cumulatively carried a large percentage of the annual loads. The increase in the percentage declined rapidly after the top 6 to 7 events on average. The average contribution of the top 5 load events to annual loads for all pollutants was substantial for the Maumee and other agricultural watersheds. On the other hand, for the urbanized watershed Cuyahoga, the annual loads were more evenly distributed amongst the top 10 load events. The top 5 load events were chosen for predicting annual loads, balancing the need for accuracy in predicting loads with potential monitoring expense. There were some scenarios in which contributions from the 6^{th} to 10^{th} biggest events were substantial, but such cases were rare.

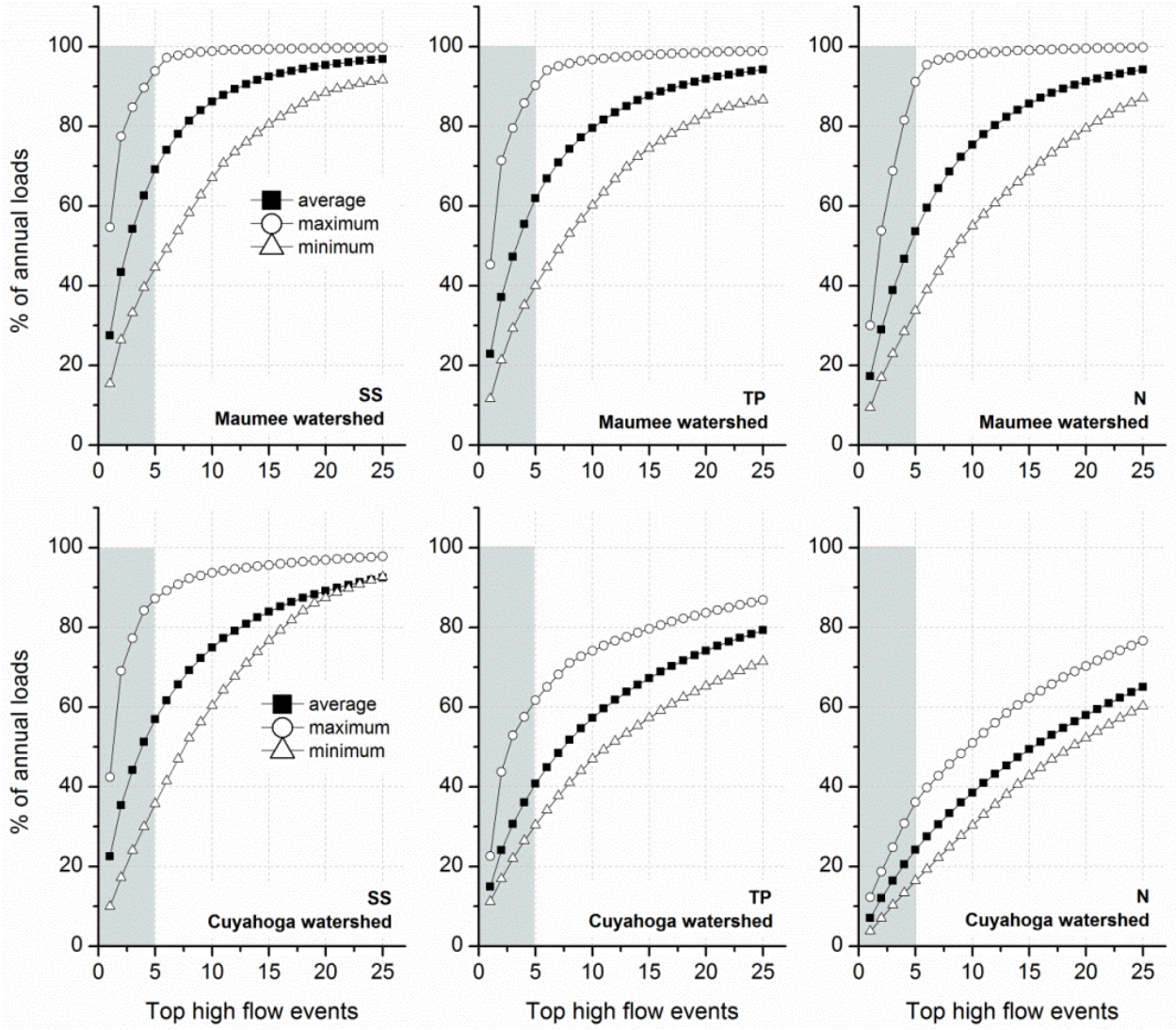

Figure 3.6: Contribution of top high flow events to annual SS, TP, and NO_3-N (N) loads for Maumee and Cuyahoga watersheds

4. Trends and Uncertainty in Estimating Annual NO_3-N Loads[1]

4.1 Introduction

Accurate calculations of seasonal, annual, and long-term nutrient loads passing a given monitoring station are critical in designing appropriate remediation management strategies. Determining nutrient loads typically combines frequently (daily) monitored discharge data and relatively less frequently (monthly or quarterly) monitored nutrient concentration data. As a result, the determination of nutrient loads is an estimation problem subjected to many potential sources of uncertainty, including data and modeling errors.

A wide variety of load estimation modeling approaches have been developed and used to estimate loads of various water quality constituents (e.g., Verhoff et al., 1980; Dolan et al., 1981; Ferguson, 1987; Cohn et al., 1989, 1992; Walker, 1996; Guo et al., 2002; Crowder et al., 2007). These different approaches generally can be divided into averaging, ratio, and regression estimators (Preston et al., 1989; Cohn, 1995; Guo et al., 2002). More recently, residual adjustment techniques that utilize the autocorrelation in concentration residuals, such as the composite method (Aulenbach and Hooper, 2006), have been introduced. Similar to the composite method, Verma et al. (2012) proposed triangular and rectangular shape functions to account for residuals in the vicinity of observed concentrations, using proportional and residual adjustment methods. To remove the effects of random variations of streamflow on estimated concentrations and flux, Hirsch et al. (2010) suggested a new approach using Weighted Regression on Time, Discharge, and Season (WRTDS). The WRTDS method was applied to study trends in nutrient concentration and flux in the Mississippi River and its tributaries, including the Illinois River for 1980 to 2008 (Sprague et al., 2011).

This research uses the above estimation methods to calculate daily NO_3-N concentrations and loads in the Lower Illinois watershed without any detailed assessment of sources of nitrate variability in this watershed such as denitrification and effects of floodplains and wetlands (e.g., Panno et al., 2008). This research evaluates selected estimators used to determine annual NO_3-N loads. The main goals of this study were (1) to calculate annual average NO_3-N concentration and annual total loads in the Lower Illinois River and its tributaries for 1975–2010 using several approaches; and (2) to determine how different approaches affect calculated loads and concentrations and their trends. These approaches included the regression estimator approach (Cohn et al., 1992), coupled with several residual adjustment methods (Aulenbach and Hooper, 2006; and Verma et al., 2012) and the WRTDS method (Hirsch et al., 2010).

4.2 Methods

Two general approaches were compared in this study to examine trends in annual nitrate loads and concentrations (Figure 4.1). The first approach includes the rating curve estimator method (Cohn, 1995) coupled with several residual adjustment techniques (Aulenbach and Hooper, 2006; Verma et al., 2012). The second approach was based on the WRTDS method (Hirsch et al., 2010).

The rating curve estimator based on the seven-parameter linear regression model was developed by Cohn et al. (1992) specifically for nutrient concentration estimation. This regression model was tested by Robertson and Roerish (1999) for small streams in Wisconsin and by Short (1999) for the estimation of nutrient loads from Illinois watersheds. Similar approaches were used in load calculations for the Upper

[1] This chapter is a modified version of an article published by Markus et al. (2014) in the American Society of Civil Engineers (ASCE) Journal of Hydrologic Engineering. It is published with permission of ASCE.

Sangamon River in Illinois (Guo et al., 2002) and in the Gulf of Mexico hypoxia assessment (Aulenbach et al., 2007). The seven-parameter log-linear model relies on correlation between the discharge and the load. The model requires estimation of the following parameters: a constant, a quadratic fit to the logarithm of discharge, a quadratic fit to time, and a sinusoidal function to remove the effects of annual seasonality (Cohn et al., 1992). These approaches are described in more detail in subsequent sections.

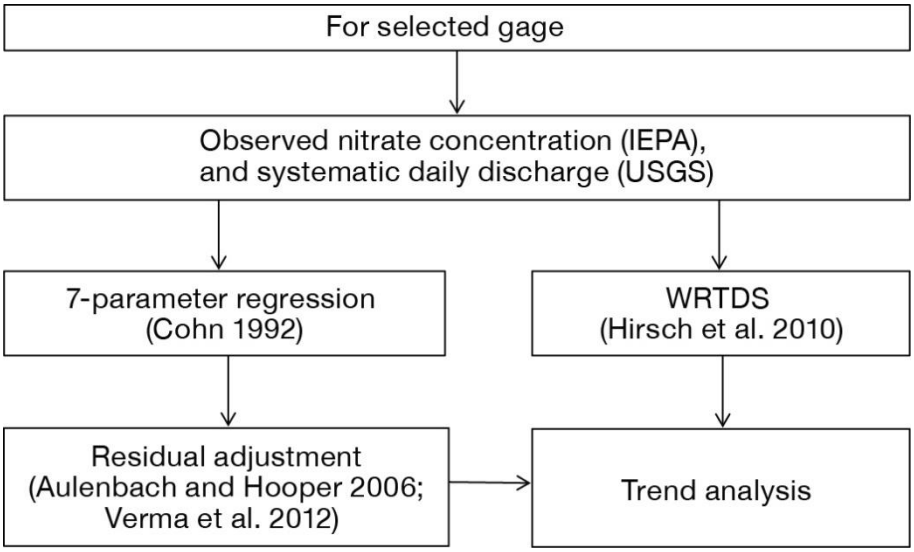

Figure 4.1: Schematic of the methods used in the study

4.2.1 Regression Estimator

The estimator developed by Cohn et al. (1992) is a multiple non-linear regression model that develops and utilizes a relationship between a sparsely collected dependent variable (i.e., concentration) and continuous independent variables such as flow rate and time of year. Logarithmic transformations are used in the model to achieve a better linear relationship between the dependent and independent variables and to reduce the influence of extreme flows on load calculations:

$$\ln(C) = \beta_0 + \beta_1 \ln\left(\frac{Q}{Q'}\right) + \beta_1 \left[\ln\left(\frac{Q}{Q'}\right)\right]^2 + \beta_3 (T - T') + \beta_4 (T - T')^2 + \beta_5 \sin(2\pi T) + \beta_5 \cos(2\pi T) + \varepsilon \quad \textbf{(4.1)}$$

where *ln ( )* denotes natural logarithmic function, C denotes the NO_3-N concentration, Q denotes the flow rate, T denotes time measured in years, ε denotes the errors (assumed to be normally distributed with a mean of 0 and a variance of σ_ε^2), β_0, $\beta_1 \ldots . \beta_6$ denote the various regression parameters estimated from the available dataset, and Q' and T' denote centering variables used in the model. Concentrations from sampled days are used along with the corresponding mean daily flow and Julian days to compute the seven parameters. The model is then used to estimate concentrations on days without sampled NO_3-N

concentrations. The complete concentration dataset is then used to estimate NO_3-N load for the monitoring period. For shorter time periods, the seven-parameter equation (4.1) can be simplified by removing the terms corresponding to β_3 and β_4. Details of this model can be found in Cohn et al. (1992).

The concentration residual time series term ε in Eq.(4.1) was found to have a significant serial correlation (autocorrelation). For example, Aulenbach et al. (2007) found an autocorrelation of 0.20 for a monthly sampling frequency at a 41-ha experimental basin in Georgia. Verma et al. (2012) calculated autocorrelation values between 0.25 and 0.30 for a four-week sampling interval at two watersheds in central Illinois ranging in size between 3,161 km^2 and 3,424 km^2. By capturing residual autocorrelation, it is possible to improve load estimates or maintain the same accuracy of load estimates using fewer observations than the traditional methods require. The methods capturing the residual autocorrelation are described below, followed by the description of WRTDS and trend tests used in this study.

4.2.2 Composite Method

Aulenbach and Hooper (2006) proposed an alternative approach to estimating constituent loads called the composite method which combines the strengths of regression and period-weighted approaches. The method was tested using an extensive dataset collected at the outlet of the Panola Mountain Research Watershed (PMRW) near Atlanta, Georgia. Residual concentrations are computed for all sampled days by subtracting concentrations estimated using the regression model from the corresponding measured values, and a piecewise continuous linear function of the residual concentrations over time is developed. The residual concentration from this composite function is then subtracted from the regression concentrations on days without water quality data.

Aulenbach and Hooper (2006) demonstrated that the composite method improved load estimation accuracies over short time intervals and allowed for better trend analysis of load estimates. The composite method is based on the principle of autocorrelation amongst the residual concentrations. It uses a piecewise linear interpolation to distribute residuals in between sampled concentrations. This concept is an advanced form of curve fitting, which has created a new class of error-correction techniques for load estimation models. Based on this concept, by optimizing the distributions used to assign residuals in between sampled concentrations, potentially more accurate error correction techniques may be developed.

4.2.3 Residual Adjustment

Verma et al. (2012) utilized the temporal correlation in modeling errors (residuals) by assigning errors on days without water quality data based on known errors on proximate sampled days. Residual concentrations were calculated on sampled days by finding the difference in regression-model-predicted concentration and observed concentrations. The mid-points of the time interval between all the pairs of consecutive sampled days were then determined. These midpoints were set as vertices in the estimation of the residuals on adjacent days without water quality observations. Verma et al. (2012) used rectangular- and triangular-shaped distributions to assign errors in the vicinity of a known error (Figure 4.2) instead of using stepwise linear interpolation as in the composite method. For the rectangular distribution, the residual at a day without a water quality observation was assigned the value of the residual on the closest sampled day. For the triangular distribution, the residual was assumed to vary linearly from the calculated residual on days with water quality observations to zero at mid-points of the time-intervals between consecutive sample days.

In addition, Verma et al. (2012) used a set of correction techniques based on proportional concentrations rather than residual concentrations. A proportional concentration was defined as the ratio between the observed concentration and the model estimated concentration on a sampled day. Once the

set of proportional concentrations was obtained for all sample observations, the rectangular and triangular distributions again were used to assign concentrations in the vicinity of known proportional concentrations.

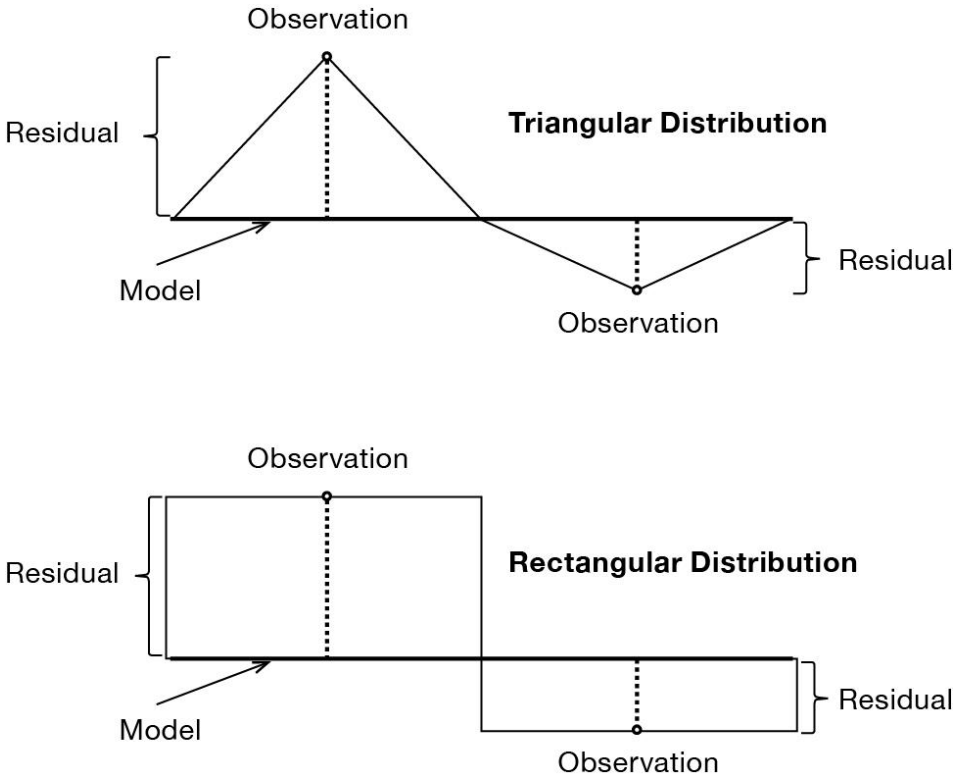

Figure 4.2: Triangular and rectangular distributions, adopted from Verma et al. (2012)

4.2.4 Weighted Regressions on Time, Discharge, and Season (WRTDS)

The WRTDS method suggested by Hirsch et al. (2010) uses the following equation to calculate daily concentration:

$$\ln(C) = \beta_0 + \beta_1 \mathrm{t} + \beta_2 \ln(Q) + \beta_3 \sin(2\pi T) + \beta_4 \cos(2\pi T) + \varepsilon \quad \textbf{(4.2)}$$

where *ln*() is natural logarithm, *c* is concentration, β_i are fitted coefficients, *Q* is daily mean streamflow, *t* is decimal time, and ε is the unexplained variation. A unique set of coefficients was estimated for every combination of *Q* and *t* in the period of record. The coefficients in Eq. (4.2) are estimated for every combination of *Q* and *t* using weighted regression. The weights on each observation in the calibration dataset are based on the distance in time, streamflow, season between the observation, and (*Q*, *t*).

A flow-normalization (FN) method is suggested to remove the effect of random streamflow variations on annual fluxes computed by WRTDS (Hirsch et al., 2010). The FN concentration estimates are computed for a given date using weighted regressions that estimate concentration on that date with the streamflow value set to each one of the historical streamflow values for that day. The FN concentration on

the given date is then calculated as a mean of estimated concentration values from each of the weighted regressions.

4.2.5 Kendall's Tau Trend Test

Statistical trend tests were required to provide an objective method to detect significant linear trends in calculated annual average concentrations, total loads, and average discharges. The Kendall's Tau test (Kendall, 1955; Helsel and Hirsch, 1995) was used, although there is uncertainty based on the selection of trend tests (Keefer et al., 2010). For each trend test, one has to select a level of confidence with which the null hypothesis (no-trend) will be rejected. In water resources literature, most authors use the confidence level of 95 percent (Neumann et al., 2003), but some also use 90 percent (Walker, 2003). A set of confidence levels (80, 90, 95, and 99 percent) was selected for this study to investigate the significance of trends and to evaluate the degree of change for different datasets

4.2.6 Şen Trend Test

Şen (2012) offered a new technique for trend analysis justified by a set of restrictive assumptions such as independent structure of the time series, normality of the distribution, and length of data, characteristics commonly used for trend identification techniques. This new technique for trend detection is based on sub-section time series plots derived from a given time series on a Cartesian coordinate system. A trend free time series sub-sections appear along the 45° straight line. Increasing trends occupy the upper triangular areas of the square area defined by the variation domain of the variable concerned. Decreasing trends occupy the lower triangular areas of the square area. Details on the technique and applications can be found in Şen (2012).

4.3 Principal Findings and Significance

4.3.1 Trends in Flow Data

Flows have a significant impact on NO_3-N transport. It is important to understand trends in flow data and how subsampling the flow data may impact trends in NO_3-N.

Figure 4.3 shows trends in observed flows for the Illinois River at Havana based on complete daily records as well as a series limited to days with observed water quality data. It is generally thought that water quality samples collected at regular intervals over a long period of time would be collected over a wide range of flows with statistics corresponding to those derived from continuous long-term flow data.

Observed NO_3-N concentrations and flows are shown in Figure 4.4 and Figure 4.5 for two Illinois River sites (Havana and Valley City) and for two tributaries of the Lower Illinois River (La Moine River at Ripley and Sangamon River at Oakford), respectively, together with a line representing linear regression. For the Illinois River at Valley City (Figure 4.4) and the two tributaries (Figure 4.5), trends in flow calculated from a limited number of days with water quality data did not appear to be different from trends in flow calculated from the complete daily datasets.

However, this notion doesn't always hold true. While there is a substantial decreasing trend of 37.5 percent in discharge values for flows during days when water quality samples were collected at Havana (Figure 4.4), there is a much smaller decrease in average annual discharges of 11.9 percent calculated from all daily values at this site (Figure 4.3). This indicates that using a limited number of days with water quality data available could result in false determinations of trends even with a long and rich dataset and possibly lead to overestimation or underestimation of annual loads. As such, extending the water

quality data beyond the actual observed NO_3-N concentrations is beneficial in analyzing concentration and load trends.

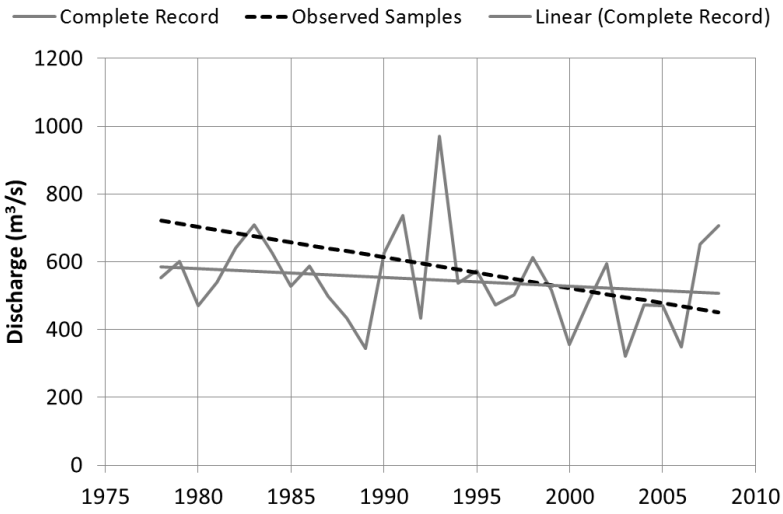

Figure 4.3: Difference in trends based on random observed samples and complete daily records at Havana

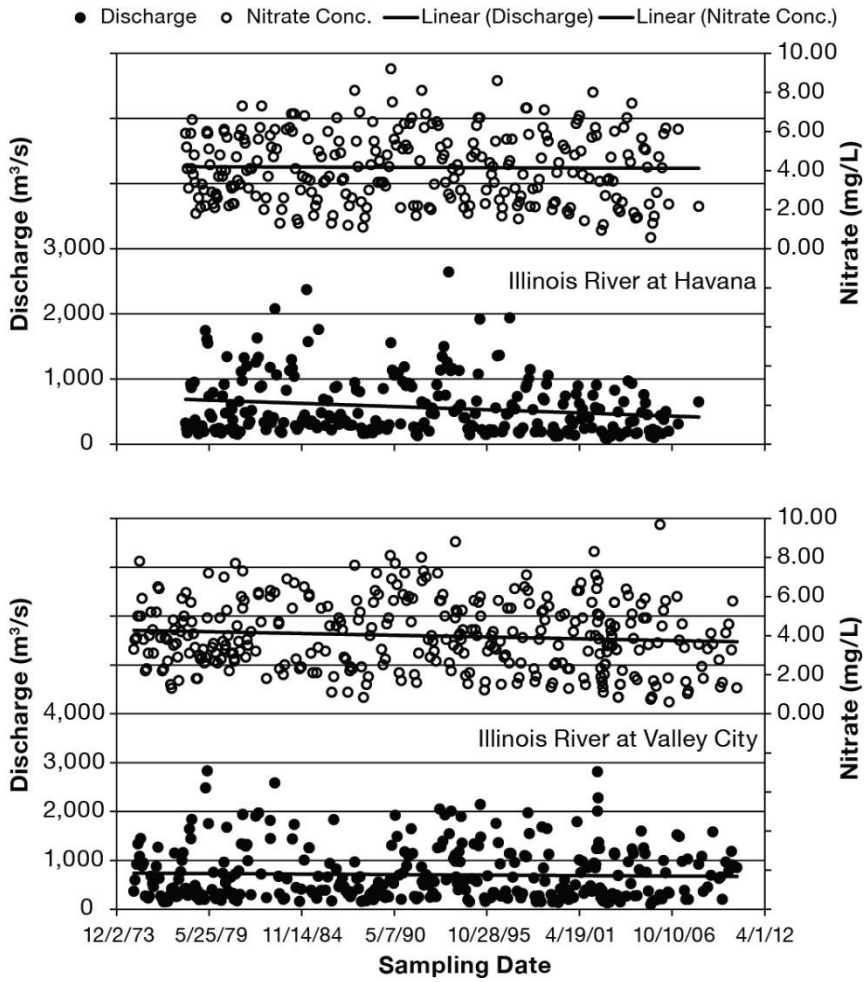

Figure 4.4: Discharge and NO_3-N concentrations at (a) Havana and (b) Valley City on the Illinois River

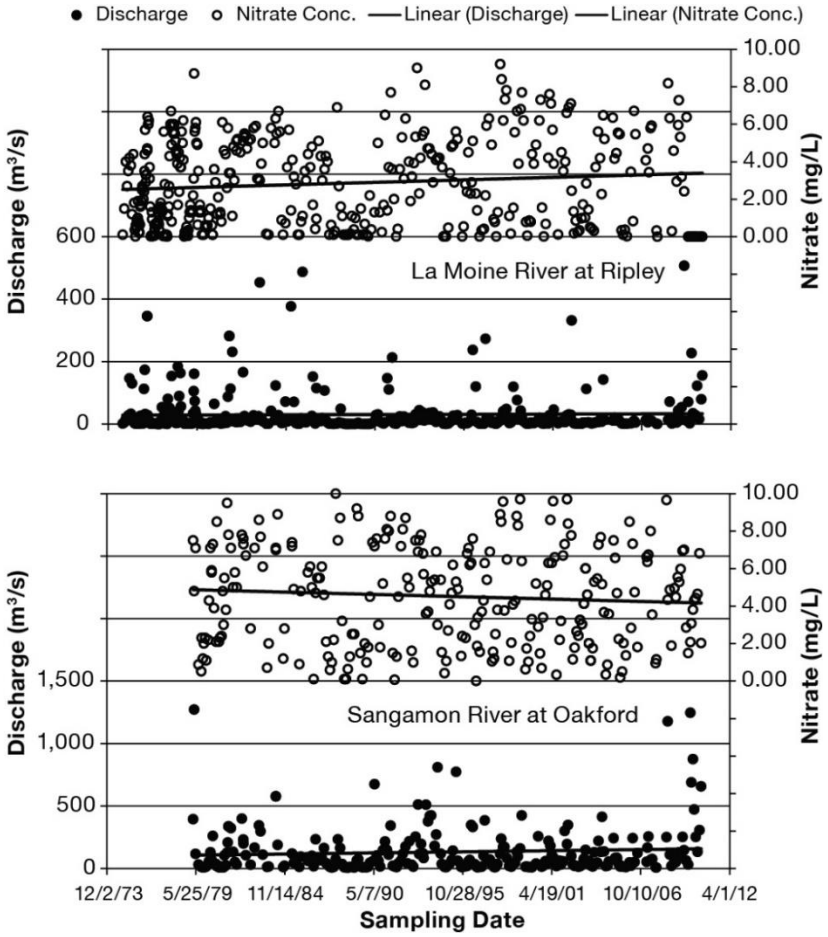

Figure 4.5: Discharge and NO_3-N concentrations in the Lower Illinois River tributaries: (a) Ripley on the La Moine River and (b) Oakford on the Sangamon River

4.3.2 Estimating NO_3-N Concentrations and Loads

The regression-based tools described in Section 4.2 were applied to all four gages in the study to provide an objective and consistent analysis. Also, as there was significant variability in flows, it was of our particular interest to test the changes in all four gages using the WRTDS method that removes the effects of flow variability.

The 7-parameter regression method (Cohn et al., 1992), one of the most frequently used models in research and applications (Short, 1999; Turner et al., 2006; Schilling and Spooner, 2006; Aulenbach et al., 2007; Hirsch et al., 2010), was used as a baseline method to calculate annual concentrations and loads. Several residual adjustment methods were used in conjunction with the 7-parameter method to assess their performance and relative differences in the methods. Figure 4.6 shows average annual NO_3-N concentrations at Havana and Valley City on the Illinois River estimated using the 7-parameter method with the following residual adjustment functions: rectangular residual adjustment (RRA), rectangular proportional adjustment (RPA), triangular residual adjustment (TRA), triangular proportional adjustment (TPA), and the composite method. There are significant differences in average annual NO_3-N concentrations depending on the method used.

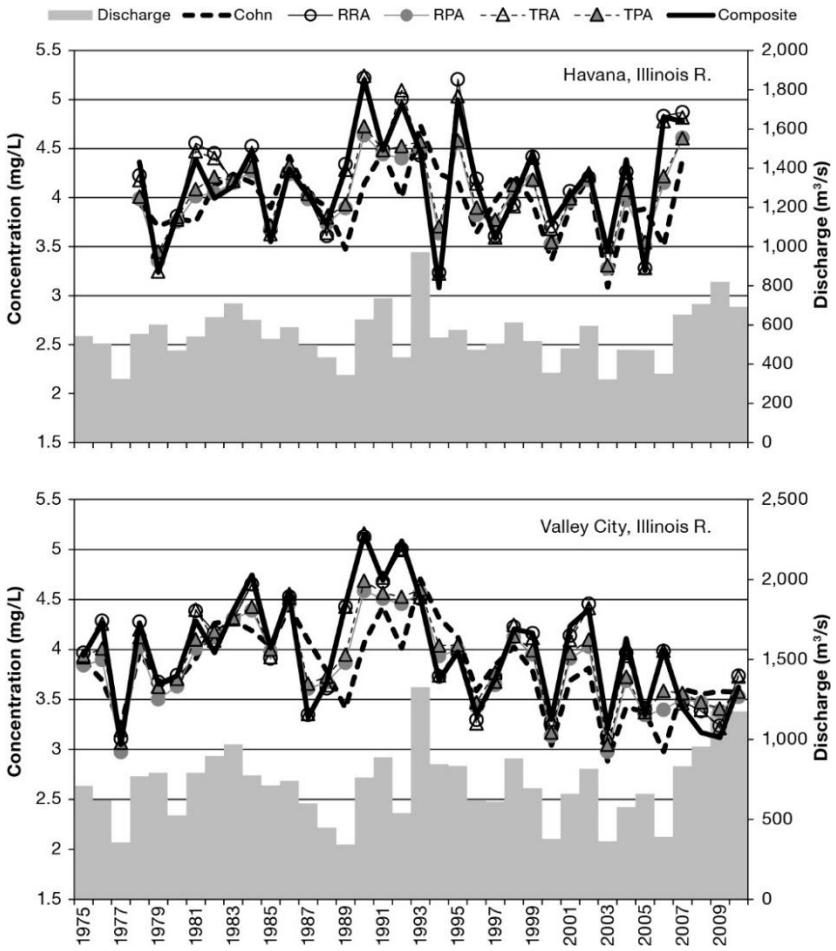

Figure 4.6: Average annual NO_3-N concentrations estimated using the 7-parameter regression approach (Cohn 1992) and four residual adjustment functions (RRA, RPA, TRA, TPA, and the composite) with annual average discharges

The basic 7-parameter method produced approximately 4 percent lower concentrations and 20 percent smaller year-to-year variability than all other methods averaged. Two distinct groups of similar results were among the residual adjustment methods. TPA and RPA produced very similar concentrations forming one group. The three remaining residual adjustment methods, RRA, TRA, and the composite method, also produced similar NO_3-N concentrations, forming another group.

Figure 4.7 shows NO_3-N concentrations estimated using the WRTDS method with and without flow normalization along with two approaches based on the 7-parameter method for comparison (RPA and the composite method). The flow-dependent (not flow-normalized) WRTDS method was denoted as WRTDS, and the flow-normalized WRTDS as FN. The RPA and the composite method represent the groups identified from Figure 4.6. These approaches were selected based on their superior performance in past research (Verma et al., 2012; Aulenbach et al., 2007).

While the annual average concentrations at Havana appear to be relatively constant, the annual average concentrations at Valley City show a generally increasing trend in the first half of the record and then a generally decreasing trend in the second half of the record based on RPA, composite, and WRTDS (Figure 4.7). The FN method shows relatively constant concentrations in the first half of the record and a

decrease in the second half. The FN method indicates that the overall reduction in annual NO_3-N concentration ranges from approximately 4.2 mg/L to about 3.2 mg/L, a 24 percent reduction.

While Sprague et al. (2011) show a relatively constant annual flow-normalized NO_3-N concentration time-series with minor fluctuations, these results show a significant decrease in the past several years. Although some of these differences might be a result of using different data, different periods of record in the computations, and different parameterization of the WRTDS in the two studies, it appears that the primary reason for these differences is the fact that the WRTDS estimates are "less reliable at the beginning and at the end of the records" (Sprague et al., 2011). This high sensitivity of the WRTDS method to the addition of the high-flow years at the end of the record is reflected in the FN method. The past 2, 3, and 4 years (2009-2010, 2008-2010, and 2007-2010) have the highest 2-year, 3-year, and 4-year flow average on the record, respectively. It is commonly accepted that the concentrations and consequently loads tend to be higher after dry years and lower after wet years (Lucey and Goolsby, 1993; McIsaac and Libra, 2003). The decreasing FN concentration in the past approximately eight years at Valley City could be a result of the method sensitivity to a sequence of wet years at the end of the record, and not necessarily an indication of achieving NO_3-N reduction goals.

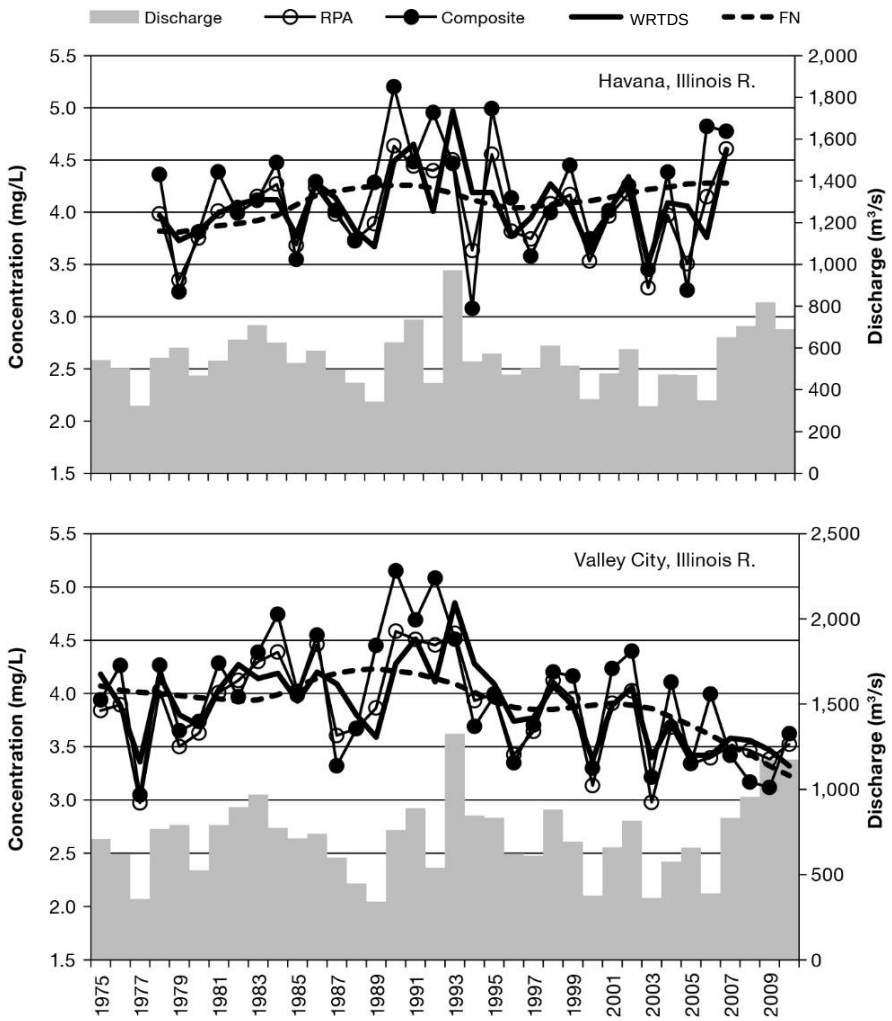

Figure 4.7: Average annual NO_3-N concentrations estimated using RPA, the composite method, the flow-dependent WRTDS ("WRTDS"), and flow-normalized WRTDS ("FN") with annual average discharges: Illinois River

This sensitivity appears to have an effect on the past approximately eight years, possibly suggesting that the effects of the end years depend on the characteristics and length of the sequence of years at the end of the record. A long sequence of non-typical conditions (such as the highest 4-year flow average) at the end of the record may result in a longer effect of the ending years conditions, and conversely, the effect of more typical ending flow conditions may not propagate back for more than one or two years (similar to Sprague et al., 2011). Adding several years past 2010 will be of a great importance for trend evaluation in the future. Additionally, the period of NO_3-N monitoring at Havana (1978-2007) did not match the monitoring periods of other stations in this study (1975-2010). This record, unlike the record at Valley City, ends with a sequence of low-flow and high-flow years, which possibly explains relatively constant concentrations in the past several years (Figure 4.7).

The corresponding annual average NO_3-N loads in the Illinois River at Havana and Valley City (Figure 4.8) show a large year-to-year variability as a result of the variability in river discharge. While the differences between RPA, composite, and WRTDS appear insignificant for long-term trends in loads, the loads from the flow normalized (FN) method are notably different and appear reasonably consistent with concentrations from the FN method for the same locations.

The curve showing annual loads from the FN method exhibits a minor increase at Havana. However, the FN curve shows a significant decrease at Valley City in the past approximately eight years of the record, which is consistent with the FN curve for concentration. As discussed above, these results need to be interpreted with caution because of the sensitivity of the results to the sequence of wet years at the end of the record.

Similar analysis was carried out for the two tributaries of the Illinois River. Average annual NO_3-N concentration (Figure 4.9) and annual NO_3-N loads (Figure 4.10) show a decrease at Oakford on the Sangamon River, and a minor increase at Ripley on the La Moine River. The annual flow pattern at the Sangamon River is similar to the flow pattern at Valley City on the Illinois River. The decrease in annual NO_3-N concentrations at the Sangamon River can similarly be attributed to the high-flow years at the end of the record. Concentrations and loads at the La Moine River did not show significant changes, possibly due to the differences in flows in the past four years. The ending four years cover a full range of flow conditions in the La Moine River, ranging from a dry year (2007) to the highest year on the record (2010).

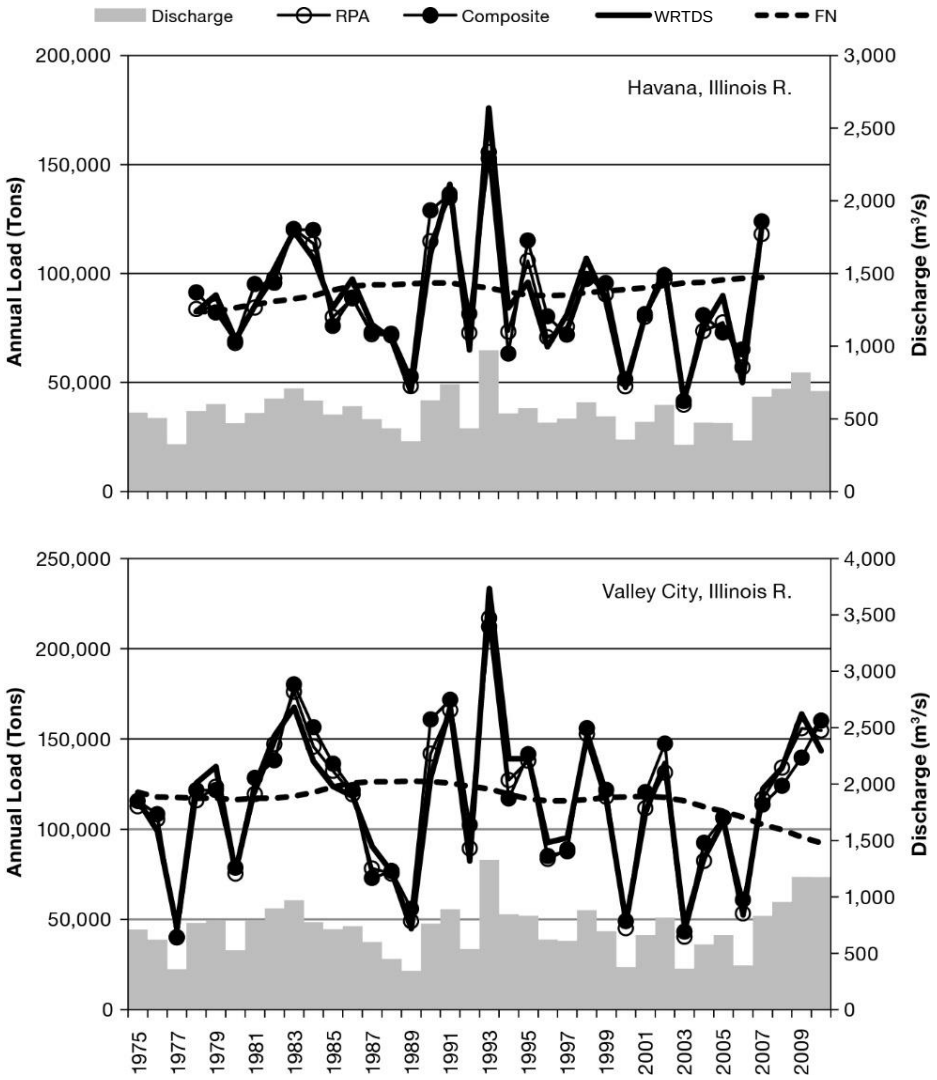

Figure 4.8: Average annual NO_3-N loads estimated using RPA, the composite method, the flow-dependent WRTDS ("WRTDS"), and flow-normalized WRTDS ("FN") with annual average discharges: Illinois River

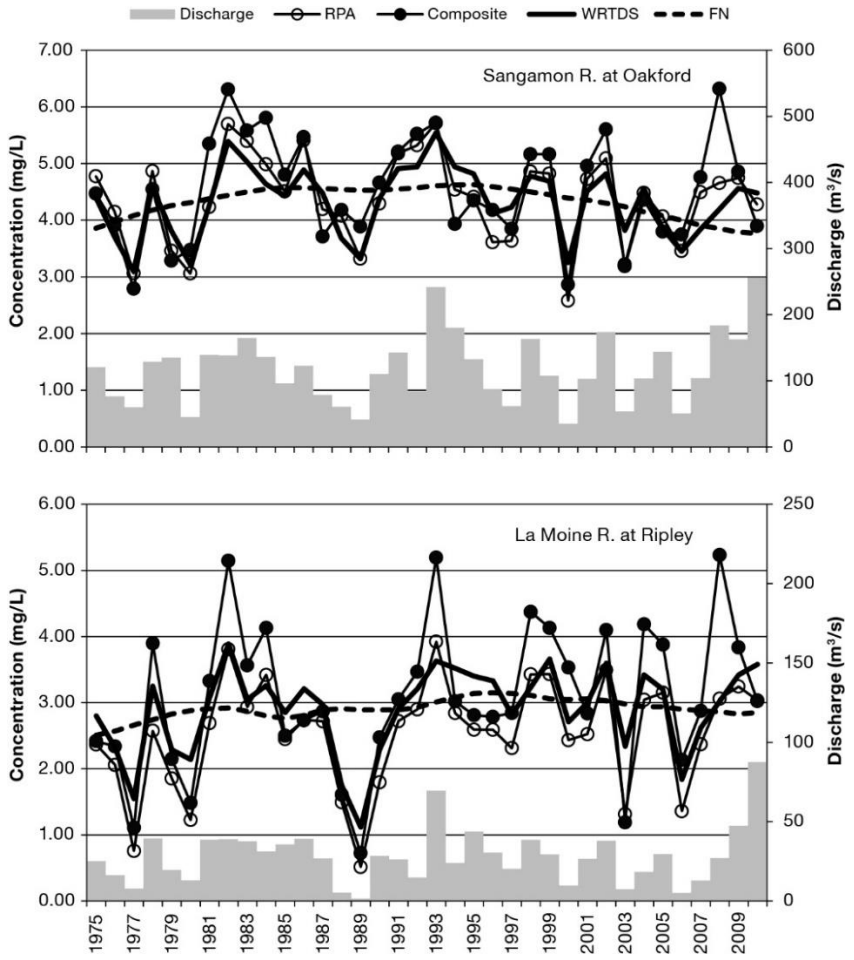

Figure 4.9: Average annual NO_3-N concentrations estimated using RPA, the composite method, the flow-dependent WRTDS ("WRTDS"), and flow-normalized WRTDS ("FN") with annual average discharges: Illinois River tributaries

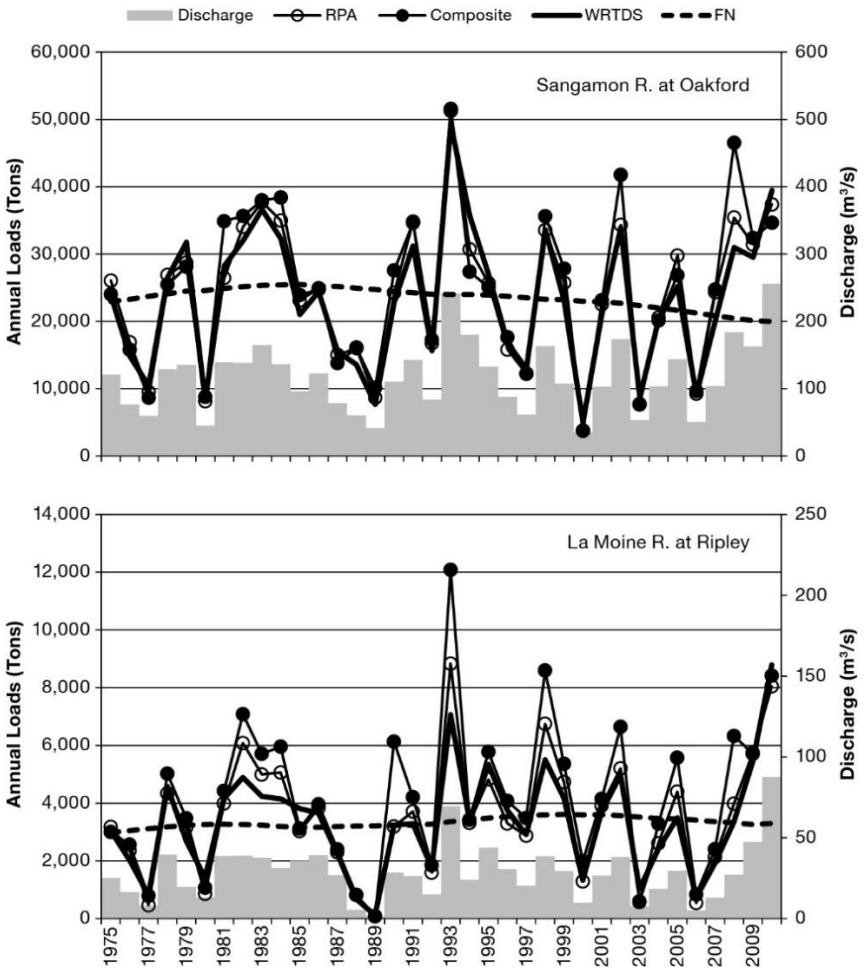

Figure 4.10: Average annual NO_3-N loads estimated using RPA, the composite method, the flow-dependent WRTDS ("WRTDS"), and flow-normalized WRTDS ("FN") with annual average discharges: Illinois River tributaries

4.3.3 Trend Tests

The Kendall's Tau trend test was applied to test the degree of change for different datasets, for 80, 90, 95, and 99 percent levels of confidence. No trend was detected for concentration, except at Valley City for some of the methods. Table 4.1 shows the results of the Kendall Tau trend method used to determine trends in annual average NO_3-N concentrations at Valley City. Most of the methods resulted in trends with the levels of confidence under 95 percent, except TPA (95 percent) and WRTDS (99 percent). Similarly, the Kendall Tau trend test was applied to test trends in annual flows and loads, but none of these trends were significant for any of the specified levels of confidence at any site. The absence of trends in flows and loads could partly be explained by the large variability in annual discharge and load data and smaller variability in concentration data.

Table 4.1: Kendall's Tau test with various levels of significance to evaluate the degree of change for annual average nitrate-N concentration at Valley City using different methods (1975-2010)

	Decreasing				*Increasing*			
Method	*99*	*95*	*90*	*80*	*80*	*90*	*95*	*99*
Cohn								
RRA								
RPA								
TRA								
TPA								
Composite								

Notes: Shaded areas signify trends along with their statistical significance

Figure 4.11 shows the Şen trend test (Şen, 2012) applied to Valley City on the Illinois River. The test splits the data into two equal parts and compares trends for different flow or concentration ranges. In this case the entire dataset is divided into two time periods, 1975–1992 and 1993–2010, which are referred to as the early and late periods, respectively. The left chart in the figure indicates that daily discharge values under 2,000 cubic meters per second (m^3/s) have increased from the early to the late period, and that the discharges above 2,000 m^3/s have decreased. The average increase in discharge is 12.6 percent. Note that the majority of highly skewed daily discharge values (96.1 percent) belong to the range under 2000 m^3/s. Similarly, the right chart indicates that the concentration decreased for the entire observed range, in particular for the values above 3.5 mg/L, which resulted in an average decrease of 6.7 percent.

It should be noted, however, that both Kendall Tau and Şen tests have limitations. The Kendall Tau test is based on the assumption that the trend is linear. This assumption does not seem to be met for all datasets in this study. For example, Figure 4.7 and Figure 4.8 suggest that the average annual NO_3-N concentrations at Valley City are best characterized by increases up through the early 1990s and decreases since that time, particularly in the past 10 years. The Şen test divides the entire dataset in two equal parts, making it well suited for data with an abrupt change occurring approximately in the middle of the record. However, the data in this study have more complex patterns. Some of the driest (e.g., 1989) and wettest (e.g., 1993) historical years on the record are in the same part of this 36-year record. These years could represent statistical outliers, making it more difficult to ascertain if "true" linear or nonlinear trends exist.

In addition, the trends in concentrations might have been affected by the periods of record, such as the sequences of wet years at the end of the monitoring records. While the record at Havana, which did not include the past three years (2008-2010), had no trend in concentration, the Valley City gage, which included the past three years, showed a decreasing trend in concentration with various levels of significance. The addition of future monitoring data as it become available will give us more insight into the processes and trends in these streams in the future.

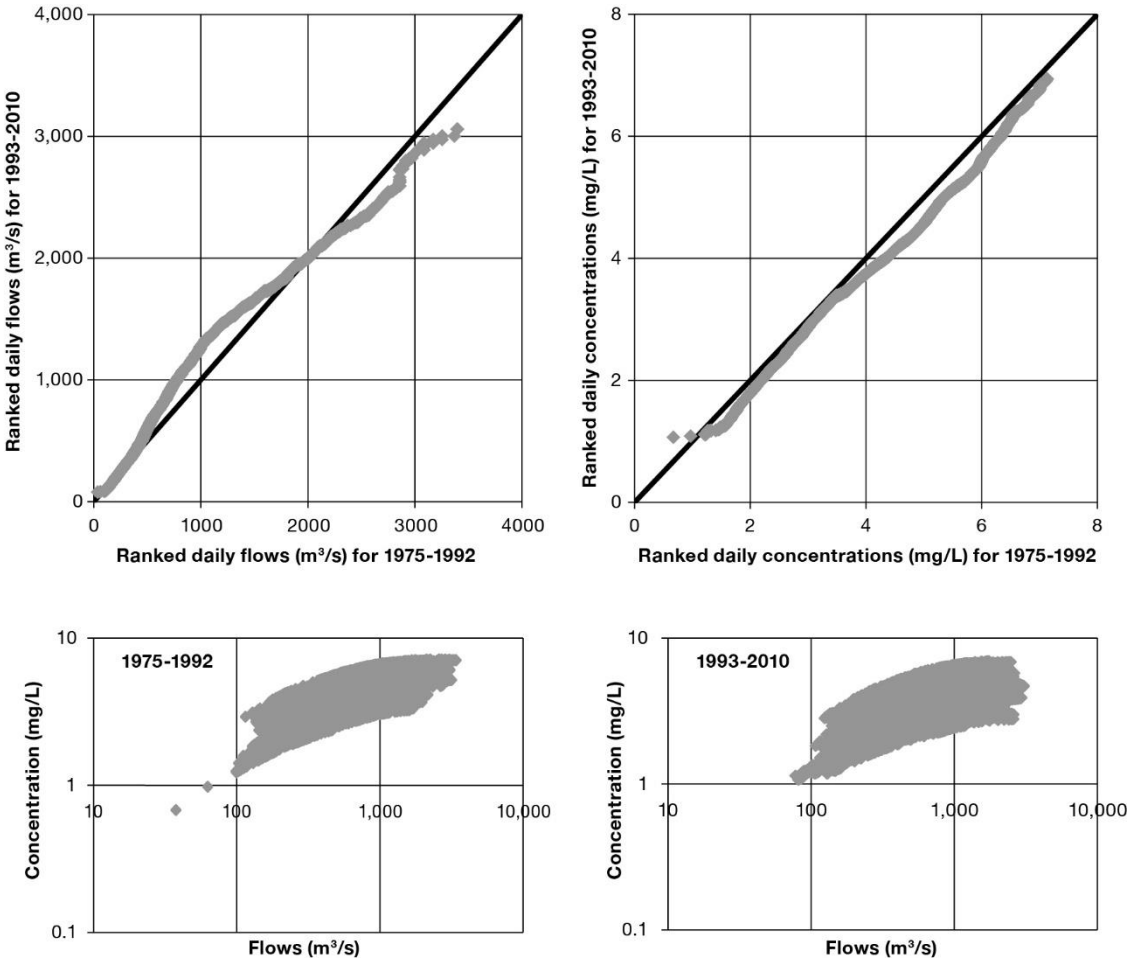

Figure 4.11: Trend tests for daily discharge (top left) and concentration (top right) at Valley City based on the Sen test. Bottom charts show relationships between flow and concentration for the two time periods.

4.4 Summary

The goal of the research presented in this section is twofold. First, several methods for annual load estimation were compared using a 36-year NO_3-N monitoring dataset from four sites in the Lower Illinois River basin. Second, long-term changes in average annual NO_3-N concentrations and total annual loads were evaluated using the selected methods at four sites in the watershed.

This research indicated that trends calculated on the samples alone could result in false determinations even with a long and rich dataset. Thus, extending the data beyond the actual observed samples using estimation techniques can be very beneficial to study long-term trends in NO_3-N concentrations and loads.

The results of this study also indicated that load estimation methods and trend analyses are highly sensitive to different periods of record. The reliability of annual concentration and loads and their trends based on all methods, particularly the FN method, is affected by the sequence of high-flow years at the end of the record. The presence of low and high outliers and driest and wettest historic years on the record added to the uncertainty of the analysis.

The results were not as sensitive to the method selection. Annual NO_3-N loads and their trends based on RPA, composite, and WRTDS methods were reasonably similar, particularly for larger watersheds, such as the Illinois River at Valley City.

The findings of the study highlight the role of data variability and signify the value of each observation year. This underscores the importance of identifying and maintaining sites with long-term nutrient and flow data records for future examination of changes in loads, which ultimately affect hypoxia in the Gulf of Mexico. Further monitoring and refinement of load calculation methods and quantification of their uncertainties are an important part in evaluating progress toward the USEPA Science Advisory Boards' (2008) recommended 45 percent reduction in the loads of nutrients to the Gulf of Mexico.

5. Data Mining Techniques for Nutrient Load Estimation

5.1 Introduction

Continuous monitoring of streams would ideally provide all information about pollutant concentrations and loads. However, such monitoring is very resource-intensive and requires significant time, personnel, and financial investments. Most monitoring programs are designed to collect water quality samples at regular intervals. Additional samples may be collected during storm events to better quantify pollutant loads.

Traditional load estimation techniques use continuously available stream flow data with available observed concentrations to estimate concentrations during times when water quality was not sampled using regression and ratio estimators. The accuracy of these estimators depends on the amount of observed streamflow and concentration data available to develop the relationships. Additional issues of bias arise from transformations between log and linear spaces.

This part of the research investigates the potential of applying data mining techniques such as nearest-neighbor methods and decision trees as an alternate way to estimate nutrient concentrations in a sparse time-series using continuous streamflow and some concentration observations. There have been a few studies that used data mining techniques such as neural networks to estimate missing concentrations (Yu et al., 2004; Antcil et al., 2009). Studies evaluating the potential and limitations of other techniques such as nearest-neighbors and decision trees for concentration estimation are scarce. These two techniques were applied to datasets from two watersheds, the Maumee River watershed and the Cuyahoga River watershed, both draining into Lake Erie. Long-term time-series datasets of streamflow and NO_3-N concentrations were used in the study.

5.2 Methods

The software package Weka (Hall et al., 2009), was used to implement two data mining methods for prediction of NO_3-N concentrations in a multiyear time-series. The methods are described below.

5.2.1 Instance Based (IBk) Classifier

IBk is an instance based classifier that is based on the k-nearest neighbor algorithm, in which k is the number of nearest neighbors in the training dataset used to define the class of the test instance. This algorithm is a simple machine learning technique that locally assigns a class to the test instance based on a majority vote of its neighbors in the training dataset with the instance being assigned a class which is most common amongst it k-nearest neighbors. A case with k=1 simply assigns the same class to the test instance as its nearest neighbor's class from the training dataset. The IBk classifier was used to predict NO_3-N concentrations for the Cuyahoga watershed dataset.

5.2.2 Reduced Error Pruning Tree (REPTree)

REPTree is an algorithm which works on the basic principle of "divide and conquer" to produce decision trees. Nodes in the decision tree represent points in which particular attributes are tested by comparison with a constant value. Further division leads to leaf nodes, and they represent the same classification for all the test instances that reach the leaf node. In the case of numeric test attributes the nodes create a two-way split with values greater or less than a constant. It is an algorithm optimized for

speed and it sorts numeric attribute values only once, saving considerable time as compared to other decision tree methods. The REPTree classifier was used to predict NO_3-N concentrations for the Maumee watershed dataset.

5.2.3 Performance Evaluation Techniques

Two techniques, cross validation and percentage split, were used to evaluate the performance of the classifiers. NO_3-N was the prediction variable (class). Daily measured streamflow, month, and a selected number of observed NO_3-N concentrations were used as training attributes. The month of measured streamflow accounts for the seasonality in the observed NO_3-N concentrations.

The first evaluation technique used was cross validation. The complete dataset was divided into a certain number of equal sets (folds). Each fold was then used as a testing dataset while all the remaining folds were used as training datasets. This process is repeated till all the folds have been used as a testing dataset at least once. This technique ensures that all instances are tested by the classifier.

The second evaluation technique, the percentage split, is a simple method in which the complete dataset is split into training and testing portions. For example, a percentage split of 66 percent would mean that 66 percent of instances in the complete dataset are used to train the classifier, while the remaining 34 percent are used to test the accuracy of the classifier. The test instances were randomly selected from the complete dataset.

5.3 Principal Findings and Significance

The IBk classifier was used to predict the missing NO_3-N concentrations for the Cuyahoga watershed dataset. Table 5.1 and Table 5.2 show results of the performance evaluation for the IBk classifier using cross validation and percentage split, respectively. The IBk classifier using cross validation predicted the missing NO_3-N concentrations for Cuyahoga fairly accurately. For 1 nearest neighbor (k=1), the IBk classifier predicted the missing values with a correlation coefficient of 0.86 for both 5 and 10 folds. For a 5-fold cross validation, the correlation coefficient increased on increasing the nearest neighbors to 0.89 and 0.90 for k=2 and k=4, respectively. The Root Mean Square Error (RMSE) was also low, ranging from 0.52 to 0.63 for different scenarios (Table 5.1). Figure 5.1 compares predicted and observed NO_3-N concentrations for different nearest neighbors for a 5-fold cross validation.

The IBk classifier using the percentage split technique also performed well. The correlation coefficient was 0.85 for a training percentage split of 66 percent and k=1. The correlation coefficient of the predicted and observed NO_3-N concentrations slightly decreased to 0.83 and 0.80 when the training dataset percentage decreased to 20 percent and 10 percent, respectively. The correlation coefficients of the predictions did not change much on increasing the nearest neighbors to 2 and 4 with a training percentage split of 10 percent. The RMSE varied from 0.64 to 0.74 for different scenarios (Table 5.2). Figure 5.2 compares predicted and observed NO_3-N concentrations for different sizes of the training datasets (percentage split) using the IBk classifier.

Table 5.1: Performance evaluation of the IBk classifier to predict NO_3-N concentrations using cross validation for Cuyahoga

Metric	*Cross Validation*			
Folds	10	5	5	5
K-Nearest Neighbors	1	1	2	4
Correlation coefficient	0.86	0.86	0.89	0.90
Mean absolute error	0.41	0.41	0.37	0.35
Root mean squared error	0.63	0.63	0.56	0.52
Relative absolute error (%)	42.36	42.68	38.27	36.59
Root relative squared error (%)	53.61	53.62	47.05	44.25
Total Number of Instances	12103	12103	12103	12103

Note: The values indicating the best fit are shaded.

Table 5.2: Performance evaluation of the IBk classifier to predict NO_3-N concentrations using percentage split for Cuyahoga

Metric	*Percentage Split*				
Training Split (%)	66	20	10	10	10
K-Nearest Neighbors	1	1	1	2	4
Correlation coefficient	0.85	0.83	0.80	0.81	0.80
Mean absolute error	0.41	0.46	0.52	0.50	0.51
Root mean squared error	0.64	0.68	0.74	0.70	0.71
Relative absolute error (%)	42.92	48.22	54.32	51.96	53.73
Root relative squared error (%)	54.47	57.26	62.35	58.95	59.72
Total Number of Instances	4115	9683	10893	10893	10893

Note: The values indicating the best fit are shaded.

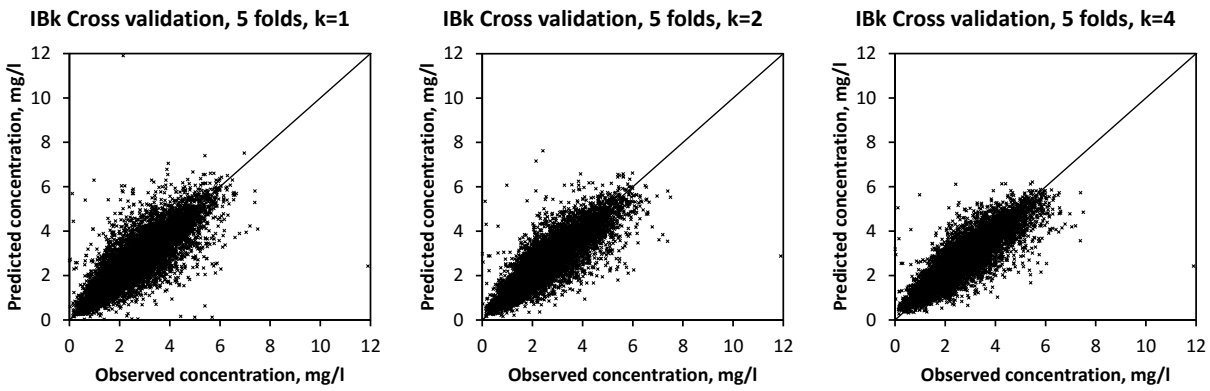

Figure 5.1: Observed and predicted NO_3-N concentrations for Cuyahoga using the IBk classifier with a 5-fold cross validation: (a) k =1, (b) k=2, and (c) k=4

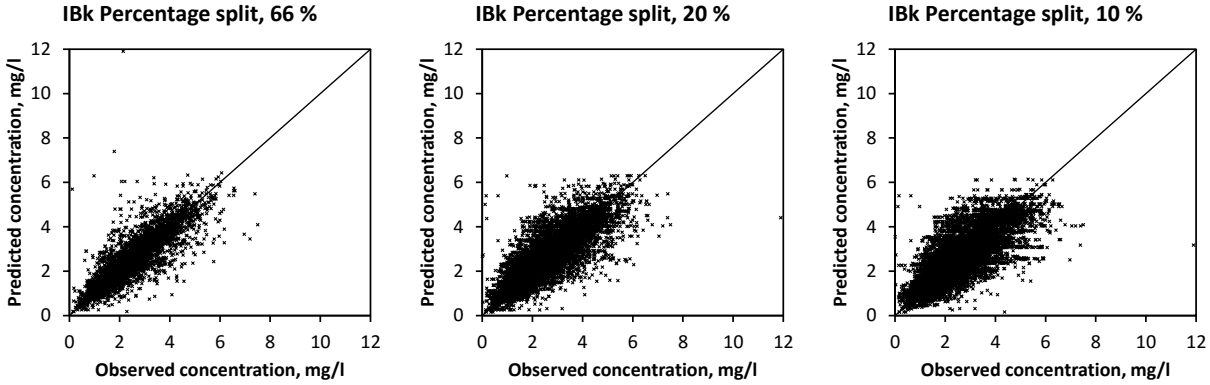

Figure 5.2: Observed and predicted NO_3-N concentrations for Cuyahoga using the IBk classifier with percentage split of: (a) 66 percent, (b) 20 percent, and (c) 10 percent

The REPTree classifier was used to predict NO_3-N concentrations for the Maumee watershed dataset. Table 5.3 and Table 5.4 show results of the performance evaluation for the REPTree classifier using cross validation and percentage split, respectively. The REPTree classifier performed very well. The correlation coefficients were 0.93 and 0.92 with an RMSE of 1.20 and 1.28 for the cross validation technique using 10 and 5 folds, respectively (Table 5.3).

The REPTree classifier using the percentage split technique also performed well. The correlation coefficient was 0.91 with an RMSE of 1.35 for a 66 percent training percentage split. The correlation coefficient decreased slightly to 0.80 and 0.71 with an RMSE of 1.94 and 2.29 when the training percentage split decreased to 20 percent and 10 percent, respectively (Table 5.4). Figure 5.3 compares the observed and predicted NO_3-N concentrations for different sizes of the training datasets (percentage split) using the REPTree classifier.

Table 5.3: Performance evaluation of the REPTree classifier to predict NO_3-N concentrations using cross validation for Maumee

Metric	*Cross Validation*	
Folds	10	5
Correlation coefficient	0.93	0.92
Mean absolute error	0.70	0.76
Root mean squared error	1.20	1.28
Relative absolute error (%)	27.19	29.33
Root relative squared error (%)	37.28	39.73
Total Number of Instances	14555	14555

Note: The values indicating the best fit are shaded.

Table 5.4: Performance evaluation of the REPTree classifier to predict NO_3-N concentrations using percentage split for Maumee

Metric	*Percentage Split*		
Training Split (%)	66	20	10
Correlation coefficient	0.91	0.80	0.71
Mean absolute error	0.81	1.32	1.62
Root mean squared error	1.35	1.94	2.29
Relative absolute error (%)	31.24	51.30	62.64
Root relative squared error (%)	41.50	60.53	71.25
Total Number of Instances	4949	11644	13099

Note: The values indicating the best fit are shaded.

The REPTree classifier is a decision tree data mining technique. It gives the same classification or prediction to all instances beyond a certain leaf node in the decision tree. This might lead to the same predictions for a certain range of observed instances. If the training dataset is small, the ranges of instances having similar predictions might be large. This is fairly evident in Figure 5.3 where horizontal bands of predicted NO_3-N concentrations can be observed for a large range of observed instances.

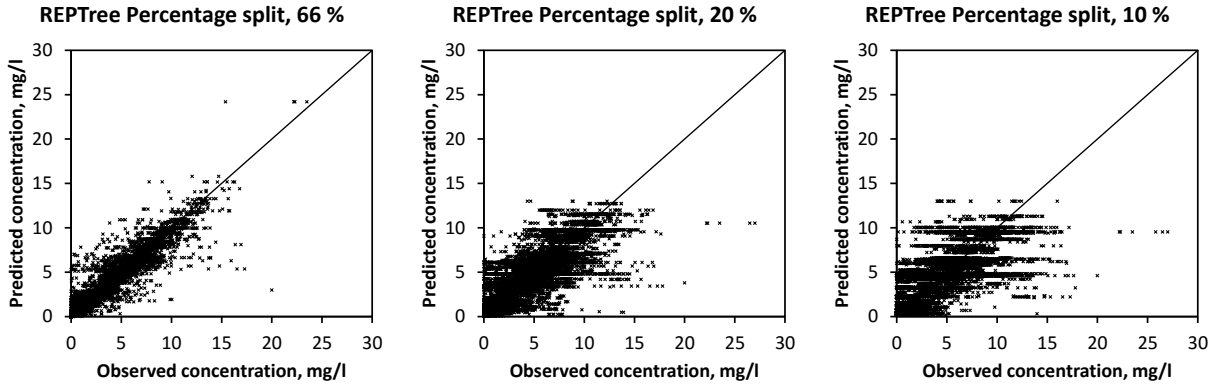

Figure 5.3: Observed and predicted NO_3-N concentrations using the REPTree classifier for Maumee with a percentage split of: (a) 66 percent, (b) 20 percent, and (c) 10 percent

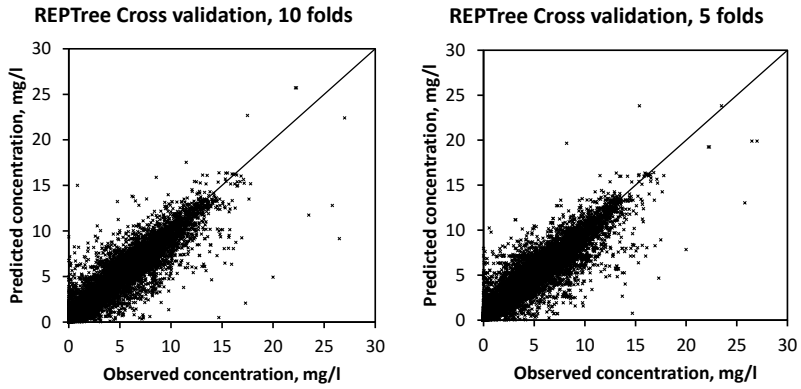

Figure 5.4: Observed and predicted NO_3-N concentrations for Maumee using the REPTree classifier with: (a) 10 fold cross validation, and (b) 5-fold cross validation

5.4 Summary

The applicability of nearest neighbor (IBk) and decision tree (REPTree) data mining methods to predict NO_3-N concentrations from long multi-year time-series was evaluated for two watersheds in the Lake Erie basin. Two different evaluation techniques, cross validation and percentage split, were used for both data mining methods to create the training and testing datasets. Both data mining techniques were successful in predicting NO_3-N concentrations with high correlation coefficients ranging from 0.80 to 0.90 and from 0.71 to 0.93 for the IBk and REPTree classifiers, respectively.

These data mining techniques present a number of advantages over the traditional statistical and physical models used in hydrology to predict nutrient concentrations. The data mining techniques are not constrained by assumptions in data such as linearity and homoscedasticity. The number of parameters

used is also unlimited. The techniques also eliminate any possible transformation biases arising from converting datasets from log to linear spaces and vice-versa that are often used with statistical methods. The data mining techniques can be implemented fairly quickly using very basic computational power.

Nonetheless, while data mining methods do not have strict data requirements, as characteristic for traditional approaches, such as normality, independence, or homoscedasticity, their limitations should also be recognized. These limitations include the large number of parameters which can lead to large uncertainty. Also, data mining methods can identify connections between variables, but they do not necessarily identify causal relationships and their significance. Data mining results require more involved interpretations than the traditional methods.

This research demonstrated that both data mining methods can be applied to watersheds with limited concentration data where daily streamflow and some observed concentrations are available to predict the missing concentrations.

The results using these and other data mining methods are expected to vary with different constituents, watersheds, and hydro-climatic zones. Future studies should be directed to evaluate the performance of these data mining methods on a large variety of watersheds from different hydro-climatic zones. Also, studies and other data mining methods should quantify the outcome of data availability on the performance of these methods.

6. Role of Large Events in Annual Pollutant Loadings

6.1 Introduction

Improving estimation accuracies and minimizing uncertainties are a concern in quantifying annual loading estimates. However, resource constraints such as inadequate funding and limited manpower can impede the collection of a large number of samples (Yaksich and Verhoff, 1983). Over the past several decades, water quality sampling strategies have also changed, moving from traditional fixed-frequency water sampling (bi-weekly, monthly, quarterly) to mixed strategies designed specifically to improve the accuracy of load estimates such as fixed-frequency water sampling supplemented with some storm-based sampling to capture high flows (Robertson, 2003; Hirsch et al., 2010). These approaches are time- and resource-intensive. All flow regimes should be characterized to capture most of the high load periods throughout the year in order to avoid underestimation of annual pollutant loading values. There are a few less data- and resource-intensive empirical or statistically-based approaches such as the Universal Soil Loss Equation, USLE (Natural Resources Conservation Service, 1983), SPAtially Referenced Regression On Watershed attributes, SPARROW (Smith et al., 1997), GIS Pollutant Load, PLOAD (USEPA, 2001), or Spreadsheet Tool for Estimating Pollutant Loads, STEPL (USEPA, 2006), but these approaches only estimate long-term average loading without a high temporal resolution.

Alternatively, to minimize monitoring costs, some research studies have evaluated different ways to estimate annual pollutant loadings, such as developing regression relationships between a few critical storm (high flow event) loads and annual loads. Richards and Holloway (1987), Preston et al. (1989), Lewis (1996), Robertson and Roerish (1999), Cooper and Watts (2002), Markus and Demissie (2006) and Salles et al. (2008) have reported that a few high flow periods carry significant amounts of sediment and nutrient loadings over a year. Yaksich and Verhoff (1983) analyzed high flow events based on sampling strategies for watersheds in the Lake Erie basin and recommended intensively sampling two to three of the largest storm events in a year to get annual suspended solids, soluble ortho-phosphorus, and total phosphorus loading estimates with small errors. Since water quality monitoring strategies have been shifting over the past few decades and water quality managers are still searching for the most cost-effective monitoring plans, a statistical approach based on large load events has the potential to estimate annual pollutant loadings with a reduction in fixed-frequency sampling, thereby reducing annual monitoring costs. It should be noted that this analysis is focused on annual load estimates which help assess downstream impacts. Studying more local impacts, which are usually most severe under low-flow conditions is beyond the scope of this study.

The main objectives of this part of the research included (i) assessing the role of a few large load events on annual pollutant loads using regression relationships, (ii) testing the statistical similarity between these regression relationships developed for different watersheds in close proximity (the Ohio watersheds), and (iii) testing the applicability of developed regression relationships for watersheds in the same geographical region with a similar land-use (the Illinois watersheds).

6.2 Material and Methods

6.2.1 Regression Relationships

Markus and Demissie (2006) reported that annual sediment loads and loads during the top high flow events (ranked by peak flows) have a high correlation, and thus annual loads can be predicted from the top high flow event loads using regression relationships. In this study, we expanded the concept and developed regression relationships for annual SS, TP, and NO_3-N loads and loads exported during the top

1, 2, 3, 4, and 5 load events. The following equation describes a general relationship between annual loads and top load events:

$$\log(L_a) = a + b\log(L_{le}) \quad \textbf{(6.1)}$$

where L_a and L_{le} are pollutant loads exported annually during a water year and cumulatively during top load events in a year, respectively (le=1, 2, 3, 4, 5), and a and b are regression parameters. The annual and top load event loads were log-transformed to normalize residual variances and reduce the skewness towards extreme values (Troutman, 1985; Driver and Troutman, 1989; and Kocic et al., 2008). Distinct regression relationships were developed for each watershed and pollutant. Additionally, aggregate regression relationships were developed by combining data for a given pollutant from all eight Ohio watersheds and similar watersheds for annual loads, and the top 1,2,3,4, and 5 load events in a water year.

6.2.2 Analysis of Covariance (ANCOVA)

Analysis of covariance (ANCOVA) was used (Snedecor and Cochran, 1980; Markus and Demissie, 2006) to test the similarity between the regression lines developed for a pollutant for different watersheds and also the spatially aggregated data. The purpose was to examine whether parameters of linear regressions for a particular watershed are the same as parameters for other watersheds or the same as parameters for regression lines developed for the spatially aggregated data from all watersheds. These regressions can differ in slope, intercept, and residual variances. ANCOVA was used to compare the following model:

$$Y_{i,j} = \alpha_i + \beta_i X_{i,j} + \varepsilon_{i,j} \quad \textbf{(6.2)}$$

where X=independent variable, high flow loads in this case; Y=dependent variable, annual load; *i*= watershed 1, watershed 2, all watersheds together; j=observations, pollutants being evaluated; α= intercept; β=slope; and ε=residuals.

This approach compares the slope, intercept, and residual variances for two regression equations based on a two-tail F test. If heterogeneous slopes, intercepts, or residual variances are found, then the regression lines are regarded as statistically different. The slope represents a rate of increase in annual loads based on top load events. For similar slopes, the intercept generally represents the overall proportion of annual loads compared to top event loads.

Regression relationships from watersheds having statistically similar regression slopes and intercepts can possibly be used interchangeably to predict annual loads based on top load events or combined to produce statistically stronger relationships. If the regression lines are similar, then regional relationships can be developed and used for monitoring sites with limited data. Reliable regional relationships would also aid in designing uniform sampling strategies and identifying representative watersheds for long-term continuous monitoring (Rozemeijer et al., 2010).

6.2.3 Transferability of Regression Relationships

Regression relationships from all Ohio watersheds (both Lake Erie and Ohio River basins) were applied to the Upper Sangamon and Vermilion watersheds in central Illinois to evaluate whether the regression relationships developed in this research can be transferred to other watersheds. The Upper Sangamon and Vermilion watersheds drain an area of 3,161 km^2 and 3,424 km^2, respectively. These

watersheds are predominantly agricultural with an extensive adoption of sub-surface drainage. Daily monitored flow and NO_3-N concentration data were available for six years for the Upper Sangamon watershed and 11 years for the Vermilion watershed. High flow events were separated for each water year using the same method described earlier that was used for the watersheds from Ohio. The separated high flow events were ranked based on loads exported, and the cumulative loads exported in the top 5 load events were used as an input for regression relationships developed from Ohio watersheds to predict annual NO_3-N loads.

6.3 Principal Findings and Significance

6.3.1 Contributions of Top Five Load Events to Annual Load

Contributions of top load events towards annual loads and their durations were computed for SS, TP, and NO_3-N (Table 6.1, Table 6.2). The average duration of the top 1 SS load event ranged from eight days (2 percent of the number of days annually) to 19 days (5 percent). The top 1 SS load event carried from 22 percent (Cuyahoga) to 31 percent (Sandusky) on average. The top 5 load events carried from 57 percent Cuyahoga to 75 percent Sandusky of annual SS load and lasted from 34 days (9 percent) for Cuyahoga to 72 days (20 percent) for Sandusky on average.

As expected, the results for TP were very similar to the result for SS. The average duration of the top 1 TP load event ranged from eight days (2 percent) to about 18 days (5 percent). The top 1 TP load event carried from 15 percent (Cuyahoga) to 28 percent (Sandusky) of the annual TP load on average. The top 5 load events carried from 41 percent (Cuyahoga) to 71 percent (Sandusky) of the annual TP load and lasted from 36 days (10 percent) for Cuyahoga to 76 days (21 percent) for Sandusky on average.

The average duration of the top 1 NO_3-N load event ranged from 14 days (4 percent) to 26 days (7 percent). The top 1 load event carried from 7 percent (Cuyahoga) to 23 percent (Raisin) of the annual NO_3-N load on average. The top 5 load events combined lasted from 60 days (16 percent) for Maumee to 90 days (25 percent) for Sandusky and carried from 24 percent (Cuyahoga) to 67 percent (Raisin) of the annual NO_3-N load on average.

The least variance for the loads contributed by the top 1 to 5 load events was observed for NO_3-N, followed by TP and SS. Cuyahoga had the smallest variance for NO_3-N among all the watersheds. Sandusky and Vermilion (OH) had the largest variance in the top NO_3-N load events. The Great Miami had the smallest variance for TP and SS. The Maumee and Vermilion (OH) had the greatest variance in contributions of the top 1 to 5 load events towards TP and SS annual loads. The biggest increase in percentage of the annual load was generally found between the top 1 and top 2 events.

Table 6.1: Average contribution percentages (%) and standard deviations (SD) for annual SS, TP, and NO_3-N loads from top load events per water year

Contribution to annual loads (%)	Top load events	Cuyahoga		Grand		Great Miami		Maumee		Muskingum		Raisin		Sandusky		Vermilion (OH)	
		%	SD	%	SD	%	SD	%	SD	%	SD	%	SD	%	SD	%	SD
SS	1	22	10	31	10	23	6	26	13	23	7	27	11	31	10	25	9
	2	35	12	47	11	36	7	41	14	38	7	42	12	48	12	42	17
	3	44	12	59	11	46	7	51	14	50	7	54	13	60	13	54	17
	4	51	12	67	10	54	7	60	14	57	7	63	13	68	12	63	14
	5	57	11	72	9	61	7	67	13	64	7	69	11	75	11	71	12
TP	1	15	6	23	7	16	4	21	9	18	6	26	10	28	11	22	10
	2	24	8	36	8	26	4	35	12	30	7	41	12	44	14	36	14
	3	31	8	46	9	34	4	45	13	39	7	52	12	56	14	45	14
	4	36	8	54	9	41	5	53	13	46	7	60	11	64	13	53	13
	5	41	8	61	10	47	5	60	12	52	7	66	10	71	12	60	13
NO_3-N	1	7	2	21	10	16	6	16	6	19	5	23	8	20	7	18	9
	2	12	3	33	11	25	6	27	7	32	7	38	9	36	11	30	11
	3	16	4	42	11	33	7	37	8	42	8	50	10	48	13	39	13
	4	20	4	49	11	40	7	44	9	50	7	60	10	57	13	46	13
	5	24	5	55	11	46	7	51	9	57	7	67	9	64	13	52	13

Table 6.2: Average yearly durations (% year) and standard deviations (SD) for annual SS, TP, and NO_3-N top load events

Duration of high flow events (%)	Top load events	Cuyahoga		Grand		Great Miami		Maumee		Muskingum		Raisin		Sandusky		Vermilion (OH)	
		%	SD	%	SD	%	SD	%	SD	%	SD	%	SD	%	SD	%	SD
SS	1	2	1	2	1	3	1	3	1	5	2	4	2	5	4	2	1
	2	4	3	5	3	5	3	7	3	9	4	8	3	9	7	5	3
	3	6	4	8	4	7	4	9	4	11	5	12	5	13	10	6	4
	4	8	5	10	6	9	5	12	5	14	6	15	6	16	13	8	4
	5	9	6	13	7	12	8	14	6	17	7	19	8	20	16	10	5
TP	1	2	2	2	1	3	2	3	1	5	2	4	1	4	4	2	1
	2	4	3	6	3	7	5	7	3	9	4	9	3	9	6	4	1
	3	6	4	9	5	11	7	10	4	12	5	12	4	13	10	7	3
	4	8	5	11	5	13	9	12	5	15	6	15	5	17	13	9	4
	5	10	6	14	7	15	10	14	6	18	8	19	8	21	17	11	6
NO_3-N	1	4	1	6	5	4	2	4	1	7	3	5	2	6	4	4	1
	2	7	2	10	7	7	4	8	3	12	4	10	3	11	8	6	2
	3	10	5	14	9	10	5	11	4	16	5	15	5	17	12	8	4
	4	14	7	16	10	14	6	14	5	21	7	19	7	21	15	10	5
	5	17	9	19	12	16	7	16	7	25	8	23	8	25	18	13	6

The Cuyahoga and Raisin were selected as two similar-sized watersheds with different land usage to illustrate differences in NO_3-N and SS loadings. The Cuyahoga watershed is a fairly urbanized watershed with almost 45 percent of its land usage being urban. Only about 20 percent of its land cover is used for agriculture, with the remaining being under wooded forests. The Raisin watershed is predominantly characterized by row-crop agriculture with about 70 percent of its land cover being agricultural. Only about 10 percent of the Raisin watershed has urban land-usage with the remaining being wooded forests.

The contribution of top 5 SS load events per water year to annual loads was calculated for both these watersheds. The results were plotted over their monitoring duration ranging from 1977 to2009. The results indicated that although the SS load contributions from the top 5 load events were generally slightly lower for Cuyahoga as compared to Raisin, there wasn't any appreciable difference (Figure 6.1). On the other hand, a similar plot for NO_3-N loadings indicated that Raisin had a much higher percentage of loads that were exported in the top 5 load events in a water year. Cuyahoga is dominated by point sources unlike the Raisin watershed, which is largely non-point source driven. Municipal wastewater treatment plants can discharge a significant amount of NO_3-N in their effluent, thus contributing a significant portion of the total NO_3-N load exported from the watershed uniformly during a year. In addition, Figure 6.1 shows that the yearly variability in NO3-N loads for the top 5 events is also lower for the Cuyahoga watershed. Agricultural watersheds characterized by row-crop agriculture and a high density of tile-drainage are more likely to export a significant amount of NO_3-N loads in a few critical high flow events occurring over late winter and early spring months than urbanized watersheds.

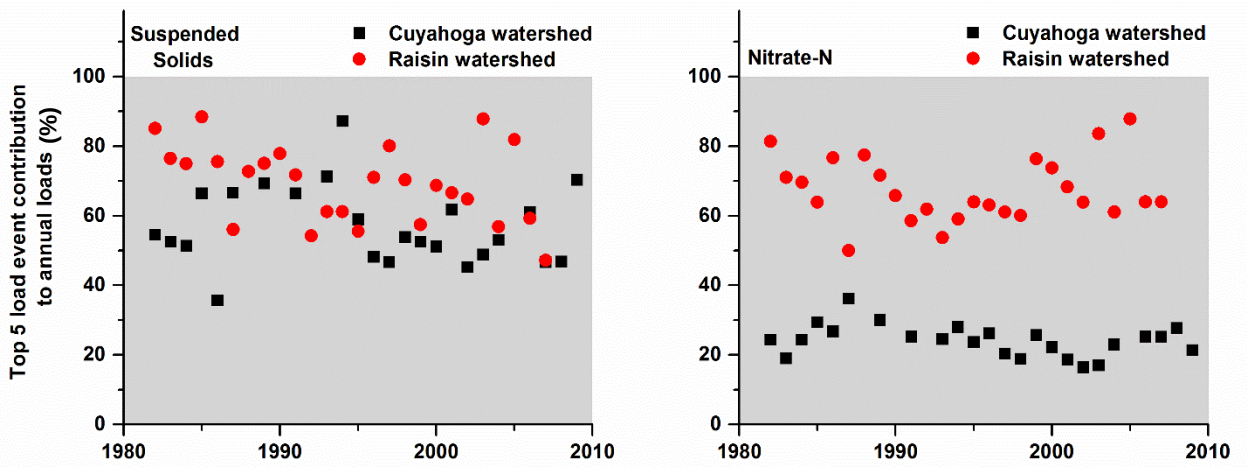

Figure 6.1: A comparison between percentage annual load contributions by top 5 SS and NO_3-N load events from Cuyahoga and Raisin watersheds over their complete monitoring durations

6.3.2 Regression Analysis

Figure 6.2 shows the total annual NO_3-N loads plotted against the loads contributed by the top 5 load events for all watersheds. Regression lines for contributions of the top 2, 3, and 4 load events towards annual loads were also developed similar to the top 1 and top 5 lines with similar results. Figure 6.2 (a) shows the individual regression lines for each watershed. Note that the Cuyahoga follows a distinctly different relationship between the annual NO_3-N load and the top 5 load events load as compared to the other watersheds. The Cuyahoga is the only highly urbanized watershed with significant point sources. Regression lines from the other watersheds align closely to one another, having visibly similar slopes. Figure 6.2 (b) shows spatially aggregated regression lines for the top 1 and top 5 load events. Two regression lines were created for the contributions of top 5 load events, with and without including data

from the Cuyahoga. A high correlation with an adjusted R^2 of 0.937 was observed for loads during the top 5 load events and total annual load for spatially aggregated data from all watersheds including the Cuyahoga (Table 6.3).

Similarly, Figure 6.3 and Figure 6.4 show the regression lines developed for TP and SS. Individual regression lines for TP from all watersheds lie in the same region, with potential differences in slopes and intercepts. Unlike NO_3-N, TP loadings from the Cuyahoga are more closely aligned with loadings from other watersheds. It is possible that watershed-scale phosphorus management changes coupled with phosphorus abatement programs implemented in these watersheds over the 1970s and 1980s contributed to a higher variability in TP loadings over the years. The adjusted R^2 for TP loads exported during top load events and total annual TP loads was high for spatially aggregated regression lines, ranging from 0.88 (top 1 load event) to 0.95 (top 5 load events).

Individual regression lines for SS are shown in Figure 6.4 (a). These regression lines were visibly the most similar among all three monitored pollutants, with most lines being indistinguishable from one another. Adjusted R^2 ranged from 0.89 (top 1 load event) to 0.97 (top 5 load events) for spatially aggregated regression lines (Table 6.3). The adjusted R^2 for spatially aggregated SS regression lines were the highest among the three monitored pollutants.

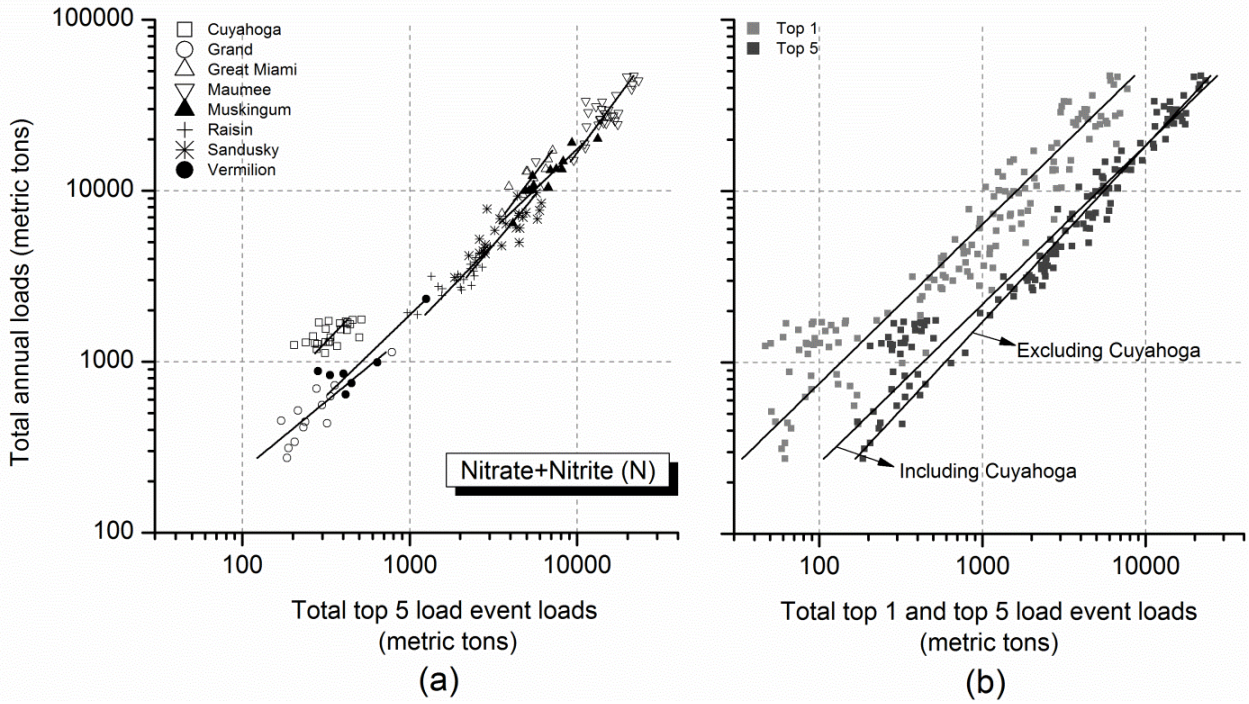

Figure 6.2: Regression relationships for total annual and top event NO_3-N loads: (a) top 5 load events for each watershed, and (b) top 1 and top 5 load events for all watersheds aggregated

Table 6.3: Correlation coefficient between annual and top 1 to 5 SS, TP, and NO_3-N load events for spatially aggregated data from all watersheds

High flow event by loads	*Top 1*	*Top 2*	*Top 3*	*Top 4*	*Top 5*
Constituent	Adjusted R^2				
SS	0.89	0.93	0.95	0.96	0.97
TP	0.88	0.92	0.93	0.94	0.95
NO_3-N	0.89	0.91	0.92	0.93	0.94

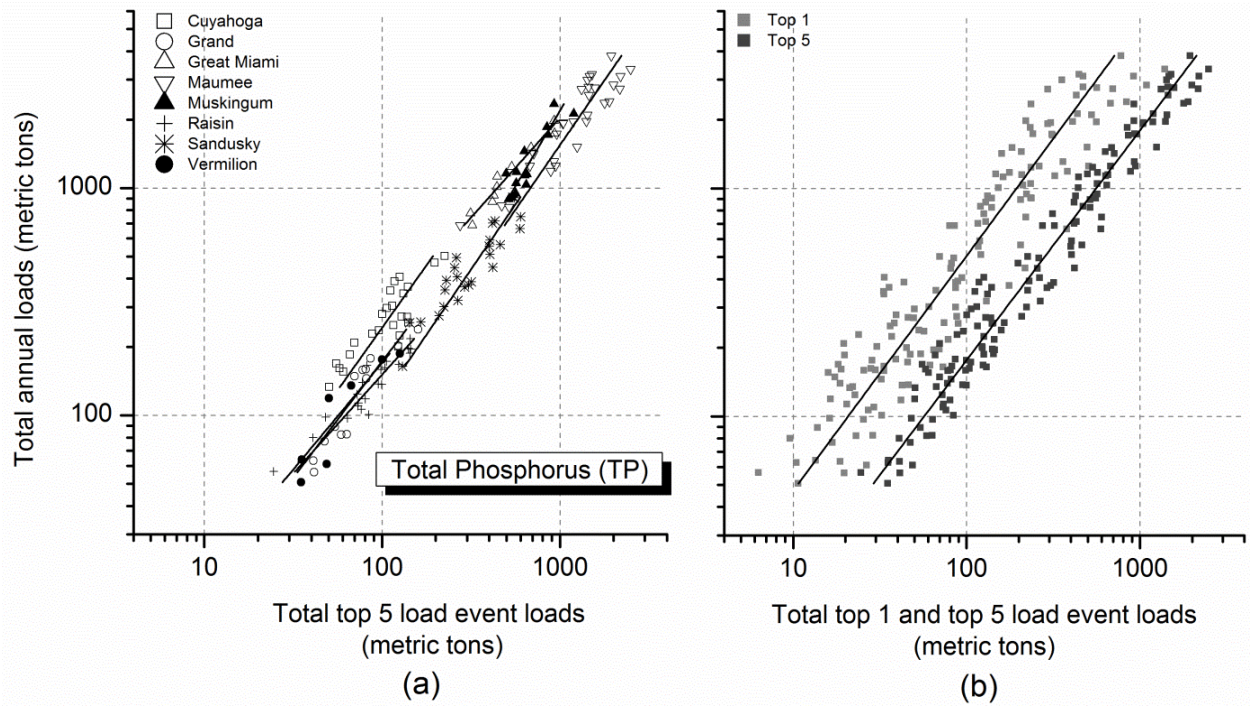

Figure 6.3: Regression relationships for total annual and top event TP loads: (a) top 5 load events for each watershed, and (b) top 1 and top 5 load events for all watersheds aggregated

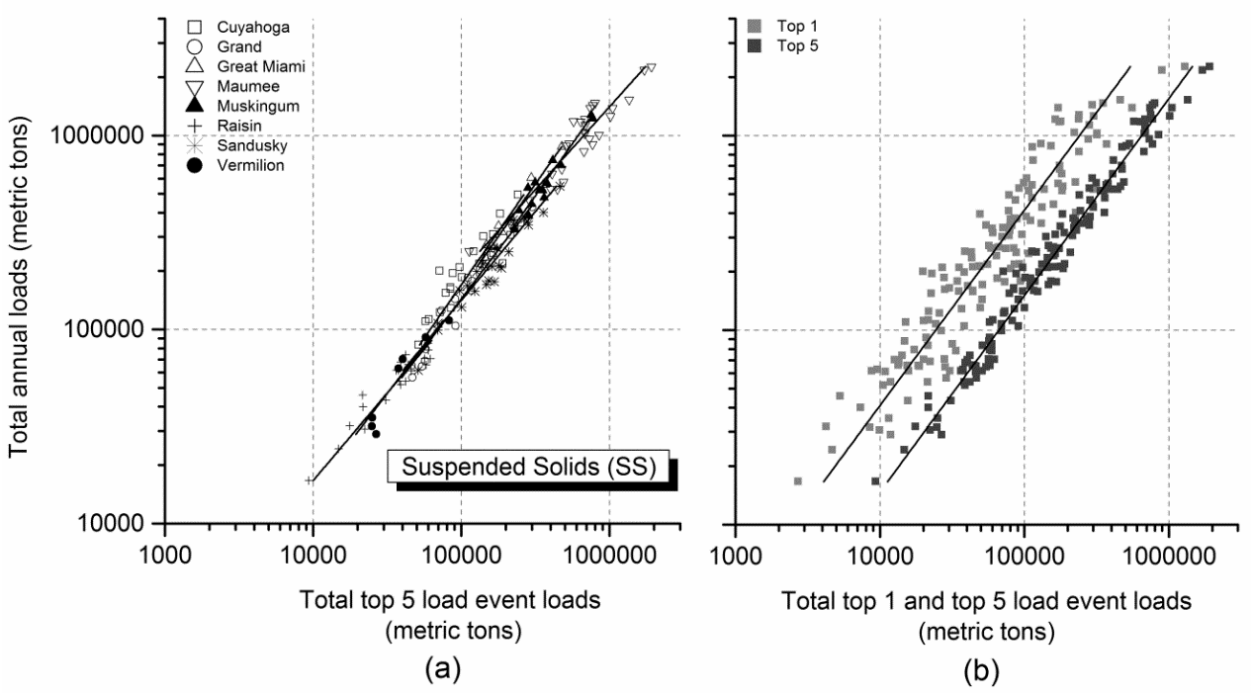

Figure 6.4: Regression relationships for total annual and top event SS loads: (a) top 5 load events for each watershed, and (b) top 1 and top 5 load events for all watersheds aggregated

6.3.3 Analysis of Covariance (ANCOVA)

ANCOVA was used to compare linear regression lines developed for total annual load estimates using loads exported during the top 1 to 5 load events for all eight watersheds in the Lake Erie and Ohio River basins (Ohio watersheds) and three monitored pollutants (Table 6.4, Table 6.5, and Table 6.6). The individual watershed-specific regression lines were also compared with a spatially aggregated regional regression line for similarity (Table 6.7). ANCOVA analysis was performed to gauge a statistical similarity between linear regression slopes, intercepts, and residual variances at α=0.05 and α=0.01 levels of significance. Watershed names indicate watershed-specific regression lines while "all watersheds together" indicates spatially aggregated data from all the watersheds. A comparison of watershed A to watershed B would be similar to a comparison of watershed B to watershed A for slope and intercept differences, while it would be different for comparing residual variances. This difference arises as the slope and intercept comparisons between two regression lines are done on pooled data (which would be similar in both cases), while residual variance comparisons are done using individual data and their associated degrees of freedom (Snedecor and Cochran, 1980 pp. 392).

The SS regression lines show the fewest statistical differences of the three pollutants (Table 6.4). Five out of the eight watersheds had similar regression lines to the spatially aggregated regional regression line (Table 6.7). The Cuyahoga had statistically similar SS regression lines to the Maumee and Vermilion (OH). A few groups of watersheds were found to have statistically similar regression lines, for example, the Maumee, Raisin, and Sandusky. The Great Miami was statistically different from most other watersheds.

Table 6.5 shows statistical differences for TP. The Cuyahoga, Grand, and Great Miami had statistically different lines when compared to most of the other watersheds. Most statistical differences rose from different regression line intercepts, except in a few cases such as the Raisin and Grand, where regression line slopes were different. The Grand, Maumee, Muskingum, and Vermilion (OH) were found to have statistically similar TP regression lines as the spatially aggregated regional regression line. A few

groups of watersheds were found to have statistically similar regression lines such as the Great Miami and Grand and the Maumee and Sandusky.

Table 6.6 summarizes results for NO_3-N. As was clearly evident from Figure 3.6, regression lines for the Cuyahoga are different from other watershed regression lines. The ANCOVA analysis indicates that slopes and residual variances of the regression lines from the Cuyahoga are statistically the same as the other lines, but the intercepts are different. Most of the statistical differences in NO_3-N regression lines were in the intercepts. The slopes and residual variances of most lines were consistently statistically similar. Four out of eight watersheds, the Great Miami, Maumee, Muskingum, and Vermilion (OH), were found to have statistically similar regression relationships when compared to the spatially aggregated regional regression line. The Maumee, Muskingum, Sandusky, and Raisin were found to have statistically similar regression relationships to each other for NO_3-N top load event contributions to annual loads.

Table 6.4: ANCOVA based statistical comparison for annual and top 1-5 SS load event regression relationships, for individual watersheds

Watershed	High flow event	Cuyahoga			Grand			Great Miami			Maumee			Muskingum			Raisin			Sandusky			Vermilion (OH)		
		R	*S*	*I*	*R*	*S*	*I*	*R*	*S*	*I*	*R*	*S*	*I*	*R*	*S*	*I*	*R*	*S*	*I*	*R*	*S*	*I*	*R*	*S*	*I*
Cuyahoga	top1				0	0	1	0	0	0	0	0	0	0	0	0	0	0	0	0	0	2	0	0	0
	top2				0	0	1	0	0	0	0	0	0	0	0	0	0	0	0	0	0	2	0	0	0
	top3				0	0	2	0	0	0	0	0	0	0	0	0	0	0	1	0	0	2	0	0	0
	top4				0	0	2	0	0	0	0	0	0	0	0	0	0	0	1	0	0	2	0	0	0
	top5				0	0	2	0	0	0	0	0	0	0	0	0	0	0	1	0	0	2	0	0	0
Grand	top1	0	0	1				0	0	0	0	0	0	0	0	0	0	0	0	0	0	0	0	0	1
	top2	1	0	1				0	0	0	1	0	0	0	0	0	0	1	0	0	0	0	0	0	2
	top3	1	0	2				0	0	0	1	0	0	0	0	0	0	1	0	0	0	0	0	0	1
	top4	1	0	2				0	0	0	1	0	0	0	0	0	0	1	0	0	0	0	0	0	1
	top5	1	0	2				0	0	0	1	0	0	0	0	0	0	1	0	0	0	0	0	0	0
Great Miami	top1	2	0	0	0	0	0				2	1	0	0	0	0	2	1	0	1	0	0	0	0	2
	top2	2	0	0	0	0	0				2	0	0	0	0	1	2	1	0	1	0	1	1	0	2
	top3	2	0	0	0	0	0				2	0	0	0	0	1	2	1	0	1	0	2	0	0	1
	top4	2	0	0	0	0	0				2	0	0	0	0	1	1	1	0	1	0	2	0	0	0
	top5	1	0	0	0	0	0				2	0	0	0	0	1	0	1	0	0	0	2	0	0	0
Maumee	top1	0	0	0	0	0	0	0	1	0				0	0	0	0	0	0	0	0	0	0	0	0
	top2	0	0	0	0	0	0	0	0	0				0	0	0	0	0	0	0	0	0	0	0	0
	top3	0	0	0	0	0	0	0	0	0				0	0	0	0	0	0	0	0	0	0	0	0
	top4	0	0	0	0	0	0	0	0	0				0	0	0	0	0	0	0	0	0	0	0	0
	top5	0	0	0	0	0	0	0	0	0				0	0	0	0	0	0	0	0	0	0	0	0
Muskingum	top1	0	0	0	0	0	0	0	0	0	0	0	0				0	0	0	0	0	0	0	0	0
	top2	1	0	0	0	0	0	0	0	1	1	0	0				1	0	0	0	0	0	0	0	1
	top3	1	0	0	0	0	0	0	0	1	1	0	0				1	0	0	0	0	0	0	0	1
	top4	1	0	0	0	0	0	0	0	1	1	0	0				1	0	0	0	0	0	0	0	0
	top5	1	0	0	0	0	0	0	0	1	1	0	0				0	0	0	0	0	1	0	0	0
Raisin	top1	0	0	0	0	0	0	0	1	0	0	0	0	0	0	0				0	0	0	0	1	0
	top2	0	0	0	0	1	0	0	1	0	0	0	0	0	0	0				0	0	0	0	1	0
	top3	0	0	1	0	1	0	0	1	0	0	0	0	0	0	0				0	0	0	0	1	0
	top4	0	0	1	0	1	0	0	1	0	0	0	0	0	0	0				0	0	0	0	1	0
	top5	0	0	1	0	1	0	0	1	0	0	0	0	0	0	0				0	0	0	0	1	0
Sandusky	top1	0	0	2	0	0	0	0	0	0	0	0	0	0	0	0	0	0	0				0	0	1
	top2	0	0	2	0	0	0	0	0	1	0	0	0	0	0	0	0	0	0				0	0	0
	top3	0	0	2	0	0	0	0	0	2	0	0	0	0	0	0	0	0	0				0	0	0
	top4	0	0	2	0	0	0	0	0	2	0	0	0	0	0	0	0	0	0				0	0	0
	top5	0	0	2	0	0	0	0	0	2	0	0	0	0	0	1	0	0	0				0	0	0
	top1	0	0	0	0	0	1	0	0	2	0	0	0	0	0	0	0	1	0	0	0	1			

Watershed	High flow event	Cuyahoga			Grand			Great Miami			Maumee			Muskingum			Raisin			Sandusky			Vermilion (OH)		
		R	S	I	R	S	I	R	S	I	R	S	I	R	S	I	R	S	I	R	S	I	R	S	I
Vermilion (OH)	top2	0	0	0	0	0	2	0	0	2	0	0	0	0	0	1	0	1	0	0	0	0			
	top3	0	0	0	0	0	1	0	0	1	0	0	0	0	0	1	0	1	0	0	0	0			
	top4	0	0	0	0	0	1	0	0	0	0	0	0	0	0	0	0	1	0	0	0	0			
	top5	0	0	0	0	0	0	0	0	0	0	0	0	0	0	0	0	1	0	0	0	0			
All watersheds together	top1	0	0	1	0	0	0	0	0	0	0	0	0	0	0	0	0	0	0	0	0	1	0	0	0
	top2	0	0	2	0	0	0	0	0	0	0	0	0	0	0	0	0	0	0	0	0	1	0	1	0
	top3	0	0	2	0	0	0	0	0	0	0	0	0	0	0	0	0	0	0	0	0	1	0	0	0
	top4	0	0	2	0	0	0	0	0	0	0	0	0	0	0	0	0	0	0	0	0	2	0	0	0
	top5	0	0	2	0	0	0	0	0	0	0	0	0	0	0	0	0	0	0	0	0	2	0	0	0

Notes: R, S, and I indicate residual variances, slope, and intercept, respectively. Significant differences at both α=0.05 and α=0.01 are indicated a "2" value and a dark shading. Differences significant at α=0.05 and insignificant at α=0.01 are indicated by "1" value and a light shading. A "0" value indicates no statistical difference between two lines at both α=0.05 and α=0.01.

Table 6.5: ANCOVA based statistical comparison for annual and top 1-5 TP load event regression relationships for individual watersheds

Watershed	*High flow event*	*Cuyahoga*			*Grand*			*Great Miami*			*Maumee*			*Muskingum*			*Raisin*			*Sandusky*			*Vermilion (OH)*		
		R	***S***	***I***	***R***	***S***	***I***	***R***	***S***	***I***	***R***	***S***	***I***	***R***	***S***	***I***	***R***	***S***	***I***	***R***	***S***	***I***	***R***	***S***	***I***
Cuyahoga	top1				0	0	0	0	0	0	0	0	0	0	0	0	0	0	2	0	0	2	0	0	0
	top2				0	0	1	0	0	0	0	0	0	0	0	1	0	0	2	0	0	2	0	0	0
	top3				0	0	2	0	0	0	0	0	1	0	0	1	0	0	2	0	0	2	0	0	0
	top4				0	0	2	0	0	0	0	0	1	0	0	2	0	0	2	0	0	2	0	0	1
	top5				0	0	2	0	0	0	0	0	2	0	0	2	0	0	2	0	0	2	0	0	1
Grand	top1	0	0	0				0	0	0	0	0	0	0	0	1	0	2	0	0	0	2	0	0	0
	top2	0	0	1				0	0	0	1	0	0	0	0	1	1	1	0	0	0	2	1	0	0
	top3	0	0	2				0	0	0	1	0	0	0	0	1	0	2	0	0	0	2	1	0	0
	top4	0	0	2				0	0	0	1	0	0	0	0	1	0	2	0	0	0	2	1	0	0
	top5	0	0	2				0	0	0	0	0	0	0	0	1	0	2	0	0	0	2	0	0	0
Great Miami	top1	1	0	0	0	0	0				2	0	0	0	0	1	1	1	1	1	0	1	1	0	0
	top2	2	0	0	0	0	0				2	0	1	0	0	1	2	0	2	2	0	2	2	0	0
	top3	2	0	0	0	0	0				2	0	2	0	0	2	2	0	2	2	0	2	2	0	0
	top4	1	0	0	0	0	0				2	0	2	0	0	2	1	0	2	1	0	2	1	0	0
	top5	1	0	0	0	0	0				1	0	2	0	0	1	0	0	2	0	0	2	1	0	0
Maumee	top1	0	0	0	0	0	0	0	0	0				0	0	0	0	0	1	0	0	0	0	0	0
	top2	0	0	0	0	0	0	0	0	1				0	0	0	0	0	0	0	0	0	0	0	0
	top3	0	0	1	0	0	0	0	0	2				0	0	0	0	0	0	0	0	0	0	0	0
	top4	0	0	1	0	0	0	0	0	2				0	0	1	0	0	0	0	0	0	0	0	0
	top5	0	0	2	0	0	0	0	0	2				0	0	2	0	0	0	0	0	0	0	0	0
Muskingum	top1	0	0	0	0	0	1	0	0	1	0	0	0				0	1	0	0	0	0	0	0	0
	top2	0	0	1	0	0	1	0	0	1	1	0	0				0	1	0	0	0	0	0	0	0
	top3	0	0	1	0	0	1	0	0	2	1	0	0				0	1	0	0	0	0	0	0	0
	top4	0	0	2	0	0	1	0	0	2	1	0	1				0	1	0	0	0	1	1	0	0
	top5	1	0	2	0	0	1	0	0	1	1	0	2				0	1	0	0	0	1	1	0	0
Raisin	top1	0	0	2	0	2	0	0	1	1	0	0	1	0	1	0				0	1	0	0	0	0
	top2	0	0	2	0	1	0	0	0	2	0	0	0	0	1	0				0	0	0	0	0	0
	top3	0	0	2	0	2	0	0	0	2	0	0	0	0	1	0				0	1	0	0	0	0
	top4	0	0	2	0	2	0	0	0	2	0	0	0	0	1	0				0	0	0	0	0	0
	top5	0	0	2	0	2	0	0	0	2	0	0	0	0	1	0				0	0	0	0	0	0
Sandusky	top1	0	0	2	0	0	2	0	0	1	0	0	0	0	0	0	0	1	0				0	0	1
	top2	0	0	2	0	0	2	0	0	2	0	0	0	0	0	0	0	0	0				0	0	1
	top3	0	0	2	0	0	2	0	0	2	0	0	0	0	0	0	0	1	0				0	0	1
	top4	0	0	2	0	0	2	0	0	2	0	0	0	0	0	1	0	0	0				0	0	1
	top5	0	0	2	0	0	2	0	0	2	0	0	0	0	0	1	0	0	0				0	0	1

Watershed	High flow event	Cuyahoga			Grand			Great Miami			Maumee			Muskingum			Raisin			Sandusky			Vermilion (OH)		
		R	S	I	R	S	I	R	S	I	R	S	I	R	S	I	R	S	I	R	S	I	R	S	I
Vermilion (OH)	top1	0	0	0	0	0	0	0	0	0	0	0	0	0	0	0	0	0	0	0	0	1			
	top2	0	0	0	0	0	0	0	0	0	0	0	0	0	0	0	0	0	0	0	0	1			
	top3	0	0	0	0	0	0	0	0	0	0	0	0	0	0	0	0	0	0	0	0	1			
	top4	0	0	1	0	0	0	0	0	0	0	0	0	0	0	0	0	0	0	0	0	1			
	top5	0	0	1	0	0	0	0	0	0	0	0	0	0	0	0	0	0	0	0	0	1			
All watersheds together	top1	0	0	2	0	0	0	0	0	1	0	0	0	0	0	0	0	1	0	0	0	2	0	0	0
	top2	0	0	2	0	0	0	0	0	1	0	0	0	0	0	0	0	0	0	0	0	2	0	0	0
	top3	0	0	2	0	0	0	0	0	1	0	0	0	0	0	0	0	0	1	0	0	2	0	0	0
	top4	0	0	2	0	0	0	0	0	2	0	0	0	0	0	0	0	0	1	0	0	2	0	0	0
	top5	0	0	2	0	0	0	0	0	1	0	0	0	0	0	0	0	0	1	0	0	2	0	0	0

Notes: R, S, and I indicate residual variances, slope, and intercept, respectively. Significant differences at both α=0.05 and α=0.01 are indicated a "2" value and a dark shading. Differences significant at α=0.05 and insignificant at α=0.01 are indicated by "1" value and a light shading. A "0" value indicates no statistical difference between two lines at both α=0.05 and α=0.01.

Table 6.6: ANCOVA-based statistical comparison for annual and top 1 to 5 NO_3-N load event regression relationships for individual watersheds

Nitrate + Nitrite Watershed	*High flow event*	*Cuyahoga*			*Grand*			*Great Miami*			*Maumee*			*Muskingum*			*Raisin*			*Sandusky*			*Vermilion (OH)*		
		R	*S*	*I*	*R*	*S*	*I*	*R*	*S*	*I*	*R*	*S*	*I*	*R*	*S*	*I*	*R*	*S*	*I*	*R*	*S*	*I*	*R*	*S*	*I*
Cuyahoga	top1				0	0	2	0	0	0	0	0	2	0	0	1	0	0	2	0	0	2	0	0	2
	top2				0	0	2	0	0	1	0	0	2	0	0	1	0	0	2	0	0	2	1	0	2
	top3				0	0	2	0	0	1	0	0	2	0	0	2	0	0	2	0	0	2	1	0	2
	top4				0	0	2	0	0	2	0	0	2	0	0	2	0	0	2	0	0	2	0	0	2
	top5				0	0	2	0	0	2	0	0	2	0	0	2	0	0	2	0	0	2	0	0	2
Grand	top1	0	0	2				0	0	0	0	0	0	0	0	0	0	0	0	0	0	0	0	0	0
	top2	0	0	2				0	0	0	0	0	0	0	0	0	0	0	0	0	0	0	0	0	0
	top3	0	0	2				0	0	0	0	0	0	0	0	0	0	0	0	0	0	0	0	0	0
	top4	0	0	2				0	0	0	0	0	0	0	0	0	0	0	1	0	0	0	0	0	0
	top5	0	0	2				0	0	0	0	0	1	0	0	0	0	0	1	0	0	0	0	0	0
Great Miami	top1	0	0	0	0	0	0				0	0	1	0	0	1	0	0	0	0	0	0	0	0	0
	top2	0	0	1	0	0	0				0	0	2	0	0	2	0	0	0	0	0	0	1	0	0
	top3	0	0	1	0	0	0				0	0	2	0	0	2	0	0	0	0	0	1	1	0	0
	top4	0	0	2	0	0	0				0	0	2	0	0	2	0	0	0	0	0	1	1	0	0
	top5	0	0	2	0	0	0				0	0	2	0	0	2	0	0	0	0	0	1	1	0	0
Maumee	top1	0	0	2	0	0	0	0	0	1				0	0	0	0	0	0	0	0	0	1	0	0
	top2	0	0	2	0	0	0	0	0	2				0	0	0	0	0	0	0	0	0	1	0	0
	top3	0	0	2	0	0	0	0	0	2				0	0	0	0	0	0	0	0	0	1	0	0
	top4	0	0	2	0	0	0	0	0	2				0	0	0	0	0	0	0	0	0	1	0	0
	top5	0	0	2	0	0	1	0	0	2				0	0	0	0	0	0	0	0	0	0	0	1
Muskingum	top1	0	0	1	0	0	0	0	0	1	0	0	0				0	0	0	0	0	0	1	0	0
	top2	0	0	1	0	0	0	0	0	2	0	0	0				0	0	0	0	0	0	1	0	0
	top3	0	0	2	0	0	0	0	0	2	0	0	0				0	0	0	0	0	0	1	0	0
	top4	0	0	2	0	0	0	0	0	2	0	0	0				0	0	0	0	0	0	1	0	0
	top5	0	0	2	1	0	0	0	0	2	0	0	0				0	0	0	1	0	0	2	0	0
Raisin	top1	0	0	2	0	0	0	0	0	0	0	0	0	0	0	0				0	0	0	1	0	0
	top2	0	0	2	0	0	0	0	0	0	0	0	0	0	0	0				0	0	0	1	0	0
	top3	0	0	2	0	0	0	0	0	0	0	0	0	0	0	0				0	0	0	1	0	1
	top4	0	0	2	0	0	1	0	0	0	0	0	0	0	0	0				0	0	0	1	0	1
	top5	0	0	2	0	0	1	0	0	0	0	0	0	0	0	0				0	0	0	1	0	1
Sandusky	top1	0	0	2	0	0	0	0	0	0	0	0	0	0	0	0	0	0	0				1	0	0
	top2	0	0	2	0	0	0	0	0	0	0	0	0	0	0	0	0	0	0				0	0	0
	top3	0	0	2	0	0	0	0	0	1	0	0	0	0	0	0	0	0	0				0	0	0
	top4	0	0	2	0	0	0	0	0	1	0	0	0	0	0	0	0	0	0				0	0	0
	top5	0	0	2	0	0	0	0	0	1	0	0	0	0	0	0	0	0	0				0	0	0

Nitrate + Nitrite *Watershed*	*High flow event*	*Cuyahoga*			*Grand*			*Great Miami*			*Maumee*			*Muskingum*			*Raisin*			*Sandusky*			*Vermilion (OH)*		
		R	*S*	*I*	*R*	*S*	*I*	*R*	*S*	*I*	*R*	*S*	*I*	*R*	*S*	*I*	*R*	*S*	*I*	*R*	*S*	*I*	*R*	*S*	*I*
Vermilion (OH)	top1	0	0	2	0	0	0	0	0	0	0	0	0	0	0	0	0	0	0	0	0	0			
	top2	0	0	2	0	0	0	0	0	0	0	0	0	0	0	0	0	0	0	0	0	0			
	top3	0	0	2	0	0	0	0	0	0	0	0	0	0	0	0	0	0	1	0	0	0			
	top4	0	0	2	0	0	0	0	0	0	0	0	0	0	0	0	0	0	1	0	0	0			
	top5	0	0	2	0	0	0	0	0	0	0	0	1	0	0	0	0	0	1	0	0	0			
All watersheds together	top1	0	0	2	0	0	1	0	0	0	0	0	0	0	0	0	0	0	2	0	0	1	0	0	0
	top2	0	0	2	0	0	1	0	0	0	0	0	0	0	0	0	0	0	2	0	0	2	0	0	0
	top3	0	0	2	0	0	1	0	0	0	0	0	0	0	0	0	0	0	2	0	0	2	0	0	0
	top4	0	0	2	0	0	1	0	0	0	0	0	0	0	0	0	0	0	2	0	0	2	0	0	0
	top5	0	0	2	0	0	1	0	0	0	0	0	0	0	0	0	0	0	2	0	0	2	0	0	0

Notes: R, S, and I indicate residual variances, slope, and intercept, respectively. Significant differences at both α=0.05 and α=0.01 are indicated a "2" value and a dark shading. Differences significant at α=0.05 and insignificant at α=0.01 are indicated by "1" value and a light shading. A "0" value indicates no statistical difference between two lines at both α=0.05 and α=0.01.

Table 6.7: ANCOVA based statistical comparison for annual and top 1-5 load event regression relationships for spatially aggregated data

Watershed	*High flow event*	*All watersheds together*								
		NO_3-N			*TP*			*SS*		
		R	*S*	*I*	*R*	*S*	*I*	*R*	*S*	*I*
Cuyahoga	top1	1	0	2	0	0	2	0	0	1
	top2	2	0	2	0	0	2	0	0	2
	top3	2	0	2	0	0	2	0	0	2
	top4	2	0	2	0	0	2	0	0	2
	top5	2	0	2	0	0	2	0	0	2
Grand	top1	0	0	1	0	0	0	0	0	0
	top2	0	0	1	1	0	0	0	0	0
	top3	0	0	1	2	0	0	0	0	0
	top4	1	0	1	2	0	0	0	0	0
	top5	1	0	1	1	0	0	1	0	0
Great Miami	top1	0	0	0	2	0	1	2	0	0
	top2	1	0	0	2	0	1	2	0	0
	top3	2	0	0	2	0	1	2	0	0
	top4	2	0	0	2	0	2	2	0	0
	top5	2	0	0	2	0	1	1	0	0
Maumee	top1	2	0	2	0	0	0	0	0	0
	top2	2	0	2	0	0	0	0	0	0
	top3	2	0	2	0	0	0	0	0	0
	top4	2	0	2	0	0	0	0	0	0
	top5	2	0	2	0	0	0	0	0	0
Muskingum	top1	1	0	0	0	0	0	0	0	0
	top2	2	0	0	1	0	0	1	0	0
	top3	2	0	0	1	0	0	1	0	0
	top4	2	0	0	2	0	0	1	0	0
	top5	2	0	0	2	0	0	1	0	0
Raisin	top1	2	0	2	0	1	0	0	0	0
	top2	2	0	2	0	0	0	0	0	0
	top3	2	0	2	0	0	1	0	0	0
	top4	2	0	2	1	0	1	0	0	0
	top5	2	0	2	2	0	1	0	0	0
Sandusky	top1	2	0	1	0	0	2	0	0	1
	top2	2	0	2	0	0	2	0	0	1
	top3	2	0	2	0	0	2	0	0	1
	top4	2	0	2	1	0	2	0	0	2
	top5	2	0	2	2	0	2	0	0	2

Watershed	High flow event	All watersheds together								
		NO_3-N			TP			SS		
		R	S	I	R	S	I	R	S	I
Vermilion (OH)	top1	0	0	0	0	0	0	0	0	0
	top2	0	0	0	0	0	0	0	1	0
	top3	0	0	0	0	0	0	0	0	0
	top4	0	0	0	0	0	0	0	0	0
	top5	0	0	0	0	0	0	0	0	0

Notes: R, S, and I indicate residual variances, slope, and intercept, respectively. Significant differences at both α=0.05 and α=0.01 are indicated a "2" value and a dark shading. Differences significant at α=0.05 and insignificant at α=0.01 are indicated by "1" value and a light shading. A "0" value indicates no statistical difference between two lines at both α=0.05 and α=0.01.

6.3.4 Error Analysis

The regression lines presented in Section 6.3.2 were used to predict total annual loads. Regression analyses were carried out at three different levels of watershed aggregations: i) all Ohio watersheds representing regional regressions, ii) watersheds identified as similar by ANCOVA representing watersheds with similar characteristics, and iii) individual watersheds. Relative errors were defined as (Toor et al., 2008):

$$Absolute\ Relative\ Error\ (\%) = \left|\left(\frac{Observed\ annual\ load - Estimated\ annual\ load}{Observed\ annual\ load} \times 100\right)\right| \quad \textbf{(6.3)}$$

First, the spatially aggregated regional regression lines for all three pollutants using all eight Ohio watersheds were used to predict annual loads from the top 1 to 5 load events. Distributions of relative errors for estimating annual loads using spatially aggregated regional regression lines are presented using box and whisker plots in Figure 6.5. The median relative errors for annual load predictions from the top 1, 2, 3, 4, and 5 load events for NO_3-N were 29 percent, 28 percent, 28 percent, 27 percent, and 26 percent, respectively, for all Ohio watersheds. Although the median errors for annual load predictions from the top 1 to 5 load events including data from Cuyahoga were fairly similar, the standard deviations declined from 36percent to 19 percent as the number of load events increased from 1 to 5. The maximum relative errors also declined from 233 percent to 96 percent as the number of load events increased from 1 to 5.

Two NO_3-N regression relationships were developed for predictions using the top 5 load events. Applying the regression line with the Cuyahoga data included resulted in median relative errors of 26 percent. Applying the regression line with the Cuyahoga data excluded resulted in median relative errors of 14 percent, about a 50 percent reduction in median relative error when compared to the regression line with the Cuyahoga data included (Table 6.8). The regression relationship for the top five load events that excluded data from the Cuyahoga considerably improved annual load predictions for the remaining watersheds as was evident by the reduction in median relative error. The maximum relative error and standard deviations were also the smallest when the Cuyahoga data were excluded (61 percent and 12 percent, respectively).

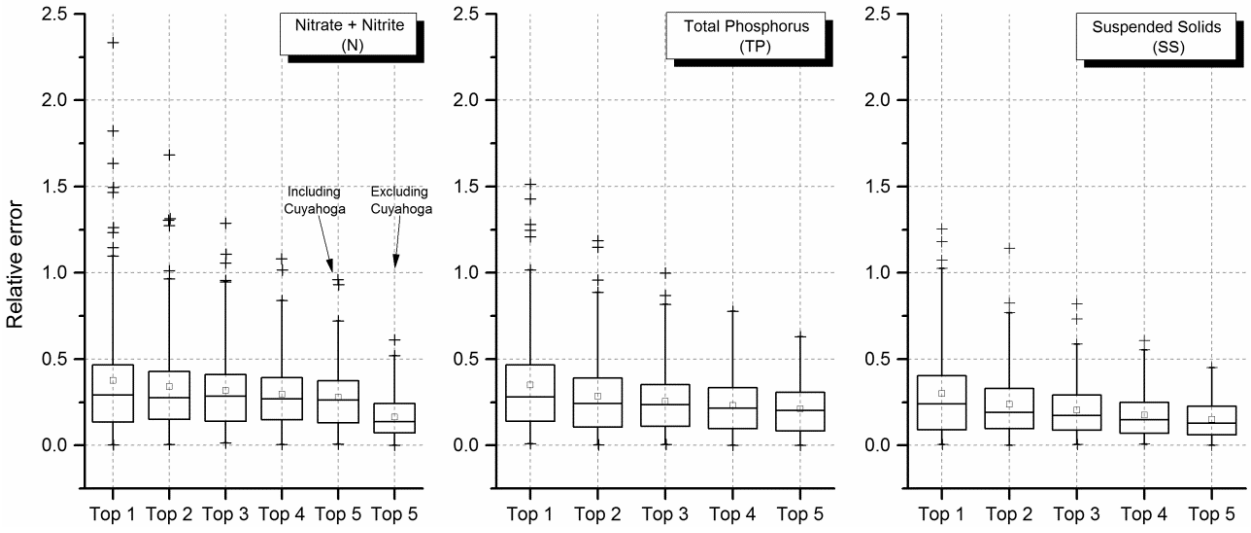

Figure 6.5: Relative error distributions for annual loads estimated using regressions developed for top 1 to 5 NO_3-N, TP, and SS load events using spatially aggregated data from all watersheds. Cross (+) symbol beyond the length of whiskers indicates outliers. A small square symbol within the boxes indicates the mean of the distributions.

The median relative errors for annual load predictions for TP and SS were slightly lower than for NO_3-N. The median relative errors for annual TP load predictions for the top 1, 2, 3, 4, and 5 load events were 28 percent, 24 percent, 23 percent, 22 percent, and 20 percent, respectively. The maximum relative errors and standard deviations also declined from 151 percent to 63 percent and 30 percent to 14 percent as the number of top load events included in the analyses increased from 1 to 5.

SS annual load predictions had the least relative errors among all three pollutants with the median values being 24 percent, 19 percent, 17 percent, 15 percent, and 13 percent for the top 1, 2, 3, 4, and 5 load events. The maximum relative errors and standard deviations for SS annual load predictions declined from 125 percent to 45 percent and 26 percent to 11 percent as the number of load events increased from 1 to 5.

The ANCOVA analysis showed that some watersheds have statistically similar regression relationships for predicting annual load. At a second level of aggregation, these watersheds with statistically similar regressions (predominantly agricultural watersheds) were grouped together to create aggregated regression lines to predict annual load using a cumulative load from the top 5 load events. The regression lines developed from aggregating similar watersheds were then used to predict annual loads. Distributions of relative errors of the predictions are presented using box and whisker plots in Figure 6.6. Note that a different group of watersheds was selected for each pollutant based on ANCOVA results.

NO_3-N data from the Maumee, Muskingum, Raisin, and Sandusky watersheds were aggregated since their individual watershed-specific NO_3-N regression lines were statistically similar to each other (Table 6.6). A new regression relationship using aggregated data from these four watersheds was developed. The median and maximum relative error for this aggregated regression was 11 percent and 53 percent, respectively, with a standard deviation of 12 percent. This represents a slight reduction in the relative errors when compared to relative errors for aggregated regression lines developed from all watersheds excluding the Cuyahoga (Table 6.8).

TP data from the Grand and Great Miami were aggregated since their individual watershed-specific TP regression lines were statistically similar to each other (Table 6.6). A new regression relationship using aggregated data from these two watersheds was developed. The median and maximum relative errors for this aggregated regression were 10 percent and 28 percent. This represents a significant reduction in relative errors when compared to spatially aggregated regression from all watersheds (Table 6.8).

SS data from the Maumee, Raisin, and Sandusky were aggregated since their individual watershed-specific SS regression lines were statistically similar to each other (Table 6.6). A new regression relationship using aggregated data from these three watersheds was developed. The median relative error for this regression was similar to that from a spatially aggregated regression for data from all watersheds (13 percent). The maximum relative error and standard deviations were 36 percent and 9 percent, respectively. This represents a slight reduction in relative errors when compared to spatially aggregated regression from all watersheds (Table 6.8).

Table 6.8: Median, maximum, and standard deviation of relative errors for annual loads estimated from top 5 load events at three levels of aggregation: all watersheds and years

Constituent	*All watersheds*			*Similar watersheds***			*Individual watersheds****		
	Median	*Maximum*	*SD*	*Median*	*Maximum*	*SD*	*Median*	*Maximum*	*SD*
SS	13	45	11	13	36	9	12	44	8
TP	20	63	14	10	28	9	10	49	9
NO_3-N	26	96	19	11	53	12	10	37	9
	(14)*	(61)*	(12)*						

Notes: * Cuyahoga data were excluded from analysis. **Similar watersheds by constituent: SS: Maumee, Raisin, and Sandusky; TP: Grand and Great Miami; NO_3-N: Maumee, Muskingum, Raisin, and Sandusky. *** Data for all years and watersheds were combined to derive this value.

Table 6.9: Median, maximum, and standard deviation of relative errors for annual loads estimated from top 5 load events at three levels of aggregation: similar watersheds only

Constituent	*All watersheds*			*Similar watersheds*			*Individual watersheds*		
	Median	*Maximum*	*SD*	*Median*	*Maximum*	*SD*	*Median*	*Maximum*	*SD*
SS	15 (12-17)	32-43	11 (9-13)	13 (13-16)	31-36	9 (8-9)	12 (10-16)	22-30	7 (6-9)
TP	16 (15-22)	31-44	13 (6-13)	10 (6-16)	26-28	9 (8-9)	9 (5-15)	11-27	8 (3-9)
NO_3-N	13 (10-15)	20-61	12 (6-16)	11 (9-13)	23-53	12 (6-15)	10 (7-19)	23-37	9 (7-10)

Notes: Range of values by watershed shown in parenthesis. Similar watersheds by constituent: SS: Maumee, Raisin, and Sandusky; TP: Grand and Great Miami; NO_3-N: Maumee, Muskingum, Raisin, and Sandusky.

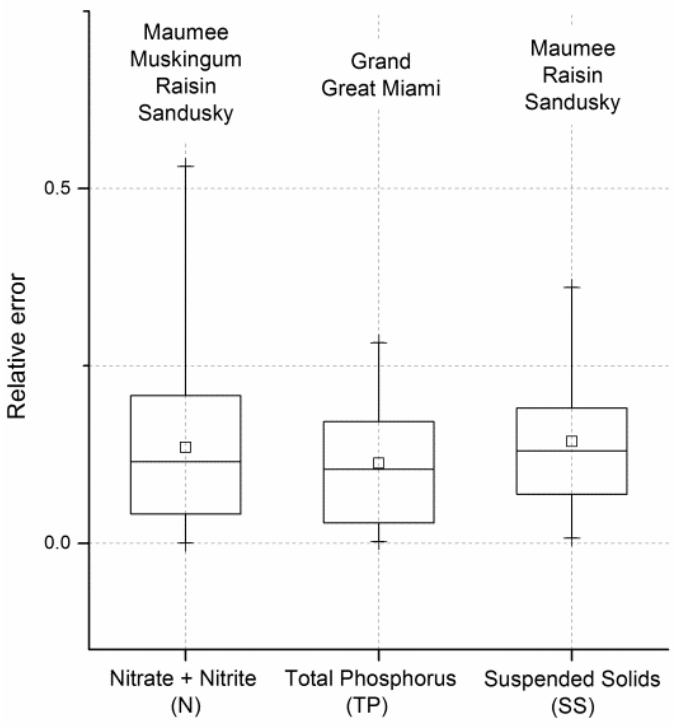

Figure 6.6: Relative error distributions for annual loads estimated using top 5 NO_3-N, TP, and SS load events for spatially aggregated data from watersheds with statistically similar regression lines. Cross (+) symbol beyond the length of whiskers indicates outliers and a small square symbol within the boxes indicates the mean of the distributions.

At a third level of aggregation, each individual watershed was used separately. Figure 6.7 shows distributions of relative errors for annual load predictions using watershed-specific regression relationships from the top 5 load events. These watershed-specific regressions generally performed better than the spatially aggregated regressions (Table 6.8).

The median relative errors to predict NO_3-N ranged from 7 percent for the Muskingum to 19 percent for the Vermilion (OH). The maximum relative error ranged from 37 percent for the Sandusky to 23 percent for the Muskingum. The average of median relative errors and maximum relative errors was 12 percent and 29 percent, respectively.

The median relative errors to predict TP ranged from 5 percent for the Great Miami to 16 percent for the Maumee. The maximum relative error ranged from 49 percent for the Cuyahoga to 11 percent for the Great Miami. The average of median relative errors and maximum relative errors was 12 percent and 30 percent, respectively.

The median relative errors to predict SS ranged from 6 percent for the Great Miami to 16 percent for the Maumee. The maximum relative error ranged from 44 percent for the Cuyahoga to 18 percent for the Great Miami. The average of median relative errors and maximum relative errors was 11 percent and 26 percent, respectively. The average standard deviation observed for these individual watershed specific regressions was 7 percent.

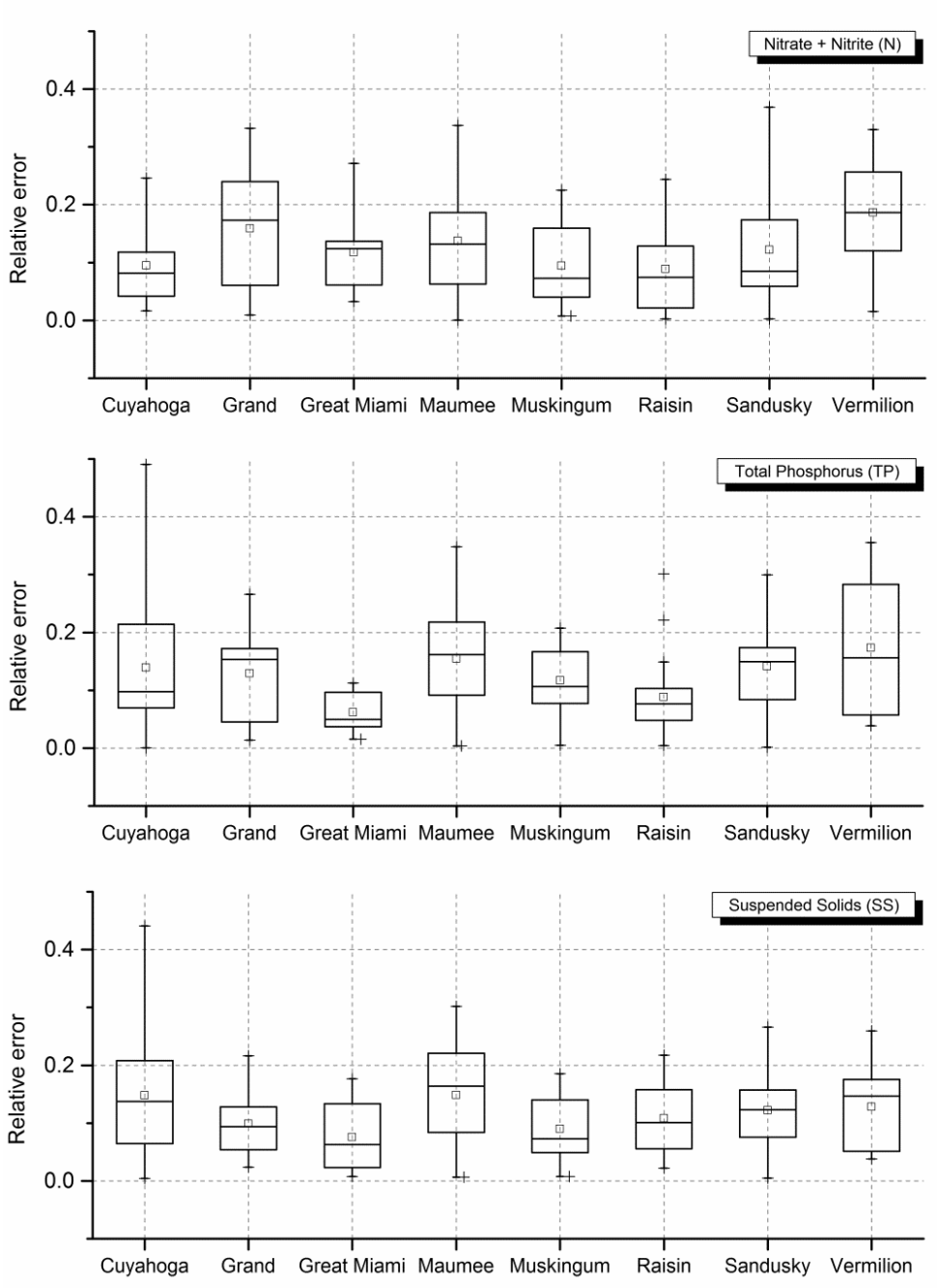

Figure 6.7: Relative error distributions for annual loads estimated using top 5 NO_3-N, TP, and SS load events for individual watersheds. Cross (+) symbol beyond the length of whiskers indicates outliers and a small square symbol within the boxes indicates the mean of the distributions.

6.3.6 Spatial Transferability of Results

The regression relationships developed in Section 6.3.2 were used to predict annual NO_3-N loads for two non-urbanized agricultural watersheds in Illinois, the Upper Sangamon and the Vermilion (IL). Regression lines from two levels of aggregation were selected for this analysis: i) aggregation of all watersheds but without the Cuyahoga, and ii) aggregation watersheds identified as statistically similar by ANCOVA (Maumee, Muskingum, Raisin, and Sandusky). Distributions of the relative error for estimating annual NO_3-N loads using both regression lines are presented using box and whisker plots in Figure 6.8.

The results indicated that the median absolute prediction error for annual NO_3-N loads using the spatially aggregated regression relationship from all non-urbanized watersheds in Ohio (all except the Cuyahoga) was 11 percent and 12 percent for the Upper Sangamon and Vermilion (IL) watersheds, respectively. The maximum errors were 42 percent and 26 percent for the Upper Sangamon and Vermilion watersheds, respectively. The median absolute prediction error declined to 10 percent and 6 percent when using the spatially aggregated regression from statistically similar watersheds for the Upper Sangamon and Vermilion (IL) watersheds, respectively. The maximum error declined to 28 percent for the Upper Sangamon watershed but increased to 31 percent for the Vermilion (IL) watershed.

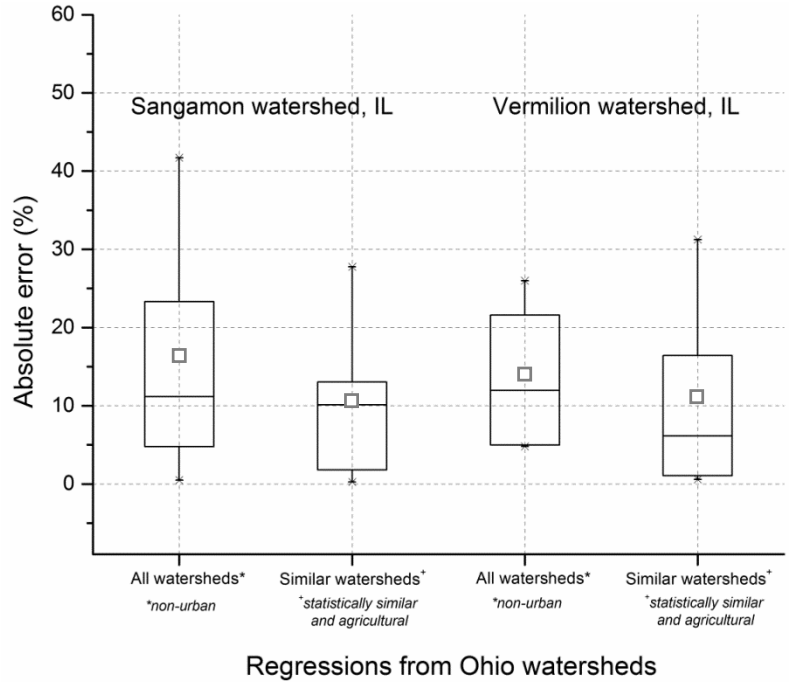

Figure 6.8: Relative error distributions for annual loads estimated using top 5 NO_3-N load events for watersheds in Illinois using two regression equations from Ohio watersheds. Small square symbol within the boxes indicates the mean of the distributions.

Table 6.10: Median, maximum, and standard deviation of relative errors for annual loads estimated from top 5 load events at two levels of aggregation for Illinois watersheds

Watershed	*All watersheds**			*Similar watersheds*		
	Median	*Maximum*	*SD*	*Median*	*Maximum*	*SD*
Sangamon	11	42	17	10	28	11
Vermilion (IL)	12	26	8	6	31	12
combined	11	42	11	7	31	11

Notes: * Cuyahoga data were excluded from regression.

6.4 Summary

The research results provided additional understanding of the pollutant dynamics as it relates to hydrologic variations. Water quality and flow data collected at 10 watersheds with different land uses in the US Midwest were analyzed. In particular, this study evaluated the role of large load events on annual pollutant load export by assessing the predictability of annual NO_3-N, TP, and SS loads by the top 1 to 5 load events in a year for eight watersheds in the Lake Erie and Ohio River basins and two watersheds in the Illinois River basin.

A pollutant-specific technique was designed to identify high flow events while considering mechanistic differences in pollutant loadings. Overall, results showed that the top load events for NO_3-N tend to last longer, carry a smaller percentage of annual loads and had higher prediction errors than TP and SS load events. High flow events defined based on pollutant loading were identified and separated by comparing the local-minimum and recursive digital baseflow filters from the WHAT baseflow separation tool (Kyoung et al., 2005). Regression relationships were developed between total pollutant loads exported by the few largest load events and total annual pollutant loads. Analysis of covariance (ANCOVA) was used to evaluate the statistical similarity of developed regression lines by comparing regressions for different watersheds for a particular pollutant.

This research shows that a majority of annual pollutant loads in Midwestern watersheds were exported in a few large load events. The top 5 load events carried on average 57 percent, 67 percent, and 56 percent of annual TP, SS, and NO_3-N loads, respectively. These top 5 load events combined lasted 15 percent, 14 percent, and 17 percent of the days in a year for TP, SS, and NO_3-N, respectively. These results clearly indicate that a small number of load events over a short period of time contribute a large portion of annual loads. Note that NO_3-N loads were carried over a longer time period than TP or SS loads associated with the same storm event.

Fairly strong regression relationships were observed for NO_3-N loads for all Ohio watersheds. The Cuyahoga, which is mainly a point-source driven watershed, had the lowest contributions to annual NO_3-N, T, and SS loads from top load events but the contributions were consistent over the complete monitoring duration.

Increased variation in annual NO_3-N, TP, and SS loads for the Maumee and Sandusky were likely related to climate-driven variations in annual loads and significant land management changes that occurred in these watersheds during the monitoring period. The strongest regression relationships for the TP load were observed for the Great Miami and Raisin watersheds. The impoundments on the Raisin tend to slow down the river flow acting as sediment sinks, altering the amount and timing of SS and TP loadings (Bosch, 2008). Impoundments also possibly minimize impacts of any land management and

nutrient abatement programs on relative contributions of top load event loads to annual loads, leading to more robust regression relationships. A strong regression relationship for TP loads was also observed for the Grand, indicating that such an approach can successfully be applied to watersheds that are not predominantly agricultural but are still dominated by non-point sources. Regression relationships developed to predict annual SS loads from top SS load events showed less uncertainty than regression relationships for TP or NO_3-N loads.

Analysis of Covariance (ANCOVA) was used to assess the similarity of regression relationships developed for different watersheds individually and for spatially aggregated data from multiple watersheds. The regression relationships from similar land use watersheds were found to be statistically similar to each other, indicating that they can be transferred spatially without losing predictive accuracy.

Annual NO_3-N loads for two watersheds in Illinois were estimated using the aggregated regression relationships to test the transferability of the developed approach to other watersheds with limited water quality data. The results indicated a reasonable estimate with absolute median errors of less than 12 percent for both watersheds. The median error decreased to less than 10 percent for both Illinois watersheds by using regression relationships from the similar land-use watersheds (agricultural). This validated the merits of this approach by showing that a regional regression relationship can be used to predict annual NO_3-N loads for similar watersheds which have the top load events monitored.

Strong correlations were identified between the pollutant loads exported during a few top load events and the total annual loads. Regression relationships were developed using top load events to predict total annual loads. These regression relationships were developed and evaluated at three levels of spatial aggregation: at the watershed level, spatial aggregation of similar watersheds, and spatial aggregation of all watersheds in a region.

The accuracy of annual pollutant load predictions increased as the level of spatial aggregation decreased. Regression relationships were weakest at the regional aggregation level and the strongest at the individual watershed level. This is expected since the watersheds differ in hydrological characteristics, geology, soils, climate, point-sources, land-use, and cropping patterns, and can have different pollutant loading patterns. A spatial aggregation of a larger number of watersheds is expected to have a larger variation in pollutant loading patterns leading to weaker regression relationships between annual loads and top load events. However, despite the slightly weaker performance of the regional-level spatially aggregated regression relationships, they still had median relative errors below 25 percent for annual load predictions. These errors are comparable or lower to other studies which have utilized the commonly used six to eight-week monitoring frequency for estimating pollutant loads for short monitoring periods (Guo et al., 2002; Robertson, 2003; Johnes, 2007; Verma et al., 2012)

Predictability of SS annual loads was the highest among the three pollutants analyzed. The prediction errors declined with the decreasing number of watersheds included in regression relationships for all three pollutants. The variation and mean errors for annual load predictions declined as more top load events were used to determine the regression relationships, indicating a trade-off in overall monitoring costs and annual load prediction accuracies.

7. Temporal Patterns of Pollutant Loadings

7.1 Introduction

This section identifies temporal patterns in pollutant loads (SS, TP, and NO_3-N) from eight watersheds in Ohio. Six of these watersheds drain to Lake Erie. They are amongst the largest draining into the lake and receive some of the highest nutrient and sediment inputs of any watersheds in all of the Great Lake basins mainly attributed to the intensive agriculture practiced in the region (Bosch et al., 2011). The majority of these watersheds are primarily agricultural, along with a few watersheds with significant presence of urban and forest lands. Collectively, they have a wide range of combinations of watershed sizes and land uses. This allows comparisons of temporal patterns in pollutant loadings for a variety of watershed characteristics.

This research and several other studies have demonstrated that pollutant loadings from watersheds mainly happen during a few high flow periods in a year (Richards and Holloway, 1987; Preston et al., 1989; Lewis, 1996; Robertson and Roerish, 1999; Cooper and Watts, 2002; Markus and Demissie, 2006; and Salles et al., 2008). The timing of nutrient loadings during a year is strongly tied to the timing of these critical events that export most of the loads from the watersheds. The loads exported during flood events were computed and analyzed in the previous section. The critical high flow periods were different for each pollutant due to mechanistic differences in loading processes for pollutants such as SS and TP whose loadings tend to peak and ebb with flow more closely than for NO_3-N whose loading tends to peak and ebb more slowly (e.g., Fig 3.3).

The temporal analysis in the study was performed in two parts, first on the top five load events, and second on daily pollutant loads and concentrations. Specifically, the objectives of this study were to apply circular statistics to (i) identify temporal patterns in the export of pollutants from the top 5 load events in watersheds in the Lake Erie and Ohio River basins, and (ii) evaluate the temporal distribution of daily average precipitation, flow, pollutant concentrations, and loads within a year in watersheds in the Lake Erie and Ohio River basins.

7.2 Methods

7.2.1 Circular Histograms

In hydrology, many commonly measured parameters which show temporal periodicity may be represented on a circular scale instead of the traditionally used linear scale. There is no fixed zero on a circular scale which perhaps better characterizes the parameters which are periodically continuous. For example, the mean daily flow at a gaging station on December 31st would be similar to that on January 1st. This continuity is better represented on a circular scale rather than on the discontinuous linear scale. Circular scales and statistics can be applied to data such as day of year which exhibit a certain periodicity, not just to parameters measured in angles such as wind speed (Berens, 2009). Continuous or average periodic data can be represented on a circular scale using circular histograms along with its mean resultant vector.

7.2.2 Mean Daily Value and Regularity

Continuous or average periodic data can also be used to compute the Mean Daily Value (MDV) over each periodic cycle with its corresponding regularity. The MDV is a statistical term that should not be confused with daily average. The MDV represents the temporal occurrence of the mean of the angular

data (through direction). It is important to note that the MDV only denotes the timing of the mean on a circular scale and not its magnitude. In a very simplistic manner, it is the day of the year that corresponds to the mean.

The daily linear time series can be converted to the angular scale using the following set of equations. The day of the maximum parameter value (example: precipitation, flow) in a year *i* can be expressed on an angular scale in radians (θ_i) by applying the following transformation (7.1):

$$\theta_i = JD_i \frac{2\pi}{ND_i} \tag{7.1}$$

where, JD_i is the Julian day of the maximum parameter value in a year and ND_i is the total number of days in year *i*.

After linear data have been transformed to an angular scale, the mean of these transformed values cannot be calculated by simply averaging the data points. The angular values need to be transformed to unit vectors in the two-dimensional plane by using the sine and cosine functions. The mean angular direction $\bar{\theta}$ is then computed using the inverse tangent function. The MDV is calculated from total number of days in a year (ND) and the mean angular direction $\bar{\theta}$. The MDV indicates the occurrence of the maximum parameter value over N years of time-series data (7.2).

$$\bar{x} = \frac{1}{N}\sum_{i=1}^{N}\cos(\theta_i)$$

$$\bar{y} = \frac{1}{N}\sum_{i=1}^{N}\sin(\theta_i) \tag{7.2}$$

$$\bar{\theta} = \tan^{-1}\left(\frac{\bar{y}}{\bar{x}}\right);(0 \leq \bar{\theta} \leq 2\pi)$$

$$MDV = \bar{\theta}\frac{\overline{ND}}{2\pi}$$

Markus et al. (2012) modified the traditional MDV by incorporating weights corresponding to daily parameter values in the calculations. These modified MDV calculations added more significance to the extreme parameter values which are essential when temporal trends are being examined. The weight w_i is calculated using the maximum parameter value P_i in the year i for the N years of record (7.3).

$$w_i = N \times \frac{P_i}{\sum_{j=1}^{N} P_j} \tag{7.3}$$

The weighted MDVs can then be calculated using the following set of equations (7.4):

$$\bar{x}_w = \frac{1}{N}\sum_{i=1}^{N} w_i \cos(\theta_i)$$

$$\overline{y_w} = \frac{1}{N}\sum_{i=1}^{N} w_i \sin(\theta_i) \qquad \textbf{(7.4)}$$

$$\overline{\theta_w} = \tan^{-1}\left(\frac{\overline{y_w}}{x_w}\right);(0 \leq \bar{\theta} \leq 2\pi)$$

$$MDV = \overline{\theta_w}\frac{\overline{ND}}{2\pi}$$

where the subscript w indicates the weighted estimates.

The regularity $\bar{r}$ can then calculated by taking the square root of the sum of squares of the unit vectors. The regularity denotes the concentration of the data around this mean direction. The regularity is usually normalized, ranging between 0 and 1. Higher regularity indicates that the data are more concentrated around the mean direction.

$$\bar{r} = \sqrt{\bar{x}^2 + \bar{y}^2}\ ;\ (0 \leq \bar{r} \leq 1) \qquad \textbf{(7.5)}$$

The weighted regularity $\overline{r_w}$ can then be calculated as

$$\overline{r_w} = \sqrt{\bar{x}_w{}^2 + \bar{y}_w{}^2}\ ;\ (0 \leq \overline{r_w} \leq 1) \qquad \textbf{(7.6)}$$

7.3 Principal Findings and Significance

7.3.1 Circular Histograms

Circular histograms were created for the top 5 precipitation events and top 5 TP and SS load events in the Ohio watersheds (Figure 7.1 and Figure 7.2). The scales were normalized, by dividing the monthly totals by the maximum total number of top 5 events that occurred over a specific month for both loads exported and precipitation totals. A vector resultant (magnitude of the vector), indicated by an arrow within the circular charts, indicates the timing (net resultant direction) and degree of concentration along the vector resultant.

Most of the top 5 TP and SS load events occurred from February to May. The patterns in the concentration peaks for TP and SS are similar (very close alignment with hydrograph peaks). The top 5 load events for both pollutants were concurrent with very few exceptions. The urbanized Cuyahoga watershed with significant point sources saw the most even distribution of the top 5 SS and TP load events on an annual scale when compared to the other agricultural watersheds dominated by non-point sources.

On the contrary, most of the top 5 precipitation events occurred from May to September. TP and SS are largely exported by surface runoff and are more influenced by precipitation events. The late spring, early summer months are generally characterized by higher flows, colder temperatures, and no or a small crop presence with very shallow rooting depths. This leaves the soils and any applied fertilizers susceptible to surface runoff. As the growing season progresses, the higher temperatures, increased plant uptake, and deeper rooting depths contribute to lower flows and limit the TP and SS loadings of these constituents.

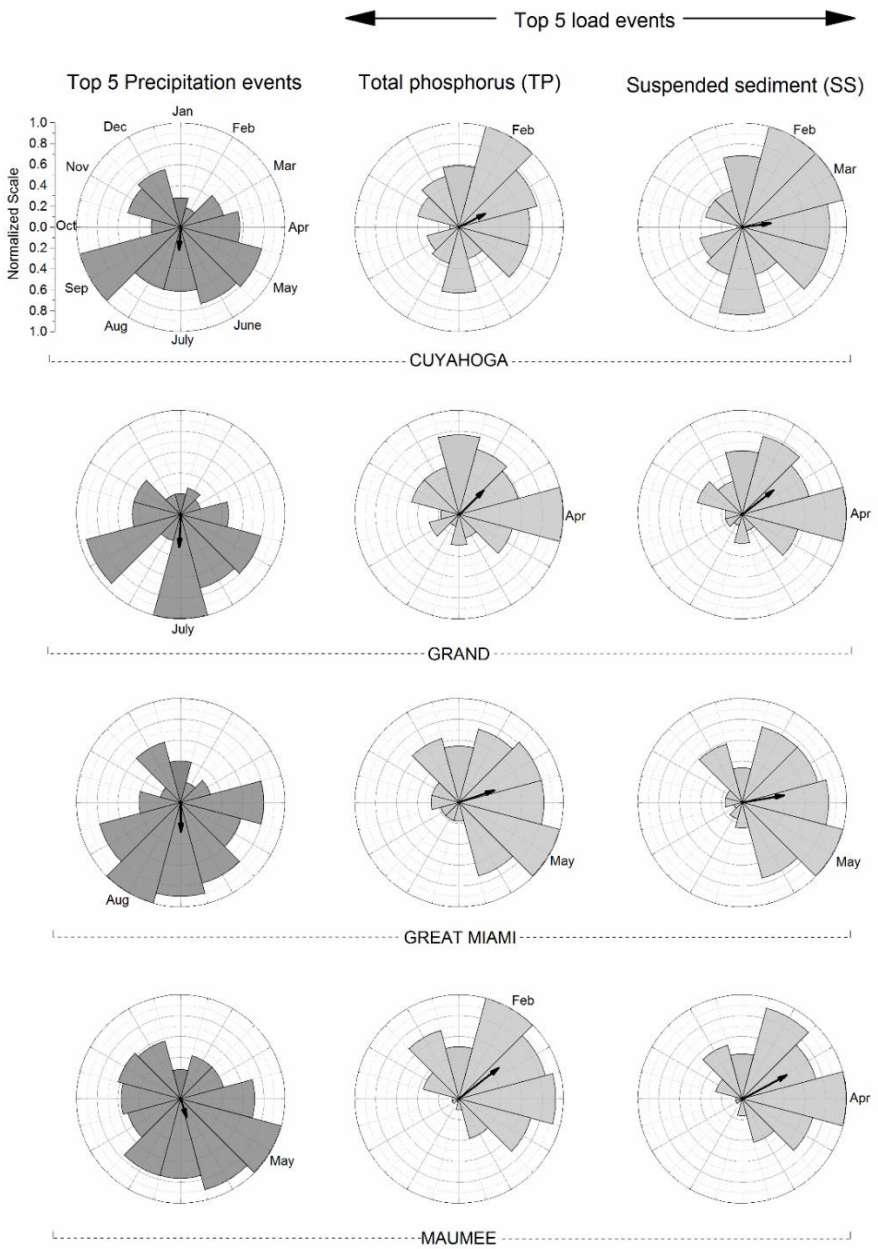

Figure 7.1: Normalized number of top 5 precipitation events, top 5 TP load events, and top 5 SS load events: Cuyahoga, Grand, Great Miami, and Maumee

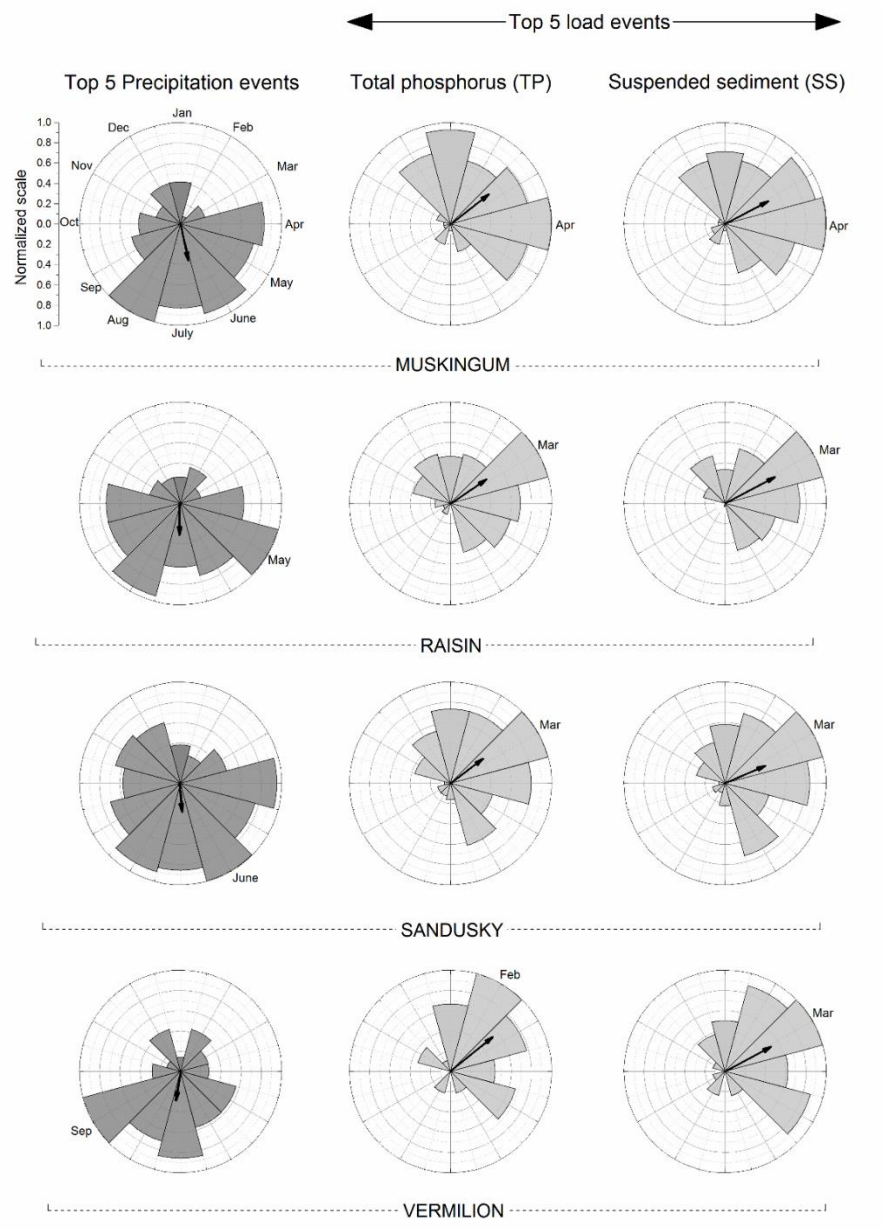

Figure 7.2: Normalized number of top 5 precipitation events, top 5 TP load events, and top 5 SS load events: Muskingum, Raisin, Sandusky and Vermilion (OH) watersheds

Circular histograms were also created for the top 5 NO_3-N load events and top 5 precipitation events (Figure 7.3). The top 5 NO_3-N load events mainly occurred in the months between November and April, a little earlier than the top 5 SS or TP load events. In the agricultural watersheds, the top 5 NO_3-N load events occurred from February to April. In the forested Grand watershed, the top 5 NO_3-N load events occurred from November to December. In the urbanized Cuyahoga watershed, the top 5 NO_3-N load events occurred from December to March.

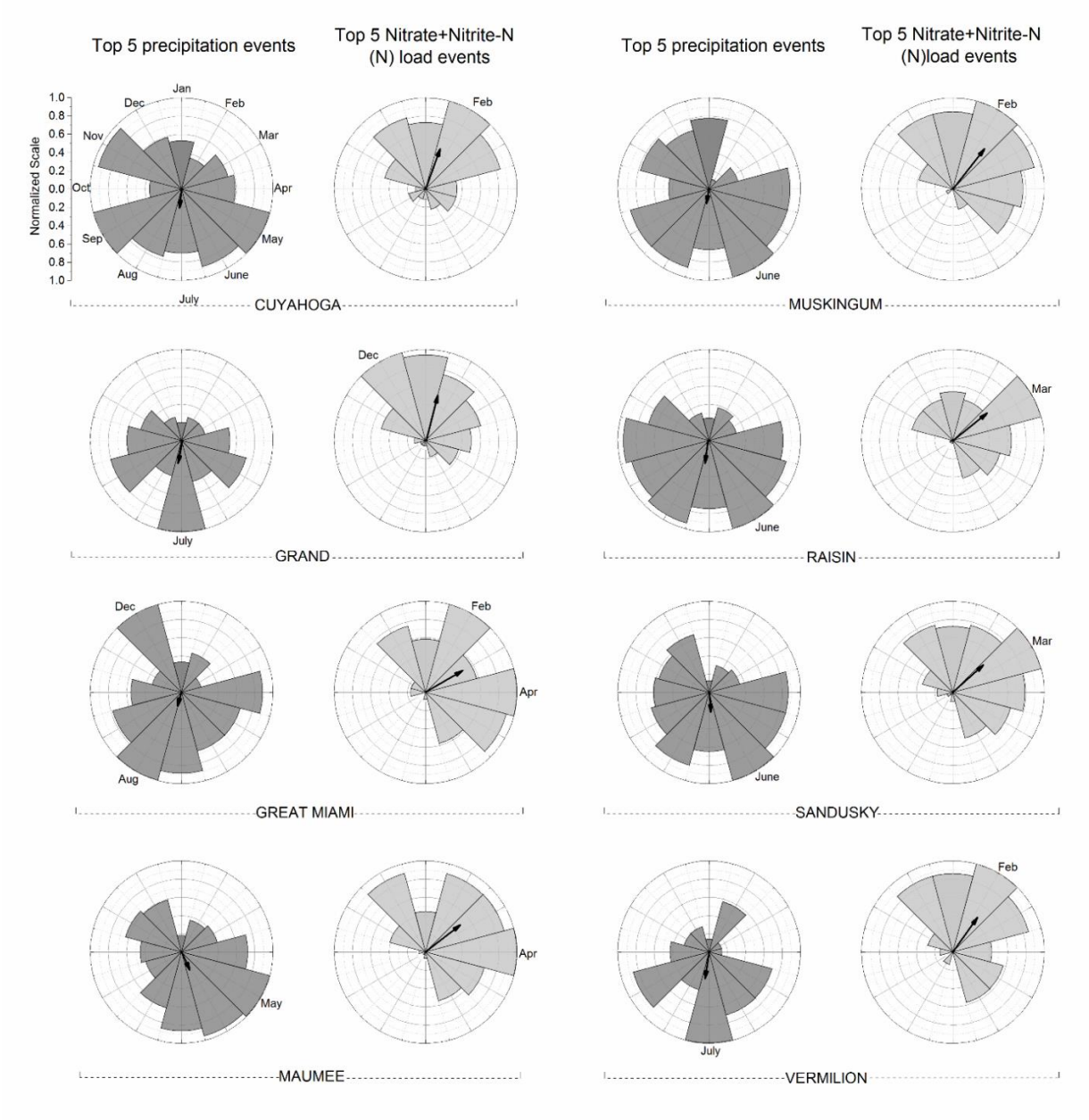

Figure 7.3: Normalized number of top 5 precipitation events, and top 5 NO_3-N load events.

Again, most of the top 5 precipitation events in these watersheds occurred over the late summer months. NO_3-N loadings typically occurred during winter or early spring. This period coincides with the fallow period in Midwestern agricultural watersheds. The lack of crops together with lower temperatures limits the amount of water taken up by vegetation. Mean monthly flows are also higher during this period. Snow melt also potentially contributes to higher flows in late winter and early spring. As nitrates are highly soluble in water, any residual and excess fertilizer within the fields dissolves and exports quickly through the extensive sub-surface tile drain network commonly present in the study area. The practice of fall application of nutrients that is still observed in the study area adds nutrients to the fields, leaving them highly susceptible to leaching with any significant precipitation event or snow melt. Any precipitation

falling over these watersheds in the winter-early spring months coupled with snow melt exports a significant amount of nitrate-rich water from agricultural fields.

Very few top 5 NO_3-N load events were observed over the summer months in spite of higher precipitation totals during such events. In summer months, the crop growing cycle is at its peak with significant uptake of water and nutrients by the crops. This inhibits the flow as well as nitrate losses considerably as compared to the winter months. However, a large precipitation event after a long dry spell can still export substantial NO3-N loads. Such occurrences were usually seen in the beginning of the summer, albeit only once or twice each year.

The vector resultants from the circular histograms were compiled together to compare the timing of the top 5 NO_3-N and TP load events as well as the top 5 precipitation events. The resultant vectors for SS load events were omitted from this analysis since they very closely followed the pattern established for TP. The vector resultants were plotted with time on the x-axis and their magnitude on the y-axis (Figure 7.4). The timing corresponds to the direction of the vector resultants in the circular histograms, and the normalized vector length corresponds to the size of the resultant vector (vector magnitude). The difference between the temporal distribution of the top 5 precipitation events, top 5 NO_3-N events, and top 5 TP events is striking. Resultant vectors for the top 5 precipitation events have a much smaller size and occur much later than resultant vectors for the top 5 TP or NO_3-N load events. There is a larger variation in timing of resultant vectors for NO_3-N than for TP. On the other hand, there is a larger variation in magnitude of resultant vectors for TP than for NO_3-N. Higher vector magnitudes for NO_3-N indicated that the top 5 NO3-N load events were concentrated around a small period in a water year. Three watersheds have a resultant vector for the top 5 TP events that are smaller than the rest: Cuyahoga, Grand, and Great Miami. This indicated a more even spread of the top 5 TP load events in these watersheds during a water year.

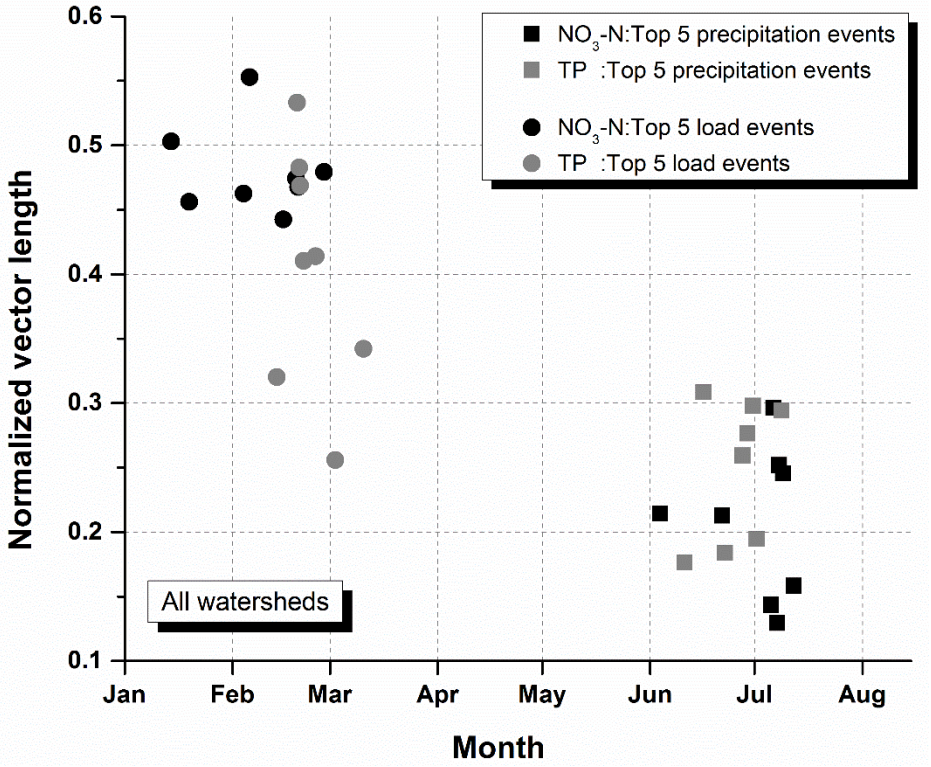

Figure 7.4: Timing and magnitude of resultant vectors for the top 5 NO_3-N and TP load events and top 5 precipitation events

Monthly averages of Thiessen weighted precipitation, flow, TP, and NO_3-N loads were computed for the Maumee using all events during the 28-year period of record. This analysis complements and validates the analyses presented above for the top 5 load events. The circular histograms are presented in Figure 7.5. The highest precipitation occurred from May to August. However, relatively lower flows were observed during the same time. The highest flows occurred from February to April. The average monthly NO_3-N and TP loads were very closely aligned with the flow pattern.

This analysis confirms that loads are very closely correlated with flow volumes, although some differences can be identified (Figure 7.6). The highest average flow occurred in March. Both February and April average flows were about 20 percent lower than the March flow. However, the TP load in April is still at 95 percent of the highest TP load that occurred in March. The NO_3-N load is even more delayed. The highest NO_3-N load occurred in April. The TP load in March was at 95 percent of the highest NO_3-N load. The TP load in May falls to 55 percent of the highest TP load. The NO_3-N load remains much higher at 78 percent of the highest NO_3-N load. Low flow months contributed smaller proportions of TP and NO_3-N load to annual loads than of flow to annual flow during the same time period (Figure 7.6).

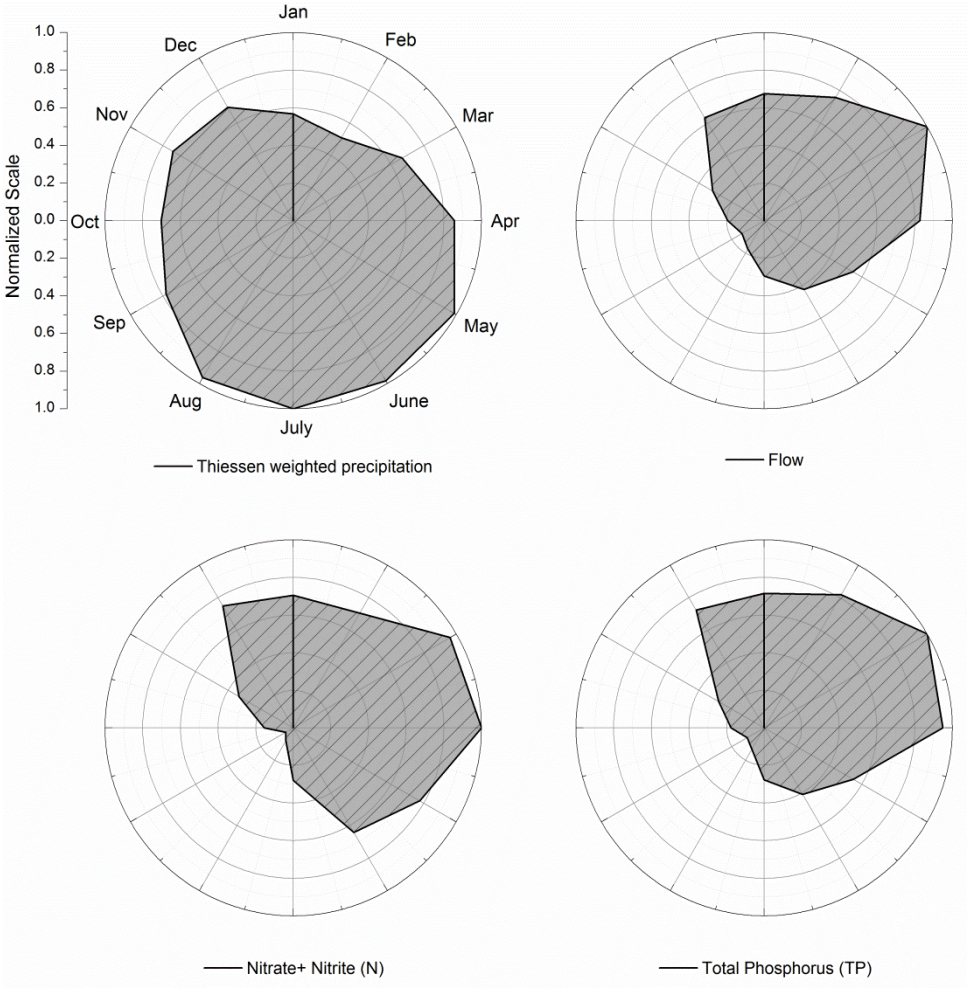

Figure 7.5: Circular histograms of monthly averages for Thiessen weighted mean areal precipitation, flows, TP loads, and NO_3-N loads: Maumee

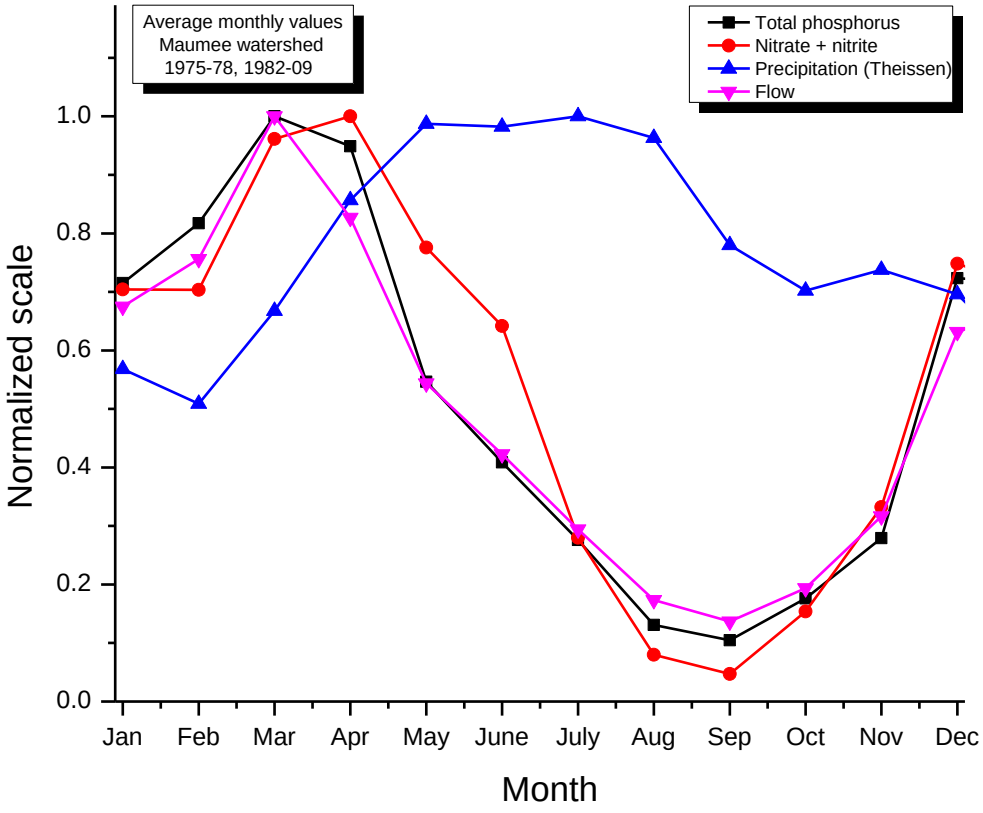

Figure 7.6: Monthly averages of Thiessen weighted mean areal precipitation, flows, TP loads, and NO_3-N loads: Maumee

7.3.2 Mean Daily Values and Regularity

MDVs and their corresponding regularity were calculated for precipitation, flow, pollutant concentrations, and loads to assess the temporal changes in watersheds for each water year during the monitoring period. Four Ohio watersheds with the longest duration of monitoring data were selected for this analysis: the Maumee, Sandusky, Cuyahoga, and Raisin. The Maumee, Sandusky, and Raisin watersheds are primarily agricultural. The Cuyahoga watershed is predominantly urbanized. The Raisin watershed is unique as it has many impoundments dotting the course of the Raisin River. Table 7.1 summarizes the MDVs and Table 7.2 the corresponding regularities for the four watersheds.

Table 7.1: Average and standard deviation for MDVs: precipitation, flow, and SS, TP and NO_3-N concentrations and loads

Watershed	Precipitation		Flow		SS				TP				NO_3-N			
					concentration		load		concentration		load		concentration		load	
	μ	σ	μ	σ	μ	σ	μ	σ	μ	σ	μ	σ	μ	σ	μ	σ
Maumee	187	12.8	145	26.4	169	20.3	141	38.9	177	13.4	143	35.7	161	18.9	147	29.4
Sandusky	187	12.6	138	27.8	162	18.9	134	34.6	170	16.5	137	36.1	154	25.9	137	33.1
Raisin	191	14.5	146	23.7	172	20.7	139	37.9	182	14.1	142	35.9	163	18.5	143	35.8
Cuyahoga	190	11.7	161	16.1	176	24.3	163	38.8	191	10.6	166	25.3	200	10.8	176	13.7

Notes: *The MDVs are represented in days after the beginning of the water year (1 = October 1st).

Table 7.2: Average and standard deviation for regularities: precipitation, flow, and SS, TP and NO_3-N concentrations and loads

Watershed	Precipitation		Flow		SS				TP				NO_3-N			
					concentration		load		concentration		load		concentration		load	
	μ	σ	μ	σ	μ	σ	μ	σ	μ	σ	μ	σ	μ	σ	μ	σ
Maumee	0.17	0.08	0.45	0.17	0.26	0.12	0.56	0.20	0.13	0.07	0.51	0.18	0.31	0.13	0.48	0.17
Sandusky	0.17	0.07	0.49	0.13	0.36	0.13	0.57	0.16	0.19	0.1	0.55	0.16	0.33	0.15	0.50	0.14
Raisin	0.17	0.08	0.42	0.12	0.21	0.10	0.53	0.15	0.12	0.08	0.5	0.14	0.30	0.11	0.51	0.17
Cuyahoga	0.13	0.07	0.30	0.11	0.27	0.12	0.39	0.17	0.15	0.07	0.28	0.11	0.21	0.07	0.15	0.07

Precipitation

Figure 7.7 presents the MDVs and the corresponding regularities for precipitation over the four watersheds for each water year. The dark blue circular markers in the figure show MDVs, i.e., the timing of precipitation for different water years (1-366 days after the beginning of the water year, 1= October 1st). The sizes of the circular markers were rescaled based on total maximum precipitation observed in a single water year in all four watersheds. As expected, the results indicated that the precipitation patterns in these watersheds are fairly similar to each other with comparable annual amounts, timing of MDVs, and also temporal distribution. The average MDVs ranged between 187 and 191 days after the start of the water year with standard deviations ranging between 12.6 and 14.5 days for the four watersheds individually.

The regularity of the MDVs was the same at 0.17 for the three agricultural watersheds and slightly lower at 0.13 for Cuyahoga. The standard deviation of the average regularity values was very close for all

four watersheds (from 0.07 to 0.08). The low regularity values show that precipitation is fairly evenly distributed throughout the year in all these watersheds. No significant differences or trends in precipitation occurrence and amounts were identified among the four watersheds. Any potential differences in MDVs or regularities for flows, pollutant concentrations, and pollutant loads can thus be assumed solely due to differences in watershed characteristics or the pollutant itself.

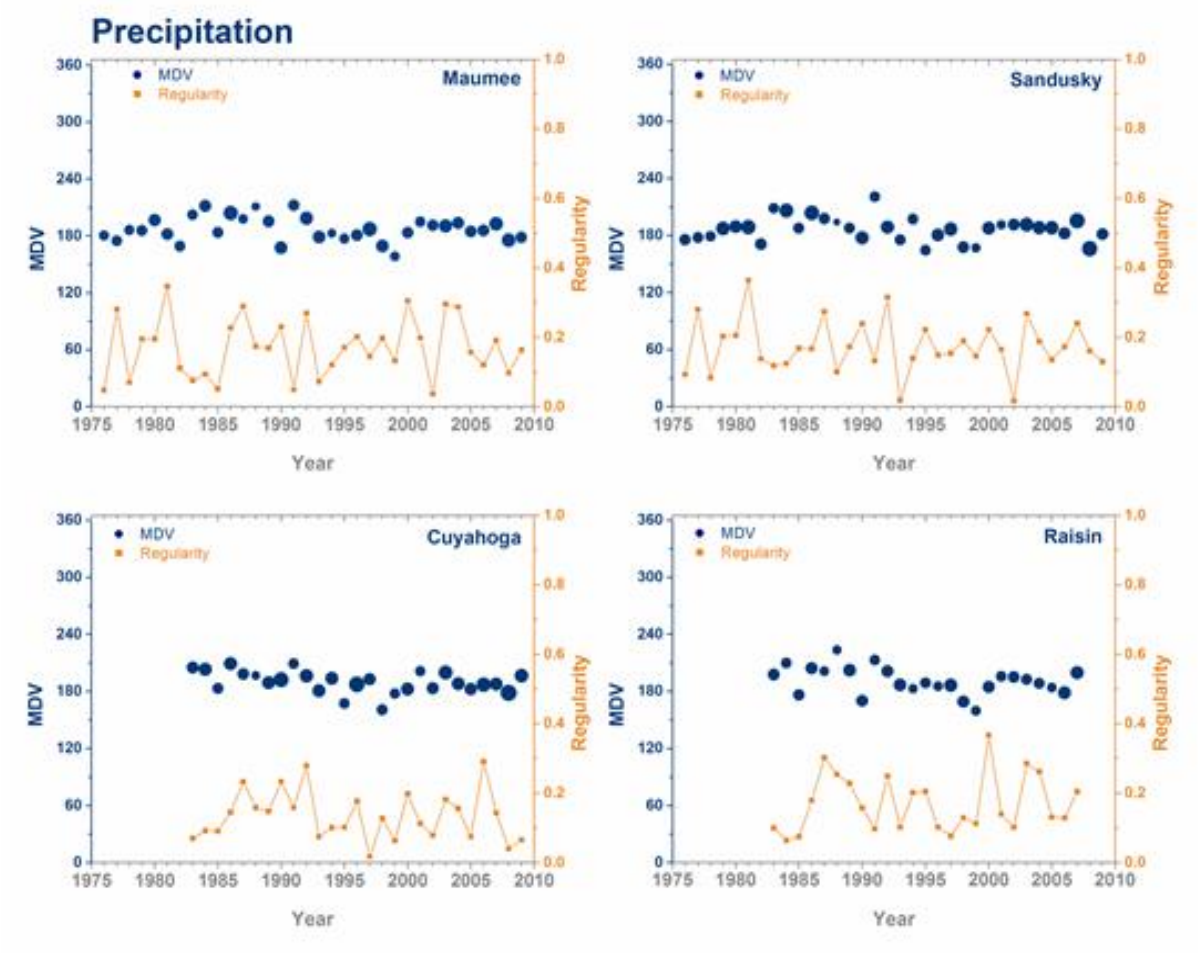

Figure 7.7: MDVs and their corresponding regularity values for precipitation. The MDVs are represented by dark blue circular markers (shown in days after the beginning of the water year). Circular markers are proportional to the maximum annual precipitation.

Flow

Figure 7.8 presents the MDVs and their corresponding regularities for flows in the four watersheds for each water year. The size of the dark blue circular markers is relative to the average annual unit area flow (i.e., average annual flow divided by the watershed area). No significant trends were observed in the MDV values, indicating there hasn't been a change in the temporal distribution of flow during the two to three decades of monitoring in these watersheds.

The average MDVs for the three agricultural watersheds ranged from 138 to 146 days after the beginning of the water year. The average MDV for flow for the Cuyahoga watershed was 161 15-23 days later than the average MDVs of the agricultural watersheds. Impervious surfaces do not provide the infiltration, retention, and evapotranspiration that lower runoff from pervious surfaces with vegetative cover provide. This leads to a higher seasonal fluctuation in average monthly flows in non-urbanized watersheds than in urbanized watersheds. Urbanized watersheds produce relatively higher floods as a response to precipitation events during the warm season than non-urbanized watersheds. The higher flows later in the season then reflect in the higher MDVs for the urbanized watershed than for the agricultural watersheds.

Impervious surfaces also affected the average unit area flow. The Cuyahoga had consistently the highest average unit area flow when compared to the agricultural watersheds. The Maumee and Sandusky showed a large variability in average unit area flows. The average annual unit area flow from the Raisin was the smallest amongst the four watersheds. The lower unit area flows are probably related to the presence of impoundments in this watershed which increase the water residence time and surface storage, allowing for higher evapotranspiration. Many of these actively operated dams managing impoundments are regulated to be managed as " instantaneous run-of-river mode," as recommended by the Michigan Department of Natural Resources, ensuring impoundment inflows equal outflow which limits water-level fluctuations (Bosch, 2008). However, as also reported by Bosch (2008), it is not clear if these requirements are followed closely as inferred by communications from downstream communities regarding seasonal fluctuations in lake levels and lowering in preparation for large precipitation events for flood control.

The highest regularity (0.49) was observed for the Sandusky watershed (Table 7.2). The value was comparable to flow regularities for the other two agricultural watersheds, the Maumee and Raisin (0.45 and 0.42, respectively). The average regularity for the Cuyahoga flow was the lowest amongst the four watersheds at 0.30 along with the least variability with a standard deviation of 0.11. The Cuyahoga flows are more evenly distributed throughout the year and have the least amount of variation among the four watersheds.

The Maumee watershed showed the highest variability in the regularity with the standard deviation of 0.17. The standard deviation for the Sandusky and Raisin regularity was 0.13 and 0.12, respectively. The highest regularities generally occurred in these agricultural watersheds for years with lower average annual unit area flows.

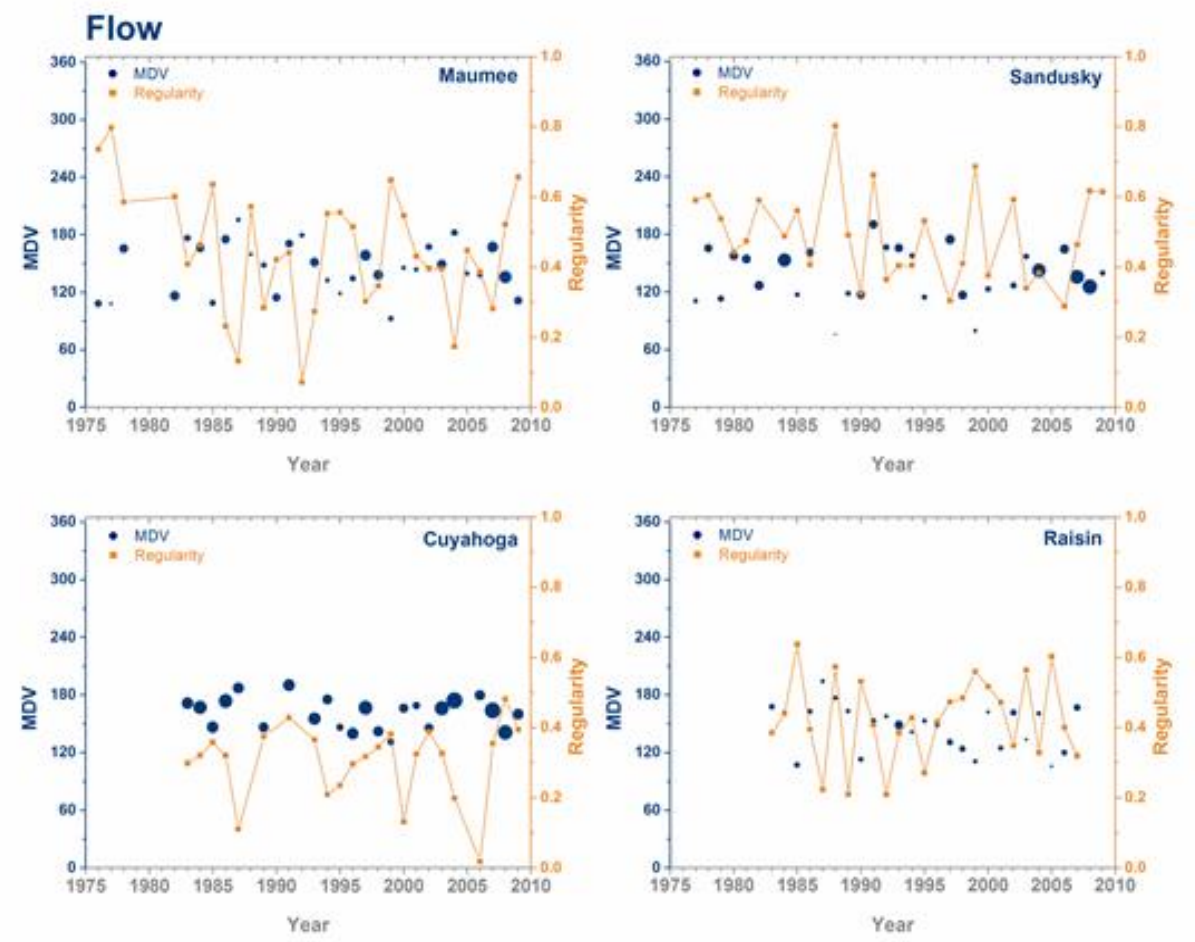

Figure 7.8: MDVs and their corresponding regularity values for flow. The MDVs are represented by dark blue circular markers (shown in days after the beginning of the water year). Circular markers are proportional to the maximum average annual flow.

Suspended Solids (SS)

Figure 7.9 shows the MDV and regularity values for SS concentrations in the four watersheds. The size of the circular markers is proportional to the maximum average annual SS concentration observed in any of the four watersheds over all water years. Table 7.1 and Table 7.2 summarize the mean and regularity values for the average SS concentration MDVs and observed in the watersheds, respectively. The MDVs for SS concentrations for all the watersheds were very close to each other with individual averages ranging between 162 and 179 days after the start of the water year. The standard deviations in the MDVs were also similar for all the agriculture watersheds (19 to 21 days). The standard deviation in MDVs was slightly higher for the Cuyahoga (24 days).

The Raisin watershed had the lowest average regularity value at 0.21. This indicates that the SS concentrations were more evenly distributed throughout the year in the Raisin watershed than in the other watersheds. The Sandusky watershed had the highest average regularity at 0.36 and the lowest average MDV at 162 days. Interestingly, these extremes in average regularity values were found between the Raisin and Sandusky watersheds which are very similar in size and land use.

SS concentrations in the Maumee and Sandusky watersheds were higher in the first half of their respective monitoring periods, with some of the highest average annual concentrations recorded after the drier water years (e.g., 1988 was a dry year and higher concentrations were observed in 1989-1990). The highest annual average SS concentrations were observed in the Cuyahoga watershed, the smallest amongst all the watersheds. The highly urbanized landscape coupled with the largest share of the point source pollution probably caused an export of SS with higher concentrations.

The MDV and regularity results for SS loads are summarized in Figure 7.10 and Table 7.1. The circular dark blue dots denoting MDVs were sized according to average annual unit area SS loads (loads divided by the watershed area). The average MDVs for SS loads for the three agricultural watersheds were found to be similar, ranging between 134 and 141 days. The average MDV for SS loads for the Cuyahoga watershed was 163 days, 22-29 days later than the agricultural watersheds. The standard deviations of MDVs for SS loads ranged from 35 to 39.

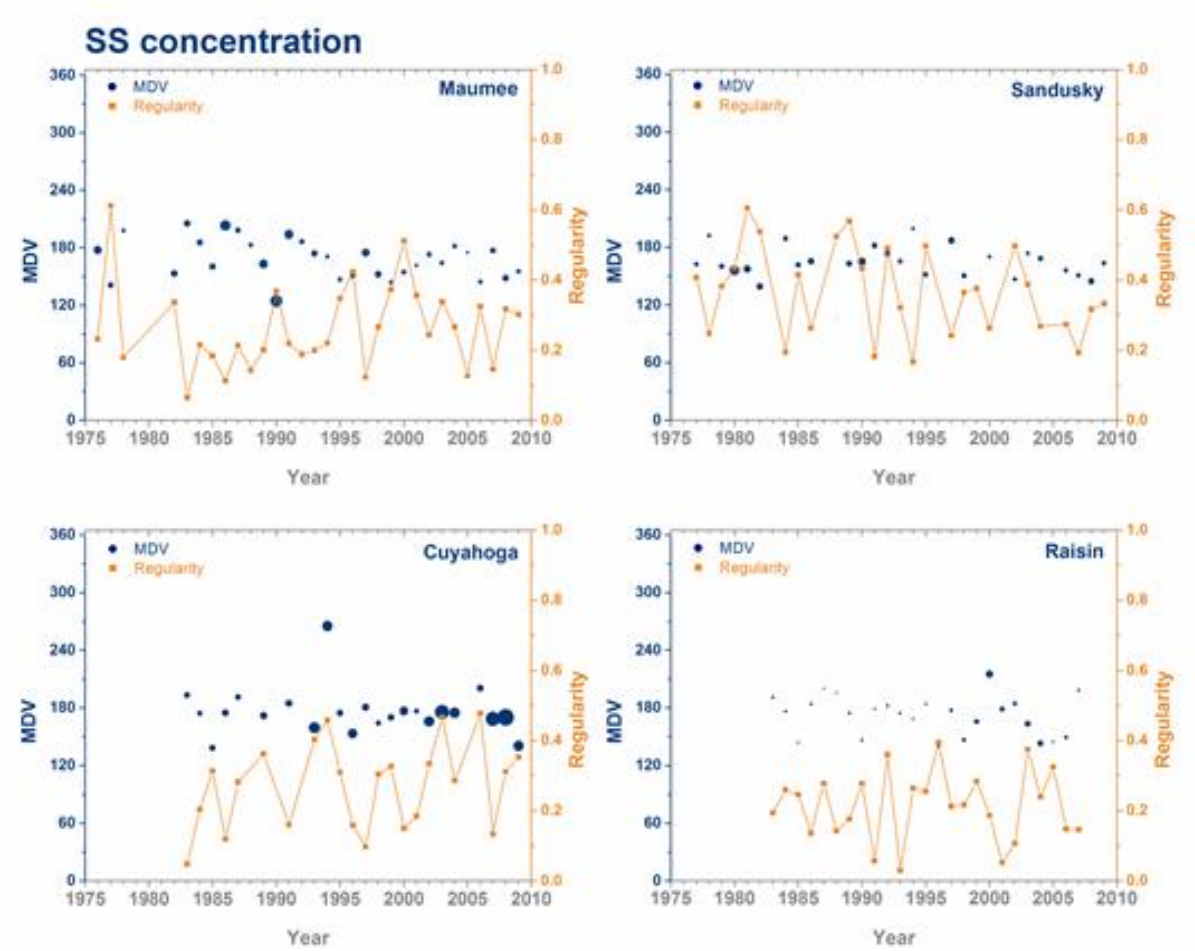

Figure 7.9: MDVs and their corresponding regularity values for SS concentrations. The MDVs are represented by dark blue circular markers (shown in days after the beginning of the water year). Circular markers are proportional to the maximum average annual SS concentration.

The average regularity values for SS loads were also similar among the agricultural watersheds, ranging from 0.53 to 0.57. The average regularity for the Cuyahoga was 0.39, slightly lower than regularities for the other watersheds. The peaks in regularity for the Maumee and Sandusky watershed typically occurred during water years with smaller annual average SS loads per unit area as is visually evident in Figure 7.10. The regularity values for SS loads were significantly higher than regularity values for SS concentrations or even flows, indicating that SS loads were more concentrated in a year than flows or concentrations.

The Cuyahoga watershed had the highest average annual unit area SS loads amongst all watersheds (Figure 7.10). Both the Maumee and Sandusky showed a large variability in average annual unit area SS loads. Several high average annual unit area SS loads were observed for the Sandusky watershed in the earlier part of its monitoring period before 1985.The differences in annual average SS concentrations for the Cuyahoga and Raisin watersheds noted previously were magnified when the SS loads were analyzed; note the relatively large dots for the Cuyahoga watershed and virtually indistinguishable ones for the Raisin watershed.

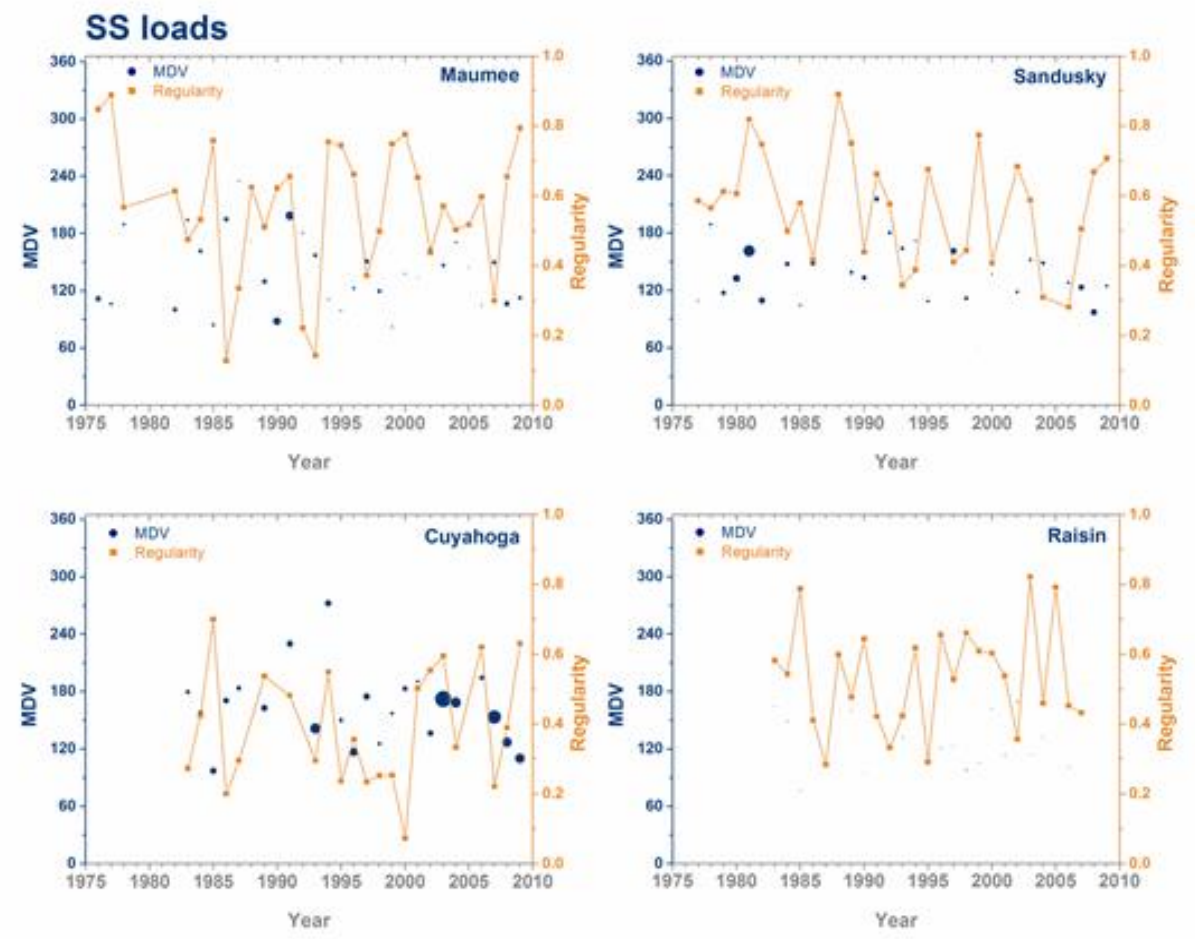

Figure 7.10: MDVs and their corresponding regularity values for SS loads. The MDVs are represented by the dark blue circular markers (shown in days after the beginning of the water year). Circular markers are proportional to maximum of average annual unit area SS loads.

Relatively low SS concentrations and SS loads were observed in the Raisin watershed. The presence of numerous impoundment dams along the Raisin River possibly altered the river sediment export dynamics. Impoundments are expected to act as nutrient and sediment sinks in river systems as reported by numerous studies (Alexander et al., 2002; Dixit et al., 2000; Kling et al., 2000). The impoundments increase water residence time allowing sediment and associated nutrients to settle out, thereby removing them from the river flow (Stanley and Doyle, 2002). Vorosmarty et al. (2003) reported that possibly 25-30 percent of the world's annual sediment flux in rivers is trapped in reservoirs. Settling in impoundments reduces average sediment concentrations and loads, and also possibly offsets the impacts of extreme events which might export high SS concentrations and loads from the watershed.

Total Phosphorus (TP)

Figure 7.11 shows the MDVs and regularity values for TP concentrations in the four watersheds. The size of the circular markers representing MDVs was normalized based on the maximum of the average annual concentrations recorded at any of the four watersheds. The MDVs for TP concentrations followed similar relationships as those for SS concentrations. The average MDVs for the three agricultural watersheds ranged between 170 and 182 days, slightly lower than the average MDV for the urbanized Cuyahoga watershed (191 days). The standard deviations for the MDVs ranged from 13 to 17 for the three agricultural watersheds. The standard deviation for the MDV was 10.6 days for the Cuyahoga.

The regularity values for TP concentrations were the lowest of all pollutant concentrations studied in this research, ranging between 0.12 and 0.19. The highest regularity was observed in the Sandusky watershed (0.19). The variability in both MDVs and regularity values for TP concentrations was the lowest among the three pollutants analyzed.

The highest annual average TP concentrations were seen for all the watersheds in the first half of their monitoring periods. There was a distinct decline in the annual average TP concentration in the Cuyahoga watershed after the mid-1980s, likely due to implementation of the NPDES programs regulating phosphorus discharge from point sources. Even the Maumee watershed and the Sandusky watershed saw declines in annual average TP concentrations to some extent after policy regulations reducing TP loadings were implemented in the area. The highest annual average TP concentrations were observed in the Cuyahoga watershed. The Maumee had consistently high annual average TP concentrations. The Raisin watershed consistently had the lowest annual concentrations, partly due to the presence of the dams in the watershed.

The MDVs and regularity results for the TP loads are shown in the Figure 7.12. The sizes of the dark blue circular markers indicating MDVs were proportioned based on the maximum of the average annual unit area TP loads. The averages and standard deviations for the MDVs and regularity for TP loads were again very similar to those for SS loads for most watersheds. The Cuyahoga was a notable exception with a standard deviation for MDV of 25 days, standard deviation for the regularity of 0.11, and a regularity of 0.28. This indicates that SS and TP loads in the Cuyahoga may be affected by different processes with point sources and non-point sources playing different roles in transport of these constituents.

Overall there was much more variation in the temporal averages of the TP loads compared with the TP concentrations over the years these watersheds were monitored. The average MDVs ranged from 137 to 143 for the three agricultural watersheds. The standard deviation was 36 days for the three agricultural watersheds. The average for the MDVs for the Cuyahoga watershed was 166 days with a standard deviation of 25 days. Similar to the SS loads, this average was 23-29 days later than that of the agricultural watersheds.

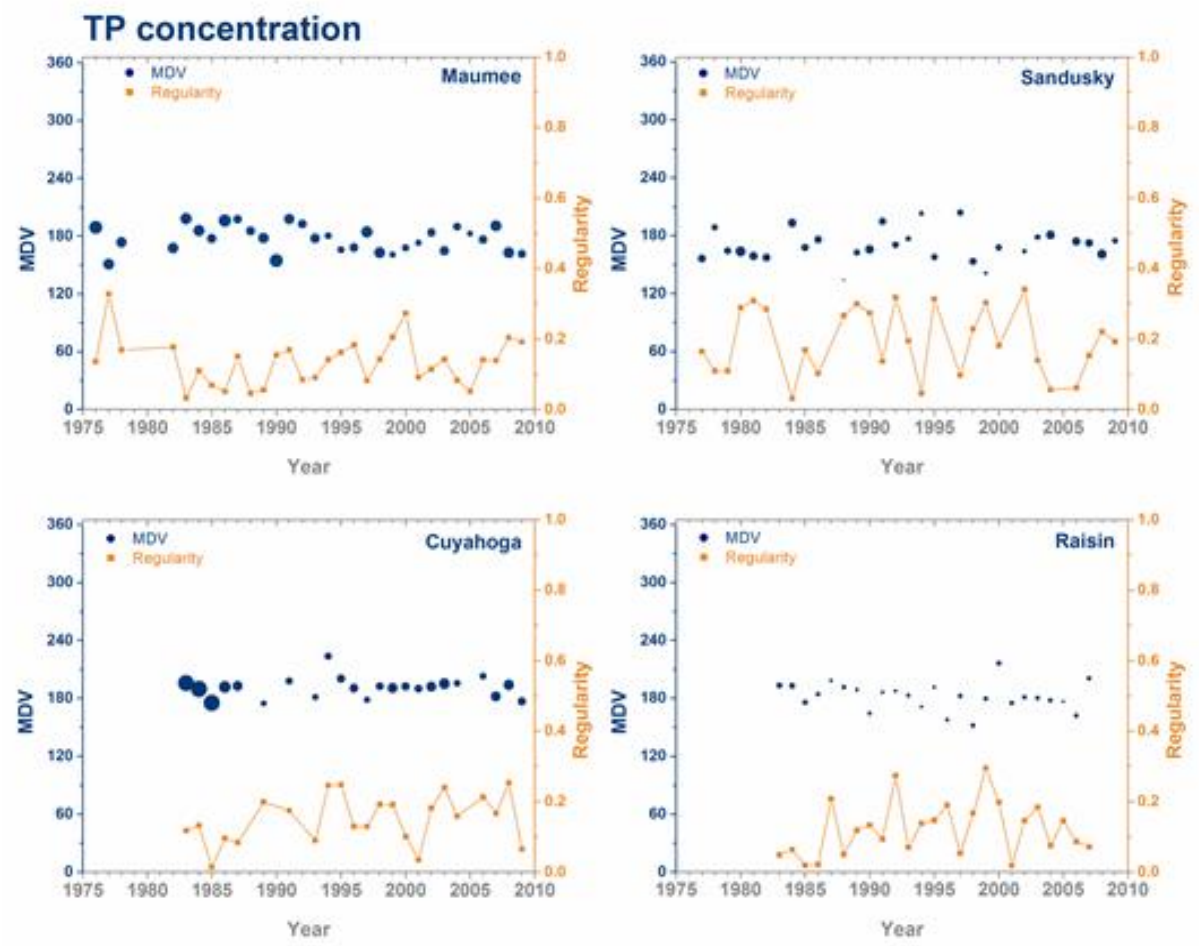

Figure 7.11: MDVs and their corresponding regularity values for TP concentrations. The MDVs are represented by dark blue circular markers (shown in days after the beginning of the water year). Circular markers are proportional to the maximum of average annual TP concentrations.

The higher regularity values show that the TP loads were much more concentrated temporally than TP concentrations in these watersheds. Regularity values for TP loads ranged from 0.50 to 0.55 for the agricultural watersheds. These values were slightly lower than regularity values for SS loads. The relatively lower average regularity seen in the Cuyahoga watershed (0.28) was likely due to the higher percentage of point sources contributing to the total TP load. Point sources are not affected by seasonal changes that can be seen in loading patterns in agricultural watersheds and attributed to crop growing cycles.

The peaks in regularity values for the Maumee and Sandusky watersheds were typically accompanied by lower average annual TP loads, very likely occurring during drier years in which the load export was low and concentration increased over a small period. For example, some of the lowest annual average TP loads per unit area along with high regularity were observed in 1988, one of the driest years in the study area in the past several decades. Conversely, a low TP load regularity value can be seen in 1993, a relatively wet year, indicating that load events transporting TP were more evenly distributed during the year.

There is a greater variability in average annual TP loads than in average annual TP concentrations. Average annual TP loads in the Sandusky and the Cuyahoga watersheds were higher prior to 1985 and declined considerably over the next few years. However these loads started rising again in these watersheds over the mid-2000s, possibly partly because of land management and climatic changes.

The average annual TP loads in the Maumee watershed were more consistent with roughly cyclic periods of high and low average annual flows. The Raisin watershed produced the lowest amount of unit area TP loads as evident by the small and virtually indistinguishable dots representing the MDVs. The dams along the Raisin River impact the transport and settling of TP similarly to SS.

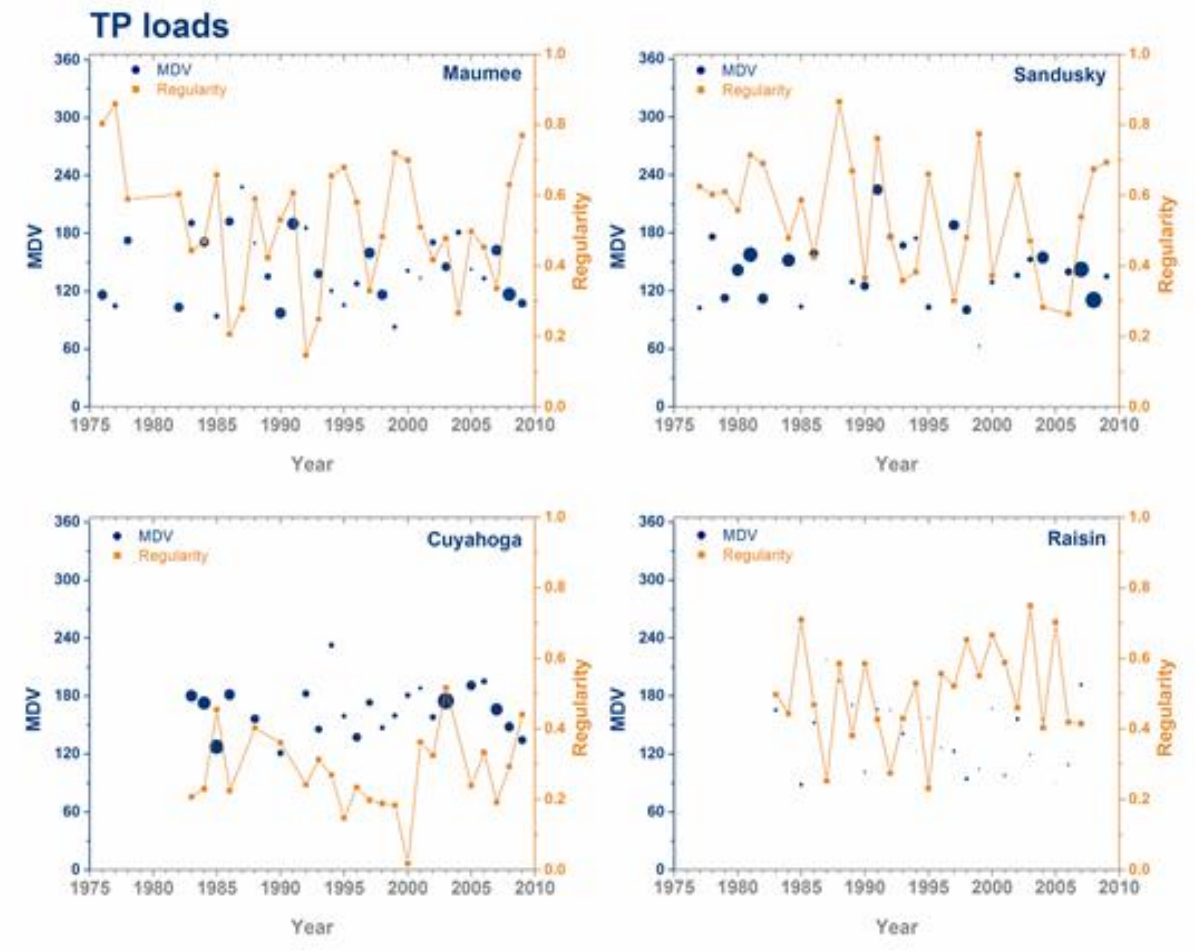

Figure 7.12: MDVs and their corresponding regularity values for TP loads. The MDVs are represented by dark blue circular markers (shown in days after the beginning of the water year). Circular markers are proportional to the maximum of average annual unit area TP loads.

Nitrate Nitrogen (NO_3-N)

The MDVs and their corresponding regularity values for NO_3-N concentrations are shown in Figure 7.13. The MDVs represented by dark blue circular markers in the figure were sized relative to the maximum annual average NO_3-N concentration recorded in all of the four watersheds.

The temporal patterns in average annual NO_3-N concentrations were distinctly different from those for SS and TP concentrations. The MDVs for NO_3-N concentrations were very similar for the three agricultural watersheds, ranging from 154 to 163 days along with an average standard deviation of 19 to 26 days. The largest average MDV of 200 days with a standard deviation of 11 days was calculated for Cuyahoga.

The regularity values ranging from 0.30 to 0.33 showed that the NO_3-N concentrations in the agricultural watersheds were fairly concentrated around the MDVs. The urbanized and point source-dominated Cuyahoga watershed had a smaller regularity of 0.21, indicating the NO_3-N concentrations were a lot more evenly distributed during a water year. The highest NO_3-N concentrations were seen in the Maumee and Sandusky watersheds which are typical agricultural watersheds. The NO_3-N concentrations in the Raisin and Cuyahoga watersheds were significantly lower.

The highest average annual NO_3-N concentrations in the agricultural watersheds occurred around 1990. It has been speculated that this increase occurred due to higher nitrate application rates and increased atmospheric deposition (Richards and Baker, 1993). Similar to the SS and TP concentrations, the peaks in regularity were typically accompanied by lower annual NO_3-N concentrations likely during the drier years (e.g., 1988). Years with high regularity which were presumably drier years were followed by years with increased NO_3-N concentrations. Drier years are typically associated with lower crop yields. Crops during drier years are not fully developed and may not consume the full amount of NO_3-N applied as fertilizer. The NO_3-N that was not exported or consumed by crops in the drier years thus stays in the watershed. The NO_3-N left in storage can then be washed out in larger amounts in the following seasons.

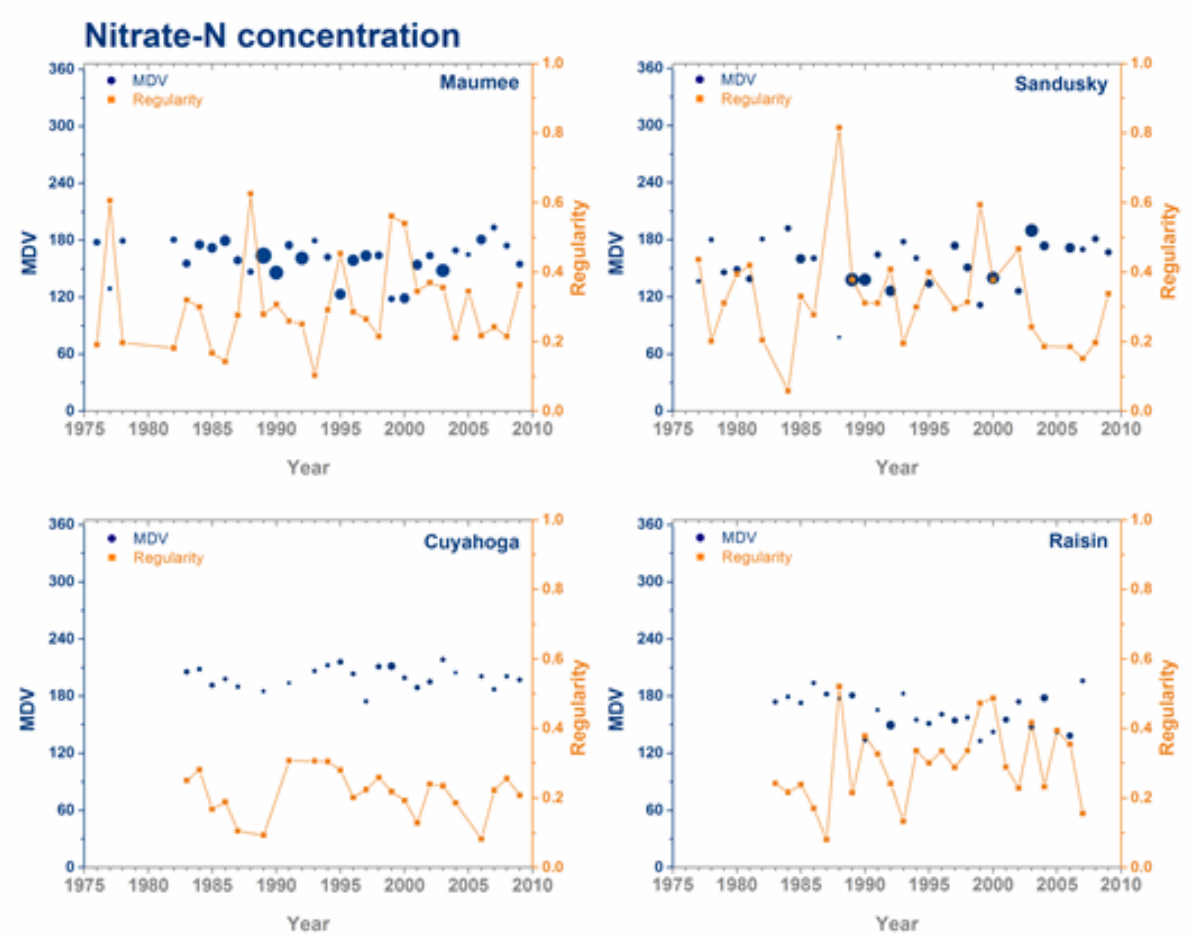

Figure 7.13: MDVs and their corresponding regularity values for NO_3-N concentrations. The MDVs are represented by dark blue circular markers (shown in days after the beginning of the water year). Circular markers are proportional to the maximum of average annual NO_3-N concentrations.

Similar findings have also been reported in Midwestern agricultural watersheds by other studies such as Raymond et al., 2012; Randall and Mulla, 2001; Gentry et al., 2009; and David et al., 1997. The average annual NO_3-N concentrations were relatively low for the Cuyahoga and Raisin watersheds when compared to the Maumee and Sandusky. However, the differences in NO_3-N concentrations between the Raisin watershed and the other two agricultural watersheds were not as large as the differences in SS and TP concentrations. NO_3-N as a dissolved constituent is less likely affected by the sedimentation behind dams, a common characteristic in the Raisin watershed. However, denitrification can occur in impoundments under certain conditions, lowering the average NO_3-N concentration.

The MDVs and regularity results for the NO_3-N loads are presented in the Figure 7.14. The MDVs shown by dark blue circular markers are sized based on average annual NO_3-N loads normalized by watershed areas. The average MDVs for NO_3-N loads ranged from 137 to 147 days in the three agricultural watersheds. The average MDV NO_3-N load was 175 days in Cuyahoga watershed, about a month later than in the agriculture watersheds. Variations in the MDVs for the agricultural watersheds ranged from 30 to 36 days, much higher than the MDV variations in the Cuyahoga watershed (14 days). The average and standard deviations in MDVs for NO_3-N loads closely follow the values for flows in these agricultural watersheds.

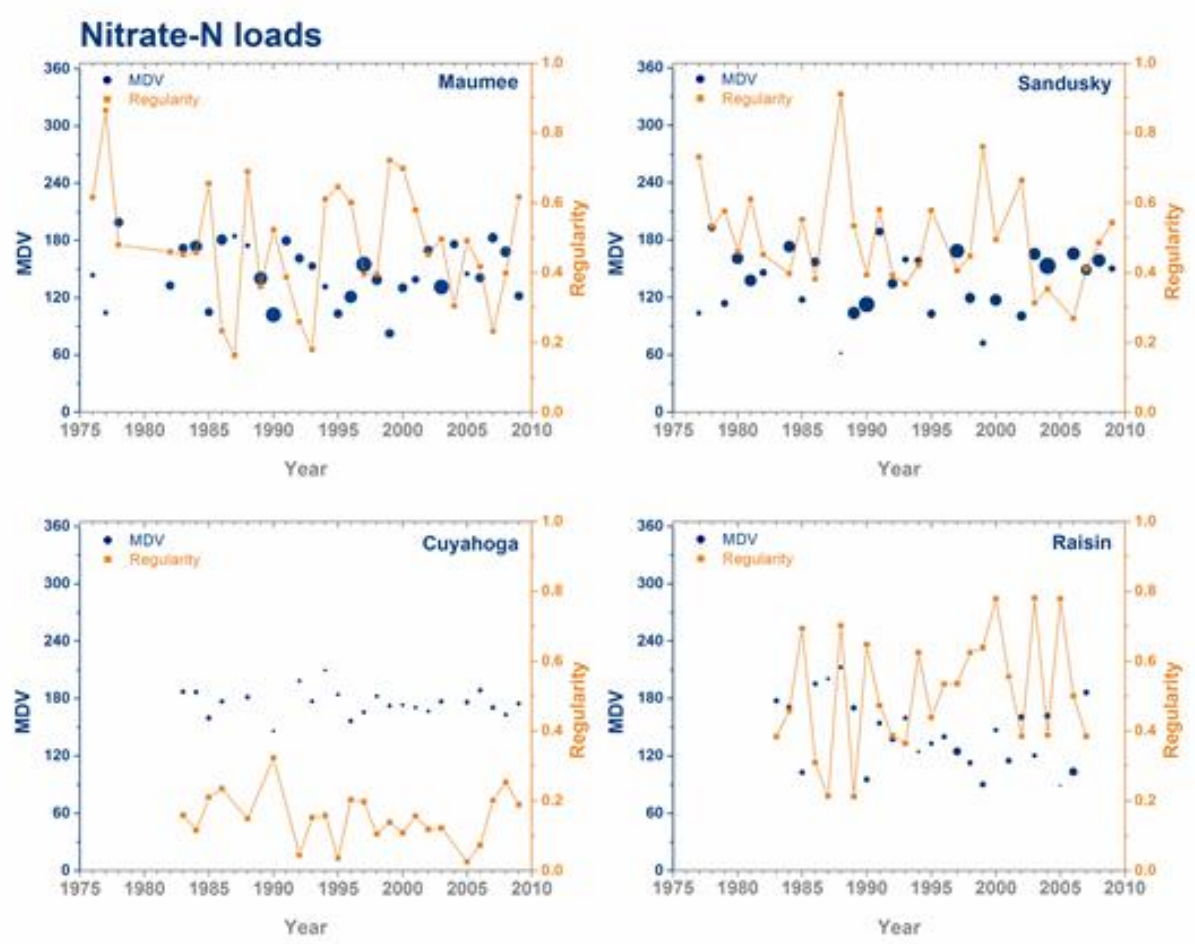

Figure 7.14: MDVs and their corresponding regularity values for NO_3-N loads. The MDVs are represented by dark blue circular markers (shown in days after the beginning of the water year). Circular markers are proportional to the maximum of average annual unit area NO_3-N loads.

The regularity for NO_3-N loads (0.48-0.51) was significantly higher than the regularity for concentrations (0.30-0.31) in the agricultural watersheds. On the contrary, the regularity for NO_3-N loads (0.15) was lower than the regularity for its concentrations (0.21) in the Cuyahoga. The highest annual average unit area NO_3-N loads were observed in the Maumee and Sandusky. There were no statistical trends that were observed in the MDVs for NO_3-N loads, indicating stationarity in the timings of the NO_3-N load export in these watersheds for the two to three decades of monitoring data.

The Cuyahoga watershed saw the smallest average annual unit area of NO_3-N loads. The average annual unit area of NO_3-N loads in the Raisin watershed were lower than the other two agricultural watersheds mainly due to lower flow volumes in the watershed attributed to the impoundments. These loads were proportionally higher than the SS and TP loads. SS and TP are more likely to be affected by the sedimentation occurring in the impoundments behind dams.

7.3.4 Long-term Temporal Variability and Agriculture Practices

This section analyses the possibility of any significant correlation between the climatic variables in a year *t* and the nitrate plus nitrite load ($N\text{-}NO_{2+3}$) in the following year *t+1*. The hypothesis maintained that the drier years are likely to be followed by the high nutrient load years. As drought quantification can be difficult and uncertain based on any assumed indicator, corn yield was used as a surrogate for drought conditions in this research. Higher yields are normally expected to occur during normal or wet years, and vice versa. The change in average corn yield during the several decades analyzed in this research is presented in Figure 7.15. Significant developments in agricultural growth over the past decades resulted in a continuous and substantial increase in corn yield. A similar trend was documented in Illinois by Mierzejewski et al. (2013). This extraordinary yield advance was associated with both breeding of improved hybrids and the ability to grow them at an increased density. The trend line in Figure 7.15 shows that the expected corn yield increased by nearly 50 percent in the past 39 years in Ohio. The fluctuations around the expected yield ranged between -25 percent and +15 percent, partly due to the fluctuation in hydrologic conditions including soil moisture.

The trend line residuals in one year were related t0 nutrient loads in the following year to eliminate the effects of increased corn yields. Figure 7.16 shows a relationship between the annual NO_3-N load and average corn yield residuals from a previous year for three watersheds, the Maumee, Sandusky, and Raisin. The decreasing linear trend line confirms with a various degree of significance the hypothesis that dry years (i.e., years with a small corn yield) are followed by high-load years. The regression slope is the steepest for the Maumee River watershed, followed by the Sandusky and Raisin watersheds. The results were confirmed for three tile-drained Illinois watersheds (Mierzejewski et al., 2013). Figure 7.17 shows a relationship between annual NO_3-N load and average corn yield residuals from a previous year for the Sangamon River watershed in Illinois. NO_3-N concentrations and loads were found to be less dependent to almost independent on the previous year's crop yield for watersheds without tile drainage (Mierzejewski et al., 2013). Tile-drain watersheds tend to have higher loads in general, as well as more significant relationships compared to no tile-drain watersheds (Figure 7.18).

Corn yield in one year could be used as a predictor for NO_3-N load for the following year. NO_3-N levels in watersheds with significant area drained by tiles are expected to be higher in the year following a drought. The results presented here can serve as a starting point to study the long-term load predictability. It is expected that a more detailed analysis with additional predictors along with fine-tuning of these preliminary predictive regressions using more sophisticated data mining tools will result in more accurate predictions.

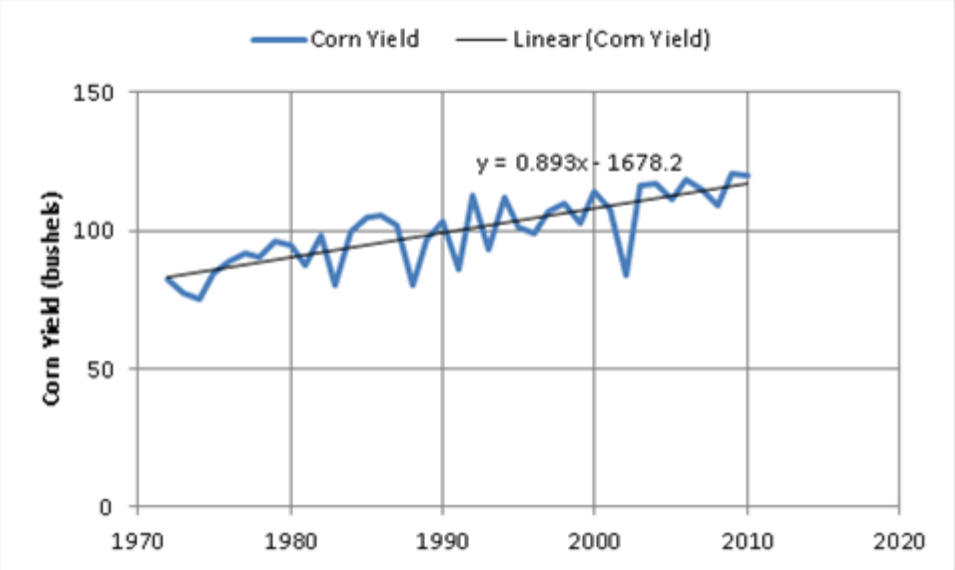

Figure 7.15: Average corn yield for Ohio

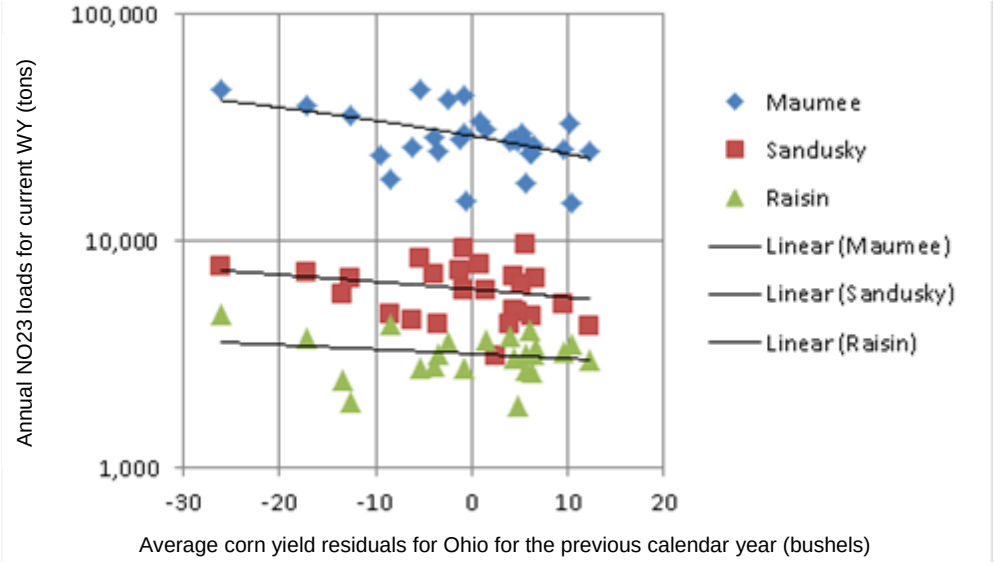

Figure 7.16: Relationship between annual NO_3-N loads and average annual residual yield in the previous year, Ohio watersheds

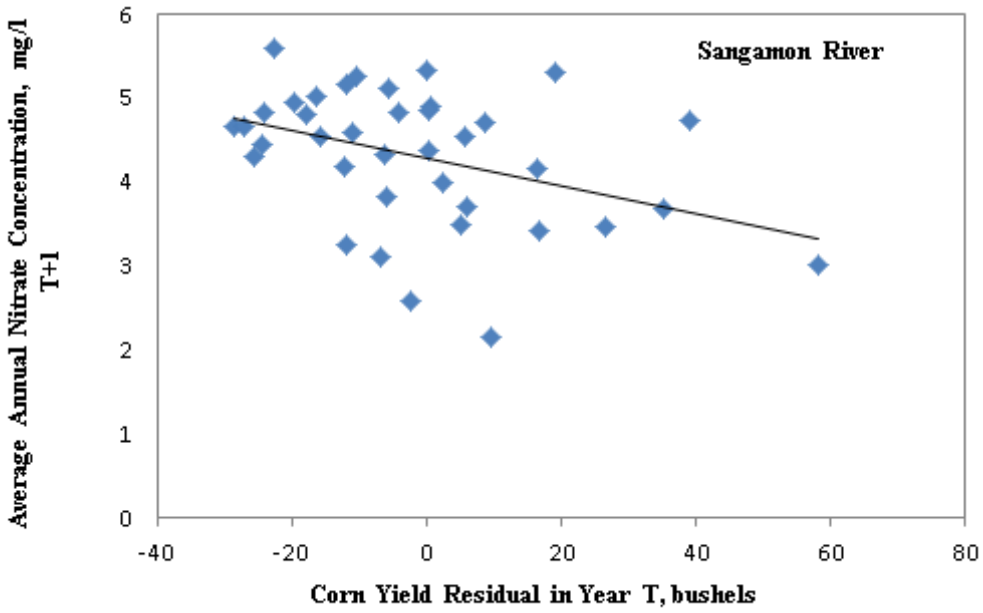

Figure 7.17: Relationship between annual NO_3-N concentration and average annual residual yield in the previous year, Sangamon River watershed in Illinois (after Mierzejewski et al., 2013)

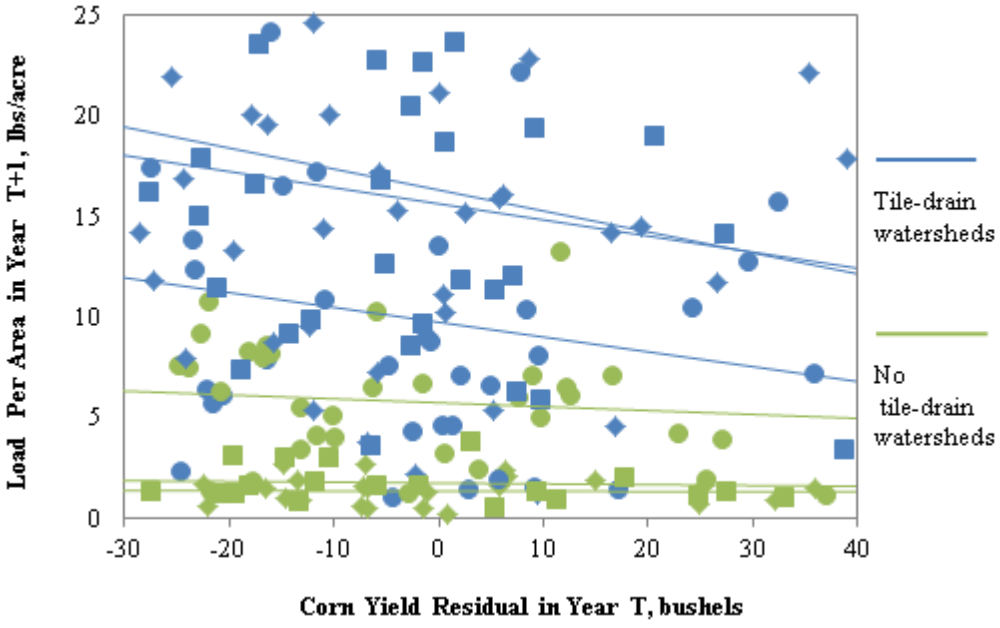

Figure 7.18: Relationship between annual NO_3-N loads and average annual residual yield in the previous year for tile drain and no-tile drain watersheds (after Mierzejewski et al., 2013)

7.4 Summary

This study utilized multiyear daily nutrient (TP and NO_3-N) and sediment (SS) datasets from eight large watersheds in the Lake Erie and Ohio River basins to assess temporal patterns in pollutant export from these watersheds. The assessment was conducted by analyzing the temporal distribution of the top 5 load events for different pollutants and watersheds over multiple years of monitoring (8-32 years). Additionally, patterns in the timing of average annual precipitation, flow, pollutant concentrations, and pollutant loads were also examined over the complete duration of monitoring for each watershed. There were no statistically significant trends observed in the timing of the average annual precipitation, flow, pollutant concentrations, and pollutant loads in the studied watersheds. A strong correlation was observed between corn yield residuals and NO_3-N loads and concentrations in the next year. Dry years were typically followed by years with higher NO_3-N loads.

There are mechanistic differences in the load export of different pollutants. This can be seen when pollutographs are plotted with hydrographs on the same chart. Pollutographs for TP and SS are typically closely aligned with hydrographs. Pollutographs for NO_3-N typically show a lag along with a slower receding curve when compared to hydrographs. This lag is well described for the predominantly agricultural tile-drained Midwestern watersheds.

There is asynchrony in the occurrence of the largest precipitation and the largest load events in the studied watersheds. Any substantial precipitation event during the winter and early spring is likely to export large percentages of annual pollutant loads from these watersheds. However, only very large precipitation events are expected to export loads with significant contributions to annual load during the growing season.

The top 5 NO_3-N load events in the studied watersheds typically occurred from November to April. The largest NO_3-N load events were typically even more concentrated temporally for the highly agricultural watersheds, occurring from February to April. The temporal patterns in the top 5 TP and SS load events annually were very similar to each other. The top 5 TP and SS events typically occurred between February and May, earlier than the top 5 NO3-N load events. The top 5 TP and SS load events were also more distributed on an annual scale with more top load events occurring in the warmer months as compared to NO_3-N.

Anthropogenic activities such as urbanization, agriculture, and constructed dams can have significant effects on the magnitude and temporal patterns of pollutant transport. The urbanized watershed had higher unit area flows and lower regularity (a wider annual distribution in flow with less overall fluctuations) than the agricultural watersheds. The lowest unit area flows and loads were seen in a watershed with numerous dams that likely impeded the flow and increased the water retention time in the watershed. Tile-drained watersheds show significantly higher unit area NO_3-N loads than watersheds without tile drainage.

The presence of point sources along with prevalent land use affects the event characteristics in these watersheds. An urbanized and point source-dominated watershed is likely to have pollutant loads more evenly distributed during a water year with lesser significance of the top load events. In comparison, an agricultural, tile-drained, non-point source-dominated watershed is more likely to have a shorter, more concentrated period when pollutants will be exported during a few top load events exporting the bulk of the annual load.

Generally, pollutant concentrations were more evenly distributed throughout the year. The pollutant loads were more concentrated around certain time periods in a year. The impoundments affected total SS and TP loads, lowering the potential contribution from a watershed by retaining a portion of the generated loads. Higher quantities of loads were exported in relatively wetter years and were more spread out on a temporal scale. Conversely, in the drier years lower annual loads were exported and were concentrated over a small temporal duration.

The peak nutrient load in these watersheds was seen in the winter and late spring. There is a time lag between this period when most of the load is generated and transported from a watershed and the period most susceptible to algal production and the imminent hypoxic conditions in receiving water bodies, typically late summer and early fall. Regulatory or management decisions aimed at improving water quality in the downstream water bodies are likely to be more effective by focusing on reducing nutrient load export from Midwestern watersheds over the cooler months. Conservation management practices such as cover crops, conservation tillage, and injecting fertilizers in soil rather than broadcasting them would help to reduce NO_3-N load export over the winter months from agricultural watersheds.

8. Climate Change Impacts on Flow, Sediment and Nutrient Loadings in a Great Lakes Watershed Using SWAT

8.1 Introduction

The past century has seen a drastic increase in carbon dioxide and other greenhouse gas emissions (Chaplot, 2007; IPCC, 2012). This increase, primarily attributed to anthropogenic sources (Wu et al., 2012), has been more rapid over the past few decades (Raupach et al., 2007). Numerous studies have estimated the magnitude and direction of such global mean changes while studying their impacts on global carbon and water balances (Trenberth, 1999; Trenberth et al., 2007; Meehl et al., 2007; Kundzewicz, 2007; Schuur et al.; 2008; Mu et al., 2011). Higher carbon dioxide concentrations in the earth's atmosphere enhance the greenhouse effect and directly affect global temperatures and consequently precipitation patterns. There is scientific consensus on the changes in global mean carbon dioxide concentration, temperature, and precipitation happening over the past several decades (Fontaine, 2001). Such global climate change along with increases in carbon dioxide concentrations are already having discernible effects on various environmental systems, including effects on the hydrological cycle at both the global and regional scales (Ficklin et al., 2009). Generally accepted impacts of climate change on the hydrological cycle include changes projected in the intensity, frequency, duration, spatial extent, and timing of extreme weather and climate events (IPCC, 2012). Such changes are likely to cause rising sea levels, glacial melting, and variations in precipitation amounts, intensity, and distribution along with an increase in the frequency of extreme events such as floods and droughts (IPCC, Dibike and Coulibaly, 2007; Milly et al., 2005; Praskievicz and Chang, 2009).

These changes are projected to further increase in this century, with the magnitude of the changes varying based on several emission scenarios along with land and ocean climatic feedbacks (Chaplot, 2007; IPCC, 2012). Consequently, the hydrological cycle is expected to be further impacted with changes occurring in various watershed scale processes such as evapotranspiration, runoff, streamflow, water yields, soil moisture, soil erosion, and nutrient losses. Labat et al. (2004), using historical climate data, demonstrated that a 1 ^{o}C rise in global temperatures increased the mean global runoff by 4 percent, attributed to increased oceanic evaporation. Changes in precipitation patterns, coupled with increases in potential evapotranspiration, might lead to significant changes in river runoff (Kundzewicz et al., 2007). Bronstert et al. (2002) explained the potential increase in surface runoff mainly through increased intensity of precipitation coupled with soil surface crusting. Arnell (2003) showed the effects of climate change on evapotranspiration rates, soil moisture, and altered flow regimes in rivers in Britain. Park et al. (2011) simulated future changes in evapotranspiration, groundwater recharge and streamflow based on climate change and land use change both separately and simultaneously for a large forested watershed in South Korea. Bouraoui et al. (2002) demonstrated how climate change modifies the transformation and transport characteristic of nutrients from a watershed in northern England. Changes in precipitation patterns are also expected to directly affect the soil erosive processes from watersheds as simulated by Pruski and Nearing (2002) who indicated that a 1 percent rise in precipitation amounts and intensity will increase soil erosion by about 1.7 percent at multiple locations in the contiguous US. Overall, changes in runoff, flow regimes, sediment and nutrient loading from watersheds attributed to climate change, mainly precipitation variations, would irreversibly affect soil resources and cause both off and on-site effects such as floods, water pollution, reservoir damage, fertility losses, and soil erosion (Chaplot, 2007). All these studies have described the sensitivity of watershed-scale processes to the changes in atmospheric carbon dioxide concentrations and increasing temperature and precipitation. Implications of such changes for water resources, water quality and quantity, agriculture, and social issues have therefore been generally identified (Fontaine et al., 2001). However, uniformly accepted conclusions are still unavailable and less understood, along with a lack of quantitative results on the effects of climate change, especially at the regional scales.

Anticipating changes in the hydrologic cycle and thereby water resources has generally been done by using physically-based hydrologic models coupled with climate scenarios which are based on General Circulation Models (GCMs). The hydrological models provide a basis to evaluate the relationships between climate parameters, anthropogenic activities along with water resources, and predict runoff volumes, water yields, evapotranspiration rates, and sediment and nutrient losses. These models are based on equations governing the conservation of mass, momentum, and energy. As the parameters of these models have physical meaning, they can use commonly measured hydro-climatic parameters such as precipitation and temperature along with physical characteristics of the watershed such as land-use, soil types, elevation, and slope as model inputs to simulate various hydrological processes at varied spatial and temporal scales. In principle, once calibrated, these models can be applied to other conditions outside those used for calibration to understand the sensitivity of the watershed processes and to examine the climate change effects. It is imperative to understand that these sensitivity assessments provide invaluable insights into the direction of possible change in the hydrological systems due to climate change, but do not necessarily give projections of the future changes (Arnell and Liv, 2001; Ficklin et al., 2009).

The objective of this study was to assess the overall impact of climate change on the hydrology of a large agricultural watershed in the Lake Erie basin. The physically based, watershed-scale hydrologic and water quality model, Soil and Water Assessment Tool (SWAT) (Arnold et al., 1998) was calibrated and validated for flow, sediment, and nutrient yields using data from 1995-2005. Ensemble climate data from three GCMs for mid-century (2045-2055) and late-century (2089-2099) scenarios, downscaled to the watershed level, were used as model inputs to analyze future changes in flow, sediment, and nutrient yields. Changes in hydrology based on the future scenarios were compared to the 10-year baseline results with the present-day climate. The climate (temperature and precipitation) projections for the future scenarios used in this study were based on the A1B emission scenario, which represents rapid economic growth and a balanced reliance on different sources of energy (IPCC, 2012).

8.2 Methods

8.2.1 Model Description

The Soil and Water Assessment Tool (SWAT) is a semi-distributed, physically based model that can simulate hydrological processes in a watershed and predict flow and pollutant loadings based on land use, nutrient application patterns, and various other management conditions in the watershed (Bosch et al., 2011; Zahabiyoun et al., 2013). It is a continuous-time, watershed-scale model that performs simulations on a daily scale (Gassman et al., 2007). SWAT is an interactively coupled climate-land use model primarily used for agricultural non-point pollution modeling (Neitsch et al., 2005). It is a physically based model simulating the crop growth and nutrient cycles and their impacts on water resources. Thus, it can be used to test the impacts of climate change on these processes (Chaplot, 2007).

SWAT relies on spatially distributed data describing the watershed characteristics, including topography, soils, land use, land management practices, and climate. SWAT divides the watershed into sub-watersheds and sub-watersheds further into smaller units called Hydrological Response Units (HRUs) that have unique and uniform land use, soil type, and slope. SWAT models all hydrological processes at the individual HRU scale (Figure 8.1) and then compiles the results for sub-watersheds and watersheds by a weighted average based on the area.

All hydrological and pollutant transport processes in SWAT are modeled in two modules, namely the land phase module covering the movement of water and pollutants into the main channel and the routing phase module dealing with the transport of water and pollutants through stream channels to the watershed outlet (Neitsch et al., 2005). The SWAT model has been continually developed and improved over the past 20 years. It has been extensively applied across the globe to various different watersheds encompassing a wide range of land uses, climate, locations and sizes. Its main strengths lie in its

capability to model watersheds without intensive monitoring data, computational efficiency, the ability to quantify the impacts of change in input data on water quality, and the ability to perform long-term simulations (Neitsch et al., 2005).

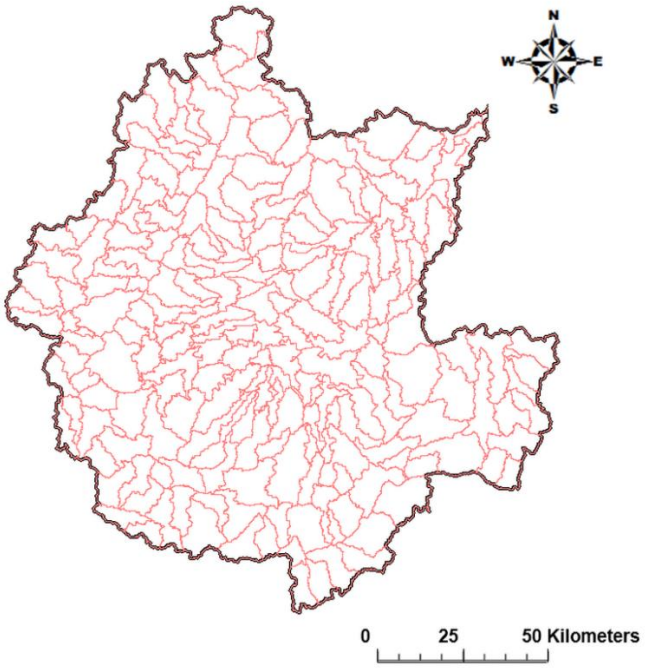

Figure 8.1: The Hydrologic Response Units (HRUs) created by SWAT for the Maumee River watershed

8.2.2 Model Inputs

ArcSWAT (version 2.1.5), a Geographic Information System (GIS) interface created for a SWAT model, was used in this study to develop the model inputs for the Maumee River basin. Elevation information for the basin was obtained from the United States Geological Survey (USGS) National Elevation Dataset. The Digital Elevation Model (DEM) with 30 x 30 m grid resolution was used in this study (Figure 8.2). The river network generated by SWAT was verified using the stream channel network obtained from USGS National Hydrography Dataset (NHD) with a 1:100,000-scale. A 30 x 30 m grid cell resolution land cover dataset was obtained from the USGS 2001 National Land Cover Dataset (Figure 8.2). Information on soil types was obtained from the Natural Resource Conservation Service State Soil Geographic Database which had 90×90 m grid cell resolution. Weather data (daily precipitation and minimum and maximum temperatures) were obtained from the National Oceanic and Atmospheric Administration (NOAA) National Climatic Data Center. Precipitation data from 27 rain gaging stations and temperature data from 21 weather stations were included in this study.

The data on impoundment characteristics were obtained from the USGS National Hydrography Dataset and Allan and Hinz (2004). Land management practices data were obtained from the USDA National Agricultural Statistics Service (NASS), various local experts, and Ruddy et al. (2006). The point source discharge data were obtained from the EPA Permit Compliance System (PCS) database. More complete point source data (average daily effluent flow, total suspended solids, organic phosphorus, organic nitrogen, nitrate, ammonia, nitrite, phosphorus, chemical/biological oxygen demand, and dissolved oxygen) were also obtained from the local sources, when available. Wetlands surface area and

volume measurement data for typical and flood stage conditions were also collected. Atmospheric nitrogen deposition data were obtained from the National Atmospheric Deposition Program (NADP) dataset.

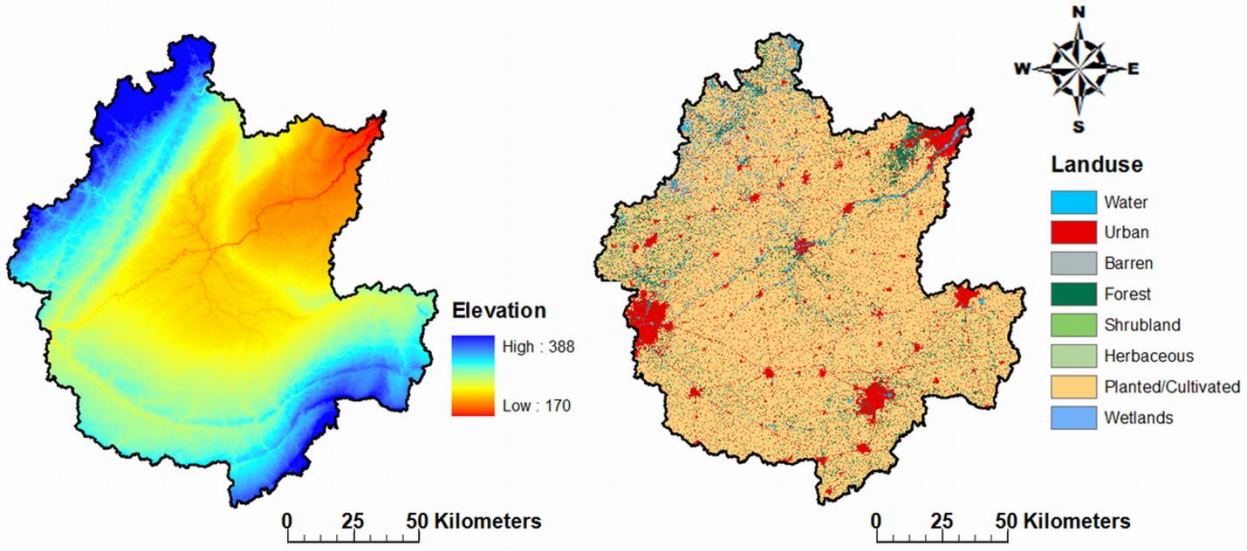

Figure 8.2: The 30x30 m grid digital elevation (DEM) and land use layers used as model inputs in SWAT for the Maumee River watershed

8.2.3 Future Climate Data

Future climate (monthly precipitation and temperature) data were obtained from the Bias Corrected and Downscaled WCRP CMIP3 Climate Projections archive (available at: http://gdo-dcp.ucllnl.org/downscaled_cmip3_projections/) to evaluate the impact of climate change on water quantity and quality for years 2045-2055 and 2089-2099 (Meehl et al., 2007). The archive provides bias-corrected and spatially downscaled to 1/8×1/8 degree resolution (12×12 km) precipitation and temperature data from multiple general circulation models (GCMs) output for different IPCC scenarios (Maurer, 2007). Future projected precipitation and temperature data from CGCM3 from Environment Canada, GFDL-CM2 from Geophysical Fluid Dynamics Laboratory of the National Oceanic and Atmospheric Administration (NOAA) in the U.S., and HadCM3 (Hadley Centre Coupled Model, version 3) from the Hadley Centre in the United Kingdom were obtained. The IPCC A1B scenario that assumes a future world of low population growth but very rapid economic growth and rapid introduction of new and more efficient technology was used in this study (Parry et al., 2007).

Weather and seasonal forecasts show improved reliability and consistency when the outputs from multiple models are combined (Knutti et al., 2010). Hence, the averages of three GCM projections were used (ensemble) to drive the SWAT model in this study rather than using outputs from a single GCM. Regional climate impact assessments require high-resolution projections (Hayhoe, 2010). The GCM projections on a monthly scale need to be downscaled to a daily scale to be used as SWAT model inputs. A relatively simple and popular technique called “delta” or “change factors” was used in this study to downscale the low-resolution future monthly projections to high-resolution daily projections (Zahabiyoun et al., 2013). In this technique, the future ensemble monthly temperature and precipitation projections (2045-2055 and 2089-2099) are compared to the observed baseline values (1995-2005). The “difference”

ΔT and "proportion" *ΔP* were computed for temperature and precipitation projections, respectively, to calculate the change factors for each month (Eq. (8.1) and Eq. (8.2)).

$$\Delta T_m = \left(\bar{T}_{ensemble,fut,m} - \bar{T}_{baseline,obs,m}\right) \quad \textbf{(8.1)}$$

$$\Delta P_m = \left(\frac{\bar{P}_{ensemble,fut,m}}{\bar{P}_{baseline,obs,m}}\right) \quad \textbf{(8.2)}$$

where, ΔT_m and ΔP_m are change factors for temperature and precipitation, respectively, *m* is the month of the year ($1 \leq m \leq 12$), and $\bar{T}_{ensemble,fut,m}$ and $\bar{P}_{ensemble,fut,m}$ are future ensemble average monthly temperatures and future ensemble average total monthly precipitations from the three GCM projections, respectively. Similarly, $\bar{T}_{baseline,obs,m}$ and $\bar{P}_{baseline,obs,m}$ are average monthly temperatures and precipitations from the observed baseline data (1995-2005), respectively.

The calculated monthly change factors for both temperature and precipitation were then used to generate high-resolution projection data for SWAT model inputs. Based on the change factors downscaling technique, the future daily time series of climate data was generated as follows:

$$T_{fut,d,m} = \left(T_{obs,d,m} + \Delta T_m\right) \quad \textbf{(8.3)}$$

$$P_{fut,d,m} = \left(P_{obs,d,m} * \Delta P_m\right) \quad \textbf{(8.4)}$$

where, *d* is the day of the month ($1 \leq d \leq 31$), *m* is the month of the year ($1 \leq m \leq 12$), and $T_{obs,d,m}$ and $P_{obs,d,m}$ are daily observed temperature and precipitation for the baseline time periods, respectively. $T_{fut,d,m}$ and $P_{fut,d,m}$ are daily projected temperature and precipitation for the future time periods, respectively, calculated after incorporating the change factors to the observed daily data.

8.2.4 Model Calibration and Validation

The model calibration process for monthly flow, SS, NO_3-N, and TP load is discussed in this section. This study used a calibrated SWAT model for the Maumee River basin developed in an earlier study by Bosch et al. (2011). Hydrological calibration is a critical step for subsequent water quality calibration for a watershed-scale water quality model like SWAT. The SWAT model was calibrated and validated for daily stream discharge measured at the USGS gage station (04193500) on the Maumee River at Waterville, OH for 1995–2005. The first three years (1995–1997) were used for model warm-up and the model output for these three years was not used in the calibration process to reduce the impact of initial model parameter values on model output. The observed data for the next four years (1998–2001) were used for calibration and the remaining four years (2002–2005) were used for model validation (Bosch et al., 2011).

Various watershed characteristics like Manning's roughness coefficient, potential evapotranspiration, channel erosion, and baseflow parameters were changed from default values to better represent characteristics of the watershed. Table 8.1 shows the various ranges and values of the SWAT parameters used in this study. In order to reflect the slightly less obstructed flow path in this agricultural watershed, Manning's *n* was set to 0.026. The Hargreaves method was selected for potential evapotranspiration estimation. The Baseflow Filter Program (Arnold and Allen, 1999) was used to estimate the baseflow alpha factor using 1995-2005 daily flow data. Following the approach outlined by Green et al. (2006), tile drainage was implemented in the watershed. Tile drainage was assumed to be present in agricultural lands with poorly drained soils (hydrologic soil group of types C and D). The depth to the subsurface drain parameter was set to 1,000 mm, time to drain soil to field capacity parameter was set to 24 hours, and the drain tile lag time parameter was set to 96 hours. Similarly, the depth to impermeable layer parameter was

set to 2,500 mm for all agricultural HRUs with poorly drained soils (Bosch et al., 2011). (Please refer to Bosch et al. (2011) for more details on stream discharge calibration and validation processes).

Impoundments located on stream channels, including natural lakes and artificial reservoirs, were included in the SWAT model. Impoundments with surface areas greater than 50 hectares were incorporated into SWAT as reservoirs, and impoundments of 10 - 50 hectares were incorporated as ponds. Parameter values for surface area and volume under average conditions for each pond and reservoir were entered based on collected data. Water quality parameters to depict NO_3-N and P removal in impoundments were adjusted on the basis of a study of 27 Midwestern reservoirs (Walker and Kuhner, 1978) that reported median settling rates of 14.0 m/y for P, and NO3-N removal rates (primarily from denitrification) equivalent to 4.7 m/y.

Water quality parameters to depict NO_3-N and P settling in impoundments were adjusted on the basis of a study of 27 Midwestern reservoirs (Walker and Kuhner, 1978) that reported median removal rates of 4.7 m/y for NO_3-N and 14.0 m/y for P.

In SWAT, terrestrial soil denitrification depends on nitrate content of the soil layer, the rate coefficient, soil temperature, soil moisture conditions, organic carbon content, and threshold moisture content. The value of denitrification threshold water content was set to 1.0 to allow denitrification when soils were saturated with water. Similarly, the denitrification exponential rate coefficient was set to 0.15 to better approximate expected denitrification rates according to previous measurements in the literature (Groffman et al., 1992; Hofstra and Bouwman, 2005).

The goodness of fit between observed and simulated water quantity and quality parameters were assessed using two popular statistical parameters: coefficient of determination (R^2) and the Nash-Sutcliffe efficiency (NSE) coefficient (Nash and Sutcliffe, 1970).

Table 8.1: SWAT model calibration parameters

Parameter	*Range (min - max)*	*Calibrated Value*
Alpha_Bf	0.01-0.3	0.2543
Canmx	0.01-10	5.7317
Ch_K2	0.01-150	0.4174
Ch_N2	0.01-0.1	0.0571
CN2	-20 - 20	-6.3791
Epco	0.01-1%	0.6381
Esco	0.01-1	1.0000
Gwqmn	0.01-500	447.58
Revapmin	0.01-500	388.62
Sol_Awc	-20 - 20	4.9695
Sol_Z	-20 - 20	-10.903
Surlag	1-24	2.8723
Timp	0.01-1	0.0611

8.3 Principal Findings and Significance

8.3.1 Baseline Climate

The total monthly precipitation observed in the Maumee River watershed over the period 1995-2005 was calculated using daily precipitation records from 27 weather stations lying within and around the watershed boundary. The daily records from all 27 stations were averaged based on the Thiessen polygon method, and average areal precipitation estimates were calculated for the whole watershed. These daily Thiessen weighted values were then summed to compute the monthly totals. The month of May received the maximum precipitation over the 11-year period, averaging 119 mm per month. The total precipitation received during the summer (May-Aug) accounted for almost 44 percent of total annual precipitation on average. The total annual precipitation varied from 804 mm in the driest year (1999) to 1,109 mm in the wettest year (2003) with the standard deviation being 95 mm. The total monthly precipitation ranged from 12 mm (February 2004) to 190 mm (July 2003).

Average daily temperature was calculated for the whole watershed based on the Thiessen polygon method using records from 21 stations in and near the watershed. Average monthly values were then calculated from the daily records. January was the coldest month with an average temperature of -4^{o}C. July was the warmest month with an average temperature of about 23 ^{o}C. 1996 was the coldest year from the simulated period (1995-2005) with an average annual temperature of 9 ^{o}C. The warmest year was 2001 with an average annual temperature 11 ^{o}C. The average monthly temperature ranged from -8 ^{o}C (December 2000) to 25 ^{o}C (July 1999). The highest and lowest maximum average temperatures were typically observed in July at about 29 ^{o}C and January at 0^{o}C, respectively. Similarly, the highest and lowest minimum average temperatures were also observed in July and January at 17 ^{o}C and -8 ^{o}C, respectively.

8.3.2 Climate Projections

Modeled total monthly precipitation and average monthly temperature data were downloaded for a mid-century period from 2045-2055 and a late-century period from 2089-2099 from three GCMs (CGCM3, GFDL-CM2, and HadCM3) for the Maumee River watershed. The IPCC A1B scenario was selected and the ensemble data were compared to the data observed in the Maumee River watershed for the 11-year baseline period from 1995-2005. Table 8.2 summarizes the correction factors obtained for both total monthly precipitation and average monthly temperature for the mid-century and late-century scenarios.

The ensemble model predictions indicated that summer and early fall precipitation (May-Oct) is projected to decrease for the mid-century period. The maximum decrease of 27 percent is expected in May and June. Conversely, the average monthly precipitation is expected to increase over the rest of the year for the mid-century period with an expected maximum increase of 36 percent in November. A large increase in average monthly precipitation of about 30 percent is also expected for the month of March. On an annual scale, the total precipitation is expected to decline from 939 mm in the baseline to 909 mm and mid-century periods.

A similar temporal pattern in the change of average monthly precipitation was seen with decreasing precipitation during May-October and increasing precipitation during the rest of the year for the late century period. However, the largest decreases in average monthly precipitation totals are projected in July (21 percent) and August (23 percent). The largest increase is projected to occur in March at about 58 percent compared to the baseline period. Overall, the annual precipitation is projected to increase from 939 mm in the baseline period to 991 mm in the late-century period.

Table 8.2: Total monthly precipitation and average monthly temperatures for the baseline period (1995-2005), mid-century period (2045-2055), and late-century period (2089-2099).

Precipitation totals (mm)		*Jan*	*Feb*	*Mar*	*Apr*	*May*	*Jun*	*Jul*	*Aug*	*Sep*	*Oct*	*Nov*	*Dec*
Observations	1995-2005	64.72	50.64	56.60	84.99	118.46	99.84	101.74	92.74	80.66	64.36	65.74	58.52
Ensemble Predictions	2045-2055	69.36	57.04	73.51	102.93	86.06	72.84	78.79	76.37	69.97	58.70	89.26	74.57
	2089-2099	74.61	61.69	89.53	106.93	107.56	84.16	80.38	71.42	70.00	80.52	89.29	75.71
Change Factor (P_{Pred}/P_{Obs})	2045-2055	1.07	1.13	1.30	1.21	0.73	0.73	0.77	0.82	0.87	0.91	1.36	1.27
	2089-2099	1.15	1.22	1.58	1.26	0.91	0.84	0.79	0.77	0.87	1.25	1.36	1.29

Average Temperature (^oC)		*Jan*	*Feb*	*Mar*	*Apr*	*May*	*Jun*	*Jul*	*Aug*	*Sep*	*Oct*	*Nov*	*Dec*
Observations	1995-2005	-4.00	-1.21	2.82	9.55	15.24	20.94	22.79	21.92	18.07	11.50	4.95	-1.64
Ensemble Predictions	2045-2055	-1.38	0.52	5.75	11.72	17.99	23.41	26.61	26.14	21.56	14.35	6.73	1.83
	2089-2099	0.21	2.29	7.12	13.78	19.26	24.92	27.89	27.68	22.92	16.18	7.58	2.74
Change Factor (T_{Pred}-T_{Obs})	2045-2055	2.61	1.73	2.92	2.17	2.75	2.47	3.82	4.21	3.49	2.84	1.79	3.47
	2089-2099	4.21	3.50	4.30	4.23	4.02	3.97	5.10	5.75	4.85	4.67	2.63	4.38

Notes: *The baseline period values were computed using observed data. The future period ensemble values were derived from three GCMs. The correction factors for precipitation totals (P_{Pred}/P_{Obs}) and average temperatures (T_{Pred}-T_{Obs}) are also shown for both the future periods.

The ensemble GCM projections for average monthly temperatures along with their respective correction factors are also summarized in Table 8.2. All the GCMs projected a warmer climate with average monthly temperatures rising in all months for the mid-century and late-century periods. The maximum rise was projected in August at 4.2^{o}C and 5.8 ^{o}C for the mid-century and late-century periods, respectively. The minimum rise was projected in February at 1.8 ^{o}C and November at 2.6 ^{o}C for the mid-century and late-century periods, respectively. Overall, the average annual temperature is projected to increase by 2.9 ^{o}C and 4.3 ^{o}C during the mid-century and late-century periods, respectively, as compared to the baseline period.

8.3.3 Flow

The modeled results from SWAT were compared to the daily flow observed at the USGS gaging station at the outlet of the Maumee River watershed located at Waterville, OH. The first three years (1995-1997) out of the 11 years in the baseline period were used as a model warm-up to minimize the impact of initial parameter values on the output. The next four years (1998-2001) were considered as the

calibration years while the remaining years from the baseline period (2002-2005) were used for validation purposes. The coefficient of determination (R^2) and NSE values for average monthly flow simulations over calibration and validation periods are shown in Table 8.3. Figure 8.3 shows the average monthly flows observed at the Maumee River watershed plotted against the SWAT simulated values. The flow simulations can be categorized as "very good" based on the classification developed by Moriasi et al. (2007).

Both the Coefficient of determination (R^2) and NSE statistical values were higher for the validation period than for the calibration period. Figure 8.4 shows the comparison of the daily flow observed at the USGS gage at the outlet of the watershed and the daily flow simulated using the SWAT model. Although SWAT under-predicted the peak flows on a daily scale, the model successfully simulated the flow conditions in the watershed overall (Figure 8.3, Figure 8.4, and Table 8.3). High goodness of fit statistics for monthly SWAT predictions indicated that the model successfully simulated the physical flow generating processes in the watershed and would be reliable for future climate simulations. Successful flow calibration is a critical step for water quality predictions (Bosch et al., 2011).

Table 8.3: Calibration and validation results for monthly flow, suspended solids loads, total phosphorus loads, and NO_3-N loads for the Maumee River watershed

	Observed mean	*Simulated Mean*	*R^2*	*NSE*
Calibration				
Flow (m^3/s)	150.61	170.49	0.93	0.91
Suspended Solids loads (Mg)	67395.60	71984.25	0.75	0.72
Total Phosphorus loads (Mg)	150.71	148.92	0.70	0.70
NO3-N loads (Mg)	2447.81	2732.55	0.74	0.70
Validation				
Flow (m^3/s)	174.25	184.97	0.96	0.95
Suspended Solids loads (Mg)	64275.58	67973.11	0.90	0.89
Total Phosphorus loads (Mg)	152.84	125.80	0.81	0.77
NO3-N loads (Mg)	2519.02	2666.10	0.72	0.69

Notes: *Coefficient of determination (R^2) and Nash-Sutcliffe efficiency (NSE) goodness of fit measures are used to compare the observed results to the SWAT modeled results.

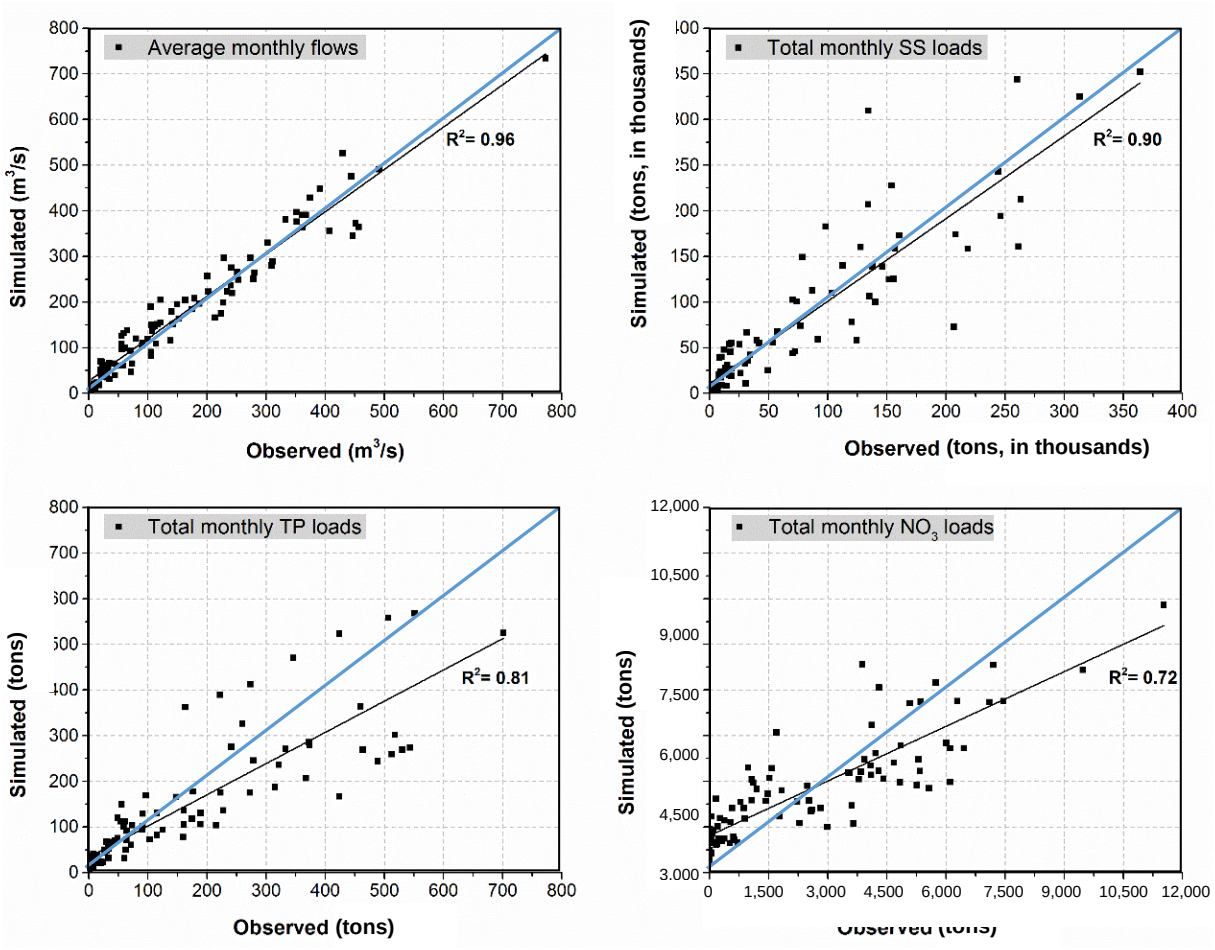

Figure 8.3: Observed and SWAT simulated monthly averages for flow, SS, TP and NO_3 loads

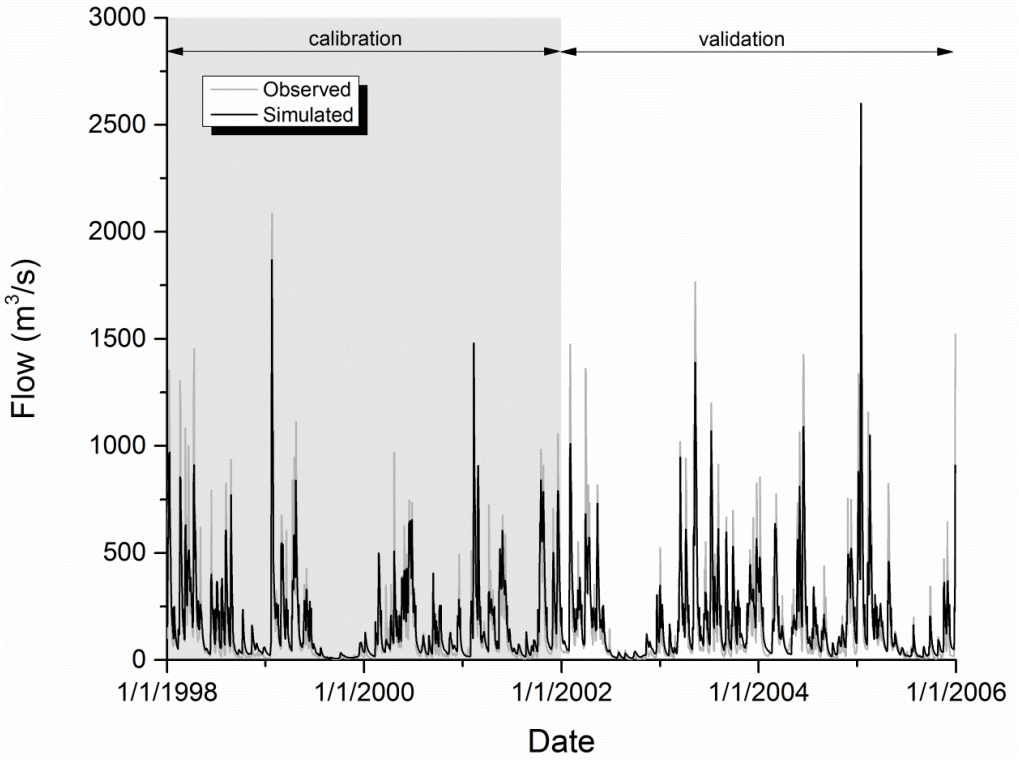

Figure 8.4: Observed and SWAT simulated daily flow data for calibration (1998-2001) and validation (2002-2005)

Changes in average monthly flows attributed to climate change (temperature and precipitation changes) in the mid-century and late-century periods as compared to the baseline period are presented in Figure 8.5 for the Maumee River watershed. The average annual flow over the mid-century and late-century periods is projected to be 162 m^3/s and 195 m^3/s, respectively. As flow is largely dependent on precipitation, the temporal change in flow patterns for future periods was similar to that of precipitation changes. The summer flows are projected to decline in the Maumee River watershed while the winter flows are expected to rise. As precipitation was projected to decline for the mid-century period on an annual scale when compared to the baseline period, flows were also projected to decrease. Similarly, precipitation was projected to increase in the late-century period as compared to the baseline period, and thereby the flows were also projected to increase.

However, these changes were not uniform as flow generation from precipitation is a fairly complex process with other variables involved. A projected 3.2 percent decrease in annual precipitation accompanied with a 2.9^{o}C rise in average temperatures over the mid-century period decreased the average flow by 8.5 percent. Similarly, a projected 5.6 percent increase in annual precipitation coupled with a 4.3^{o}C rise in average temperatures increased average flow by 9.7 percent for the late-century period compared to the baseline period.

Average flows in warmer months (May-Sep) declined by 52 percent and 36 percent for mid-century and late-century periods compared to the baseline period, respectively. Average flows in cooler months (Oct-Apr) increased by 15 percent and 35 percent in average flows for mid-century and late-century periods compared to the baseline period, respectively. The largest decrease in average flows were projected to occur in July (64 percent) and August (60 percent) for the mid-century and late-century periods, respectively. The largest increase was projected in December at 43 percent and 57 percent for mid-century and late-century periods, respectively.

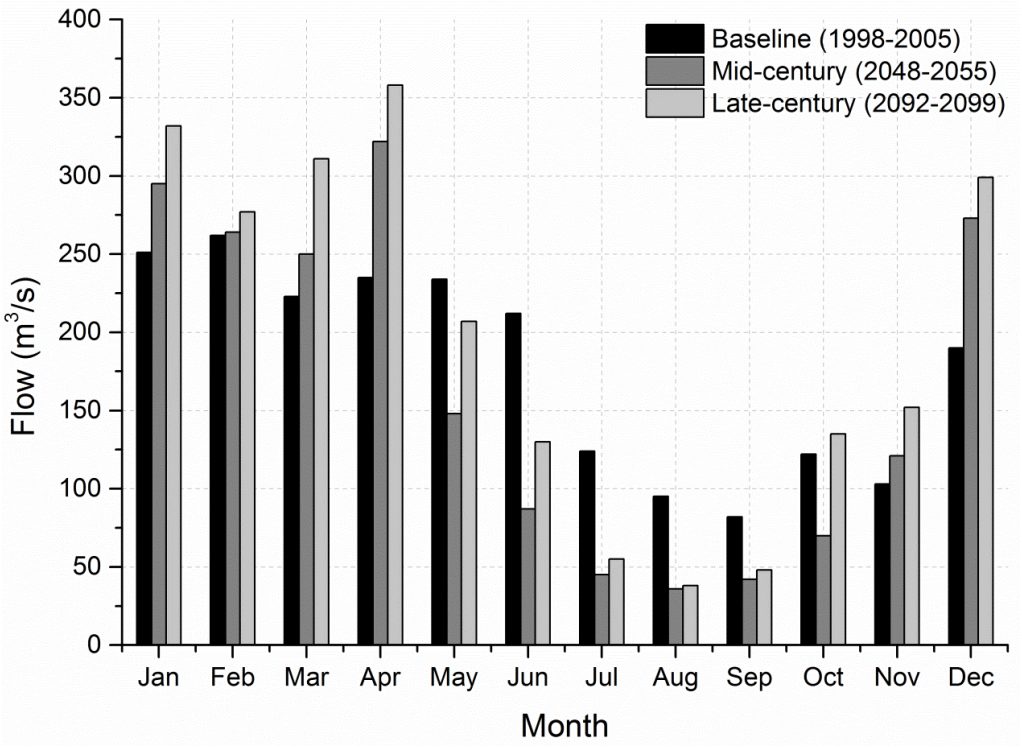

Figure 8.5: Average monthly flow for the baseline, mid-century, and late-century time periods in response to projected changes in temperature and precipitation based on ensemble GCM outputs

8.3.4 Suspended Solids (SS)

Table 8.3 and Figure 8.3 show the monthly observed and predicted SS loads in the Maumee River watershed for the calibration and validation periods. The monthly SS loads were calculated based on daily load predictions from SWAT and were compared to the observed loads at the outlet based on extensive sampling data collected by the WQL. The validation period results were slightly more accurate than the calibration period results with higher goodness of fit values for both R^2 and NSE. Figure 8.6 shows the SS load predictions from SWAT on a daily scale along with the observed loads.

It's fairly evident that SWAT under-predicted the peaks when compared to the daily load peaks. This under-prediction can possibly be attributed to the uncertainty in soil erosion and sediment yield methods used in SWAT which are based on the Modified Universal Soil Loss Equation (MUSLE). MUSLE was originally developed to estimate event-based soil erosion from agricultural fields and small watersheds. Similar under-prediction of sediment loads by SWAT has also been described in few other studies such as Benaman et al. (2005), Maski et al. (2008) and Phomcha et al. (2011). Some of the highest daily flows at the outlet of the Maumee River watershed were observed in January, 2005. There was a three-week period with high flows and no sampling data in the WQL records during this month. The monthly loads for that month were based on relatively low-flow data and probably underestimated the actual load as indicated by the very high load peaks in Figure 8.6.

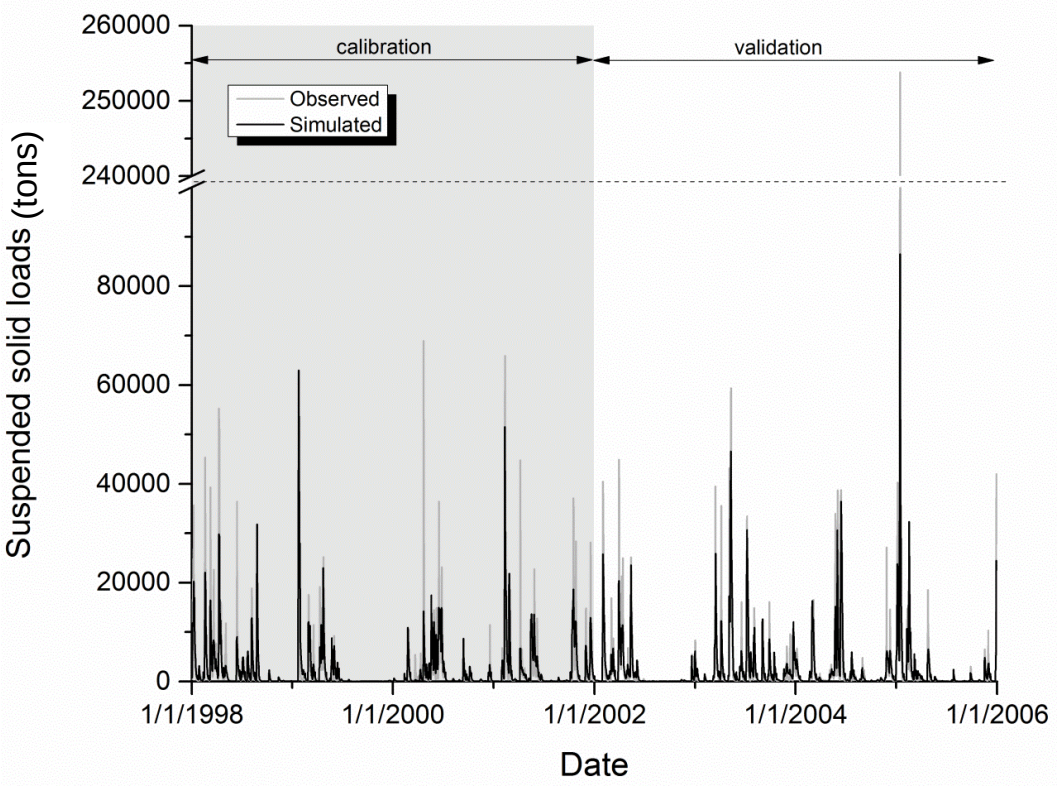

Figure 8.6: Observed and SWAT simulated daily SS loads for calibration (1998-2001) and validation (2002-2005)

Projected monthly changes in SS loads in the mid-century and late-century periods and their comparison to the baseline period loads are presented in Figure 8.7. The SS loads generally followed the same patterns as precipitation and flow changes. There was relatively negligible change projected for January SS loads. February SS loads decreased even though there was an increase in projected flow for the mid-century period. A similar trend was also seen in projected February SS loads for the late-century periods. The projected SS loads ranged from 18 percent of the corresponding monthly baseline loads (82 percent decrease) to 190 percent (90 percent increase) and from 16 percent to 238 percent for the mid-century and late-century periods, respectively. The SS loads typically increased in cooler months (except February) and decreased in warmer months for both future periods. The largest decreases in monthly SS loads were projected in July-August at 82 percent and 81 percent for the mid-century and late-century periods, respectively. The largest increases were projected in November-December and March-April, averaging 69 percent and 115 percent for the mid-century and late-century periods, respectively.

An 8.5 percent decline in average flow is projected to cause a 10.4 percent decline in annual SS loads on average. Similarly, a 9.7 percent increase in average flow is projected to cause a 19.6 percent rise in annual SS loads on average over the late-century period.

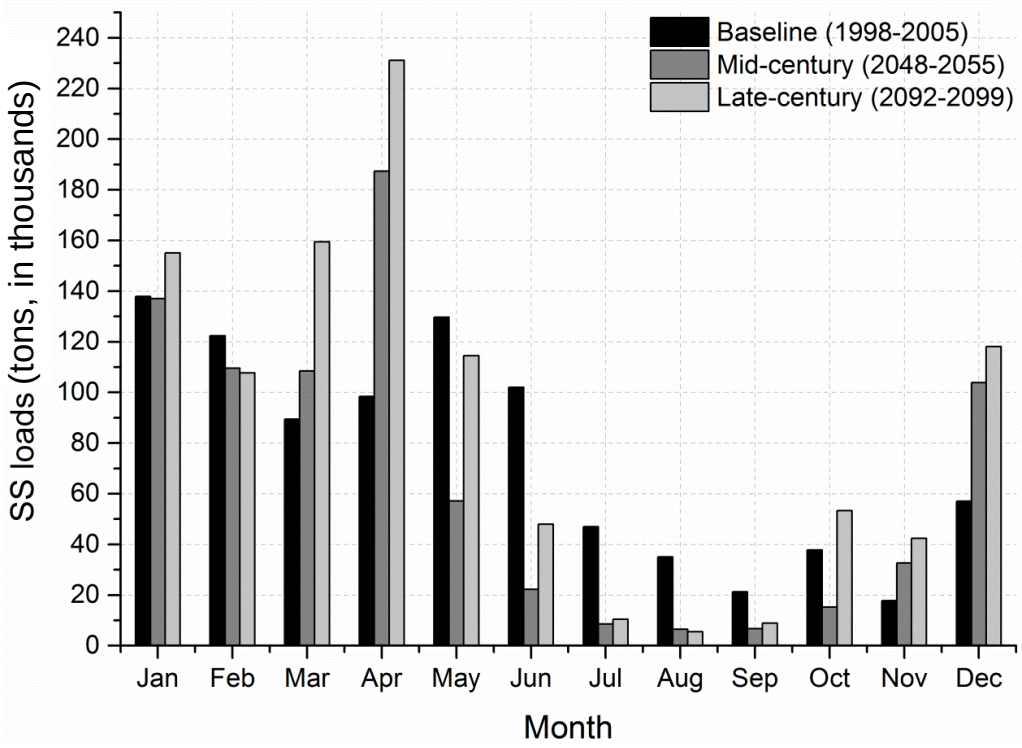

Figure 8.7: Average monthly SS loads for the baseline, mid-century, and late-century time periods in response to projected changes in temperature and precipitation based on ensemble GCM outputs

8.3.5 Total Phosphorus (TP)

Trends in TP loads for future scenarios were very similar to SS loads. TP loads typically followed changes in flow and precipitation patterns. Table 8.3 and Figure 8.3 show the average monthly TP loads using the daily data collected at the watershed outlet and daily data simulated using SWAT for the calibration and validation periods in the baseline scenario. The goodness of fit statistics were higher for the validation period when compared to the calibration period. The SWAT model predictions for TP loads were slightly worse than for SS predictions. The goodness of fit statistics were generally classified as "good" for calibration and "very good" for the validation periods, indicating that the predictions for TP loads using SWAT for the Maumee River watershed were acceptable. Figure 8.8 shows observed and SWAT simulated daily TP loads for the Maumee River watershed for the baseline period. SWAT underpredicted the peak TP loads similarly to the peak SS loads.

Figure 8.9 shows variations in monthly TP loads as compared to the baseline loads in response to the future projected changes in temperature and precipitation. The monthly loads are expected to vary from 37 percent to 165 percent and from 38 percent to 199 percent of the baseline monthly TP loads for the mid-century and late-century periods, respectively. The largest increases in monthly TP loads were projected in November, December, and April, averaging 63 percent and 78 percent for the mid-century and late-century periods, respectively. The largest decreases were projected to occur in the summer with a higher decline in the mid-century period at 62 percent and a lesser decline of 51 percent in the late-century period. The average TP loads in February showed a decline even though there was an increase projected in average flows.

An 8.5 percent decline in average flow is projected to cause an average 8.5 percent decline in annual TP loads for the mid-century period. A 9.7 percent increase in average flow is projected to cause an average 3.5 percent rise in annual TP loads over the late-century period.

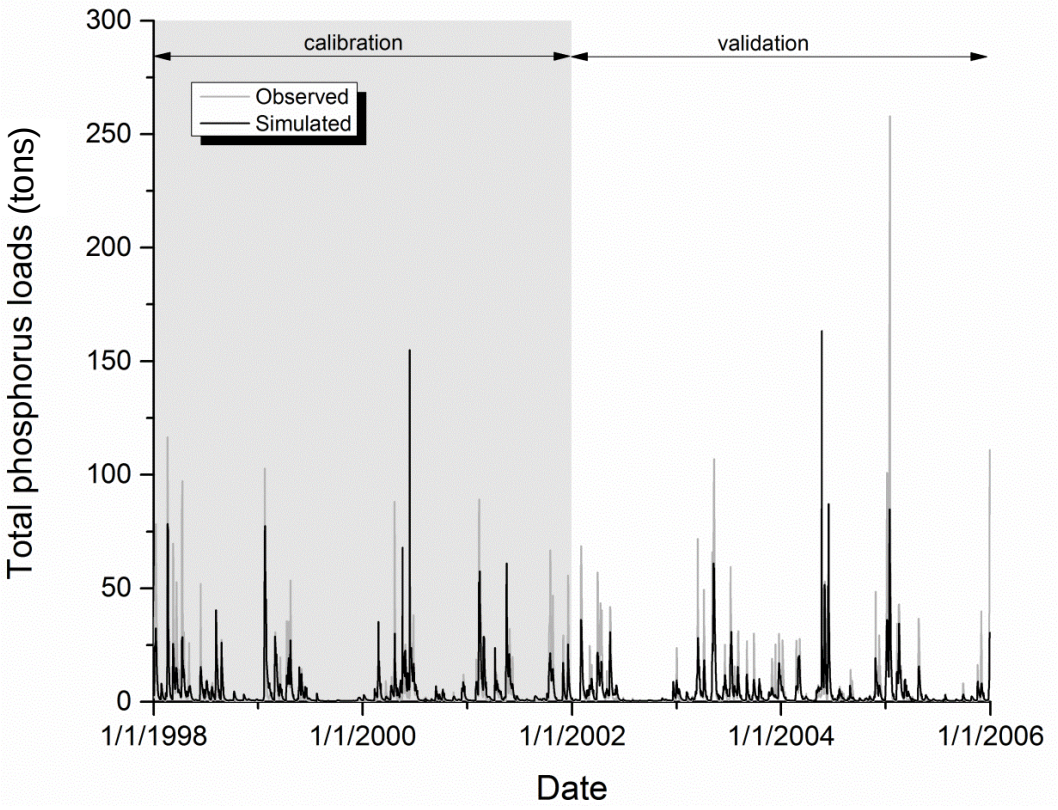

Figure 8.8: Observed and SWAT simulated daily TP loads for calibration (1998-2001) and validation (2002-2005)

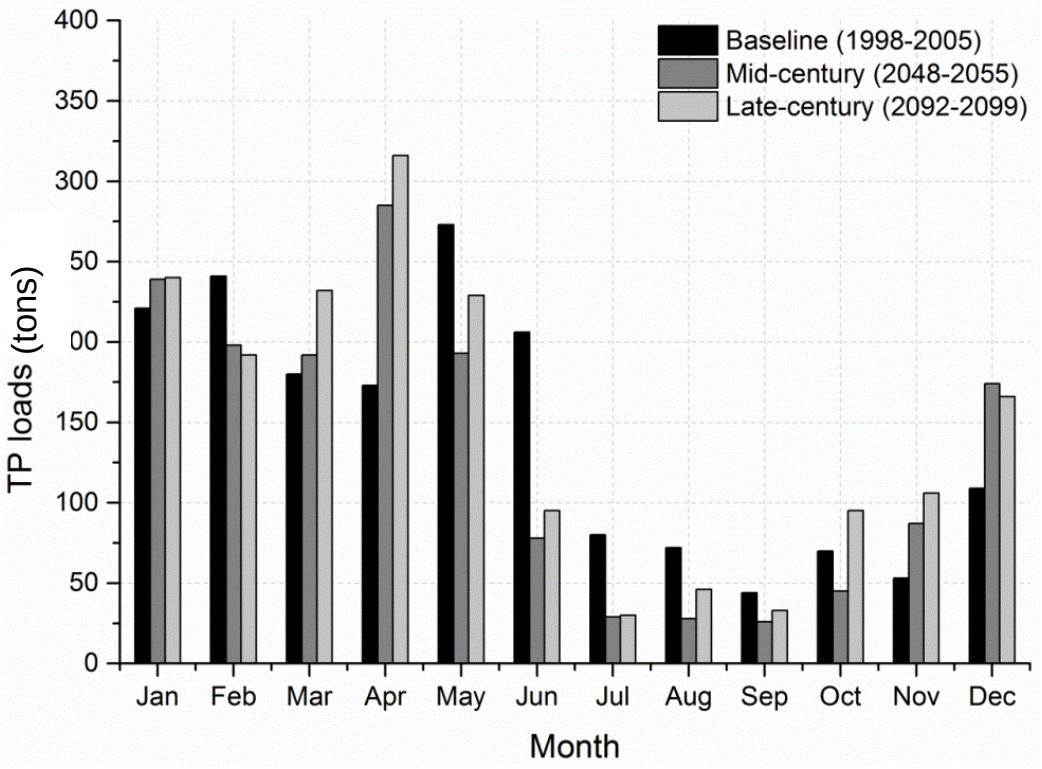

Figure 8.9: Average monthly TP loads for the baseline, mid-century and late-century time periods in response to projected changes in temperature and precipitation based on ensemble GCM outputs

8.3.6 Nitrate Nitrogen (NO_3-N)

Table 8.3 and Figure 8.3 show the average monthly NO_3-N loads observed at the Maumee River watershed outlet and the comparison to the NO_3-N loads predicted using the SWAT model for both the calibration and validation time periods. Coefficient of determination (R^2) and Nash-Sutcliff efficiency measures were higher for the calibration period (0.74 and 0.70, respectively) than for the validation period (0.72 and 0.69, respectively). Figure 8.10 shows the daily NO_3-N loads for both calibration and validation periods using observed data at the watershed outlet and simulated data from SWAT. Similar to other pollutants simulated in this research (SS and TP), SWAT under-predicted the NO_3-N load peaks.

Figure 8.11 shows the projected variations in average monthly NO_3-N loads for the mid-century and late-century time periods compared to the baseline time period. These changes are in response to projected climate change based on ensemble GCM predictions. Changes in monthly NO_3-N load patterns are very similar to changes in average monthly flows. As the flows are expected to rise over the winter and spring, the NO_3-N loads are also expected to increase over these months in the future.

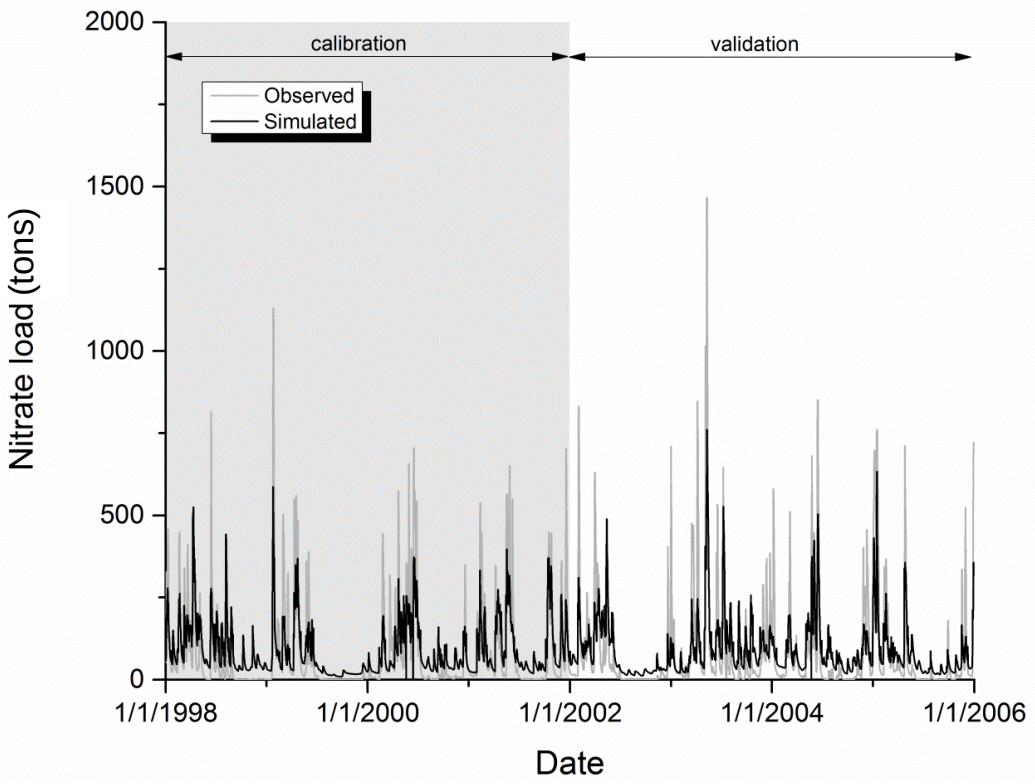

Figure 8.10: Observed and SWAT simulated daily NO_3-N loads for calibration (1998-2001) and validation (2002-2005)

A decline in NO_3-N loads compared to the baseline period is projected in the summer months for both the future time periods with a higher decline for the mid-century period. October is the first month after summer that is expected to see higher NO_3-N loads in the late-century period as compared to the baseline period. The relatively warmer months from May to October are projected to see an average decline of 43 percent in total NO_3-N loads for the mid-century period. Similarly for the late-century time period, the months from May to September are expected to see an average decline of 33 percent in total NO_3-N loads compared to the baseline period. The rest of the year, i.e., the relatively cooler months, is expected to see a rise of 17 percent and 28 percent in average monthly NO_3-N loads for the mid-century and late-century time periods, respectively.

On an individual month level, the maximum rise in NO_3-N loads is projected to occur in April averaging 39 percent and 58 percent increase compared to the baseline period for the mid and late-century periods, respectively. The maximum decline in average monthly NO_3-N loads is expected to occur over July-August averaging 56 percent and 49 percent compared to the baseline loads for the mid and late-century periods, respectively.

An 8.5 percent decline in average flow is projected to cause an average 9.9 percent decline in annual NO_3-N loads for the mid-century period. A 9.7 percent increase in average flow is projected to cause an average 6.8 percent rise in annual NO_3-N loads over the late-century period.

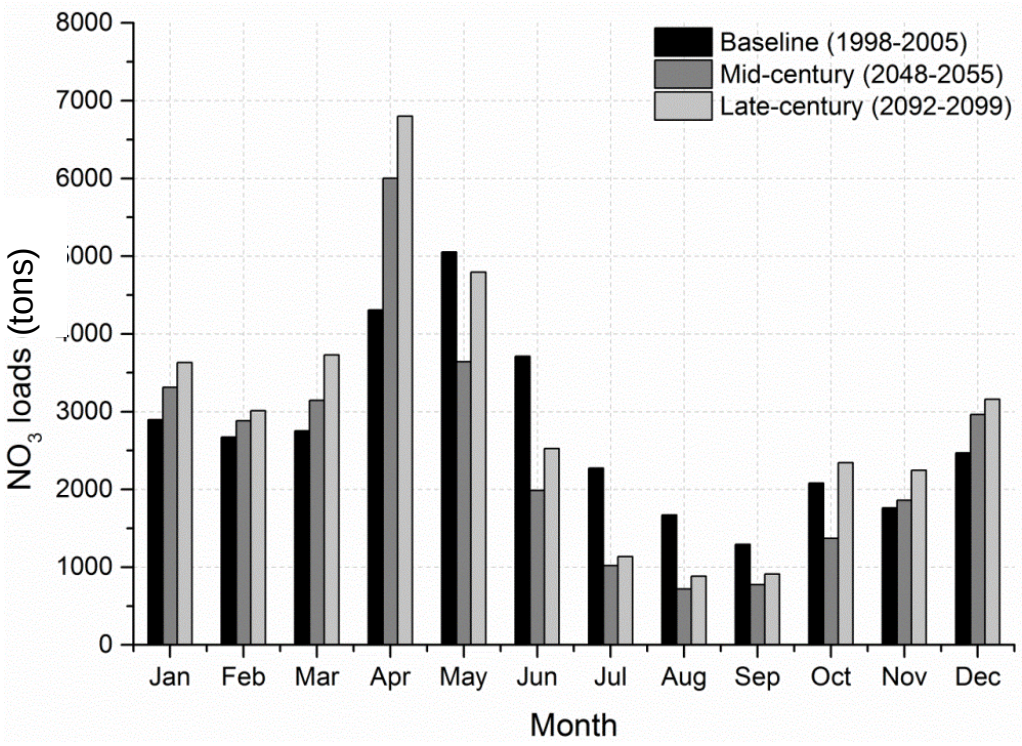

Figure 8.11: Average monthly NO_3-N loads for the baseline, mid-century and late-century time periods in response to projected changes in temperature and precipitation based on ensemble GCM outputs

8.4 Implications

The impending climate-hydrology changes may impact agriculture, natural ecosystems, and water supply in the Maumee River watershed as well as in the Great Lakes. The SWAT model was used to quantify the changes in hydrology and nutrient and sediment transport from the Maumee River watershed in response to the projected climate change in the mid- and late-century time periods. Only climate inputs to the model were modified in this study to isolate the impact of climate change. Other aspects such as urban development, agricultural practices, storm water management practices, water supply, and point source treatment would also have to be considered to fully predict future water quality changes.

The ensemble GCM predictions indicate that monthly average temperatures will rise throughout the year for the both the mid- and late-century time periods. This may have significant implications for future crop growth patterns. Each crop has its own minimum, optimum, and maximum temperature ranges for growth (Ficklin et al., 2009). Higher temperatures during the earlier part of the year coupled with longer optimum temperature periods could potentially shift the crop growing cycle earlier in a year. The length of the growing season could increase even more if temperatures stay higher during the fall. A two-crop annual cycle may then be implemented by farmers instead of the one-crop cycle practiced currently in the study watersheds if the crop growing cycle sees a large enough temporal shift.

If summer precipitation totals decline in the mid-century time period as projected, the overall flow from the Maumee River watershed will be reduced. This pattern is expected to change in the late-century period when the summer precipitation would rise compared to the mid-century period but would still be lesser than the baseline time period. This decline in summer precipitation along with an increase in temperature and evapotranspiration would lead to lesser runoff in the summer months. Flows during

summer and fall typically are already lower than flows during spring when snowmelt and spring runoff contribute to higher flows. A further decrease in summer flows could affect the water quantity in the Maumee River as well as its quality. This can have potentially negative impacts on water supply systems and other anthropogenic systems that rely on the Maumee River for their water needs. Additionally, lesser water availability during the latter part of the summer towards the end of the crop cycle may potentially cause droughts leading to crop damage.

The winter precipitation and thereby the flow is expected to rise for both the future time periods. The projected increase in precipitation in the winter months could lead to high soil moisture conditions. The related increase in runoff projected to occur in winter and spring (November through April) may potentially cause flooding in the watershed.

An increase in winter flows in the Maumee River watershed is also associated with increased sediment and nutrient loadings into Lake Erie. The increased loads could potentially affect the natural ecosystem in Lake Erie as well as the entire Great Lakes ecosystem. Higher nutrient loads coupled with increased summer temperatures and decreased inflows to Lake Erie would likely further worsen the problem of hypoxia. As shown in previous sections of this report, the majority of agricultural nutrient losses from Midwestern watersheds take place in winter months which coincides with the non-growing season in the area (also Royer et al., 2006). It would become even more critical to focus nutrient and sediment removal strategies on periods with higher loads to achieve goals aimed at reducing nutrient and sediment losses from agricultural watersheds.

8.5 Summary

This study demonstrated the potential impacts of one projected climate change scenario on hydrology and sediment and nutrient transport of the Maumee River watershed in the Lake Erie basin. The SWAT model was used to simulate hydrological and water quality processes in the watershed for the mid-century (2045-2055) and late-century (2089-2099) periods using projected ensemble climate data from three GCMs for the IPCC A1B scenario. The results indicated that the hydrology in the Maumee River watershed is sensitive to climatic variations projected to occur in the future.

It should be noted there are challenges associated with evaluating the impacts of climate change on hydrological processes. Uncertainties are related to future climate projections. There is a wide degree of variation in projections from different GCM models. Downscaling projected data to a higher spatial and temporal resolution for modeling requirements also adds to uncertainty of the resulting assessments. Additional uncertainties result from the model calibration such as under-prediction of daily pollutant peaks by SWAT in this study. Thus, in climate studies it is critical to properly define uncertainties, particularly those based on future climates, and climate model structure. This study does not account for all of these uncertainties, but rather provides a first approximation of the potential impacts of climate change. Future studies could potentially use finer scale statistical downscaling, performance-based weighted ensemble analyses, and a suite of climate change scenarios to more accurately calculate projected precipitation data and their confidence limits.

Compared to the baseline period (1995-2005), an increase of 2.9^{o}C in average annual temperatures coupled with a 3.2 percent decrease in annual precipitation decreased the flow in the watershed by 8.5 percent for the mid-century time period. This decrease in annual flow also reduced annual SS, TP, and NO_3-N loads by 10.4 percent, 8.5 percent, and 9.9 percent, respectively. A 4.3^{o}C rise in annual temperatures along with a 5.6 percent increase in annual precipitation increased the annual flow in the watershed by 9.7 percent for the late-century period. This increase in annual flow was accompanied by a 19.6 percent, 3.5 percent, and 6.8 percent increase in annual SS, TP, and NO_3-N loads, respectively.

Hydrological processes were sensitive to climate change on monthly scales as well. The summer precipitation declined for both future time periods with a greater decline in the mid-century period, while

the winter precipitation rose in both periods. Average monthly flows increased in the winter and spring and decreased during the summer. Sediment and nutrient loads also generally saw increases in the winter and spring with a few exceptions.

Overall, the results indicated that both water quantity and quality in the Maumee River watershed were affected by projected changes in climate for the mid- and late-century time periods. The results are not intended to represent actual conditions that will occur in the watershed, but do elucidate the general direction and magnitude of changes that might occur in the hydrology of the watershed under the assumptions of this study. Projected hydrological changes and potential implications for water quality could help managers in the area make more informed decisions pertaining to water management, agriculture, and urban development and to take necessary precautions to mitigate the negative impacts associated with excessive nutrient losses, erosion, floods, and droughts.

9. Overall Conclusions

The overall goal of this study was to improve the understanding of anthropogenic and natural impacts on annual pollutant loads and their corresponding spatial and temporal patterns and trends from large Midwestern watersheds. Traditional approaches to load estimation were investigated. The method of predicting nutrient concentrations can have a large impact on annual loads and their trends, as demonstrated for a large agricultural basin in the Midwestern United States by comparing a few traditional, improved, and modified statistical data mining and empirical techniques. An alternative approach to estimate annual loads was developed. The role of large load events in predicting annual pollutant (sediment and nutrients) loads using regression relationships was determined together with temporal patterns in pollutant load export from these watersheds. The impacts of projected climate change for a mid-century and late-century period on hydrology and water quality were evaluated for a large agricultural watershed using a physically-based model.

The above analyses led to these main conclusions:

- Mechanistic differences that govern the export of different constituents have a significant impact on the accuracy of load estimates. While SS and TP are primarily exported by surface runoff, large portions of NO_3-N are exported by subsurface systems including tile drains.
- Average annual pollutant concentrations, loads, and their respective trends are sensitive to the amounts of data used for calculations and observed outliers. The findings of the study highlight the role of data variability and observed outliers and signify the value of each observation year. This underscores the importance of maintaining water quality and flow monitoring sites for future analyses of changes in loads.
- Two data mining methods including the instance-based nearest neighbor classifier and the decision tree classifier exhibited a potential to be used in estimation of concentration data for days without water quality observations.
- More than half of the annual load of NO_3-N, SS, and TP is transported during the 5 largest storm events. The proportion is higher for watersheds dominated by nonpoint sources. SS and TP showed higher contributions of top load events to annual loads compared with NO_3-N. Targeted monitoring of episodes of high load events is critical for accurate estimation of annual constituent loads. These findings eventually can contribute to the design of cost-effective monitoring networks.
- A strong temporal pattern in pollutant loadings was observed. NO_3-N loadings occurred primarily between November and April. SS and TP loadings occurred primarily between February and May. No significant statistical trends were observed in timing over long monitoring durations. Pollutant concentrations were considerably more uniformly distributed throughout the year as compared to loads which were concentrated over the high flow periods in late winter and early spring months.
- The presence of point sources and impoundments in the watershed can significantly alter temporal and statistical characteristics of loads when comparing to agriculture watersheds. The presence of impoundments reduced the overall loads by limiting flow and aiding sedimentation. A significant discharge from point sources reduces the impact of nonpoint sources as well as the importance of large storm events in pollutant load transported from a watershed.
- A SWAT-based framework for evaluation of the effects on future climates on riverine loadings indicated that climate change is expected to increase annual flow volumes and total annual pollutant load export. While a more comprehensive study would be required to determine the extent of changes under various climate scenarios along with their confidence limits, this application indicates that the hydrologic system can be very sensitive to climate change.

References

Alexander, R. B., A. H. Elliott, U. Shankar, and G. B. McBride. 2002. Estimating the sources and transport of nutrients in the Waikato River Basin, New Zealand. *Water Resources Research* 38(12): 41-423.

Allan, J. D., and L. Hinz. 2004. An assessment of flows for rivers of the Great Lakes basin. Project Report, Great Lakes Protection Fund, Ann Arbor, MI.

Arnell, N. W. 2003. Relative effects of multi-decadal climatic variability and changes in the mean and variability of climate due to global warming: Future streamflows in Britain. *Journal of Hydrology* 270(3-4):195-213.

Arnell, N. W., and C. Liv. 2001. Hydrology and water resources. In McCarthy, J.J., Canziani, O.F., Leary, N.A., Dokken, D.J., White, K.S. (Eds.), *Climate change 2001: Impacts, adaptation and vulnerability*. Cambridge, UK: Cambridge University Press, 191–233.

Arnold, J. G., and P. M. Allen. 1999. Automated methods for estimating baseflow and ground water recharge from streamflow records. *J Amer Water Resour Assoc* 35:411-424.

Arnold, J. G., R. Srinivasan, R. S. Muttiah, and J. R. Williams. 1998. Large area hydrologic modeling and assessment Part I: model development. *Journal of the American Water Resources Association* 34(1): 73-89.

Aulenbach, B. T., and R. P. Hooper. 2006. The Composite Method: An improved method for stream-water solute load estimation. *Hydrological Processes* 20(14): 3029-3047.

Aulenbach, B. T., H. T. Buxton, W. A. Battaglin, and R. H. Coupe. 2007. Streamflow and nutrient fluxes of the Mississippi-Atchafalaya River Basin and subbasins for the period of record through 2005. U.S. Geological Survey Open-File Report 2007–1080.

Baker, D. B. 1985. Regional water quality impacts of intensive row-crop agriculture: A Lake Erie Basin case study. *Journal of Soil & Water Conservation* 40(1): 125-132.

Balter, M. 2013. Archaeologists say the 'Anthropocene' is here - but it began long ago. *Science* 340(6130):261-262.

Benaman, J., C. A. Shoemaker, and D. A. Haith. 2005. Calibration and validation of soil and water assessment tool on an agricultural watershed in Upstate New York. *Journal of Hydrologic Engineering* 10(5):363-374.

Berens, P. 2009. CircStat: A MATLAB Toolbox for circular statistics. *J Stat Softw* 31(10): 1-21.

Bosch, N. S. 2008. The influence of impoundments on riverine nutrient transport: An evaluation using the Soil and Water Assessment Tool. *Journal of Hydrology* 355(1-4):131-147.

Bosch, N. S., J. D. Allan, D. M. Dolan, H. Han, and R. P. Richards. 2011. Application of the Soil and Water Assessment Tool for six watersheds of Lake Erie: Model parameterization and calibration. *Journal of Great Lakes Research* 37(2):263-271.

Bouraoui, F., L. Galbiati, and G. Bidoglio. 2002. Climate change impacts on nutrient loads in the Yorkshire Ouse Catchment (UK). *Hydrology and Earth System Sciences* 6(2):197-209.

Brekke, L. D., J. E. Kiang, J. R. Olsen, R. S. Pulwarty, D. A. Raff, D. P. Turnipseed, R. S.Webb, and K. D. White. 2009. Climate change and water resources management—A federal perspective. U.S. Geological Survey Circular 1331, 65 p.

Bronstert, A., D. Niehoff, and G. Brger. 2002. Effects of climate and land-use change on storm runoff generation: Present knowledge and modelling capabilities. *Hydrological Processes* 16 (2):509-529.

Camargo, J. A. and Á. Alonso. 2006. Ecological and toxicological effects of inorganic nitrogen pollution in aquatic ecosystems: A global assessment. *Environment International* 32(6):831-849.

Chaplot, V. 2007. Water and soil resources response to rising levels of atmospheric CO2 concentration and to changes in precipitation and air temperature. *Journal of Hydrology* 337(1-2):159-171.

Cohn, T. A. 1995. Recent advances in statistical methods for the estimation of sediment and nutrient transport in rivers. *Review of Geophysics*, Supplement, 1117–1123.

Cohn, T. A., D. L. Caulder, E. J. Gilroy, L. D. Zynjuk, and R. M. Summers. 1992. The validity of a simple statistical model for estimating fluvial constituent loads: An empirical study involving nutrient loads entering Chesapeake Bay." *Water Resources Research* 28(9):2353-2363.

Cohn, T. A., DeLong, L. L., Gilroy, E. J., Hirsch, R. M., and Wells, D. K. 1989. Estimating constituent loads. *Water Resour. Res*. 25(5): 937–942.

Cooper, D. M. and C. D. Watts. 2002. A comparison of river load estimation techniques: Application to dissolved organic carbon. *Environmetrics* 13(7): 733-750.

Crowder, D. W., Demissie, M., and Markus, M. 2007. The accuracy of sediment loads when log-transformation produces nonlinear sediment load-discharge relationships. *J. of Hydrol*. 336(3-4): 250–268.

David, M. B., L. E. Gentry, D. A. Kovacic, and K. M. Smith. 1997. Nitrogen balance in and export from an agricultural watershed. *Journal of Environmental Quality* 26(4):1038-1048.

De Pinto, J. V., T. C. Young, and D. K. Salisbury. 1986. Impact of phosphorus availability on modelling phytoplankton dynamics. *Hydrobiological Bulletin* 20(1-2):225-243.

Demissie, M. 1996. Sediment load during flood events for Illinois streams. *Water Int*. 21:131-137.

Demissie, M., and L. Keefer. 1996. Watershed monitoring and land use evaluation for the Lake Decatur watershed. Misc. Publ. 169, Illinois State Water Survey Misc. Publ. 169, Champaign, IL.

Dibike, Y. B. and P. Coulibaly. 2007. Validation of hydrological models for climate scenario simulation: The case of Saguenay Watershed in Quebec. *Hydrological Processes* 21(23):3123-3135.

Dixit, A. S., R. I. Hall, P. R. Leavitt, R. Quinlan, and J. P. Smol. 2000. Effects of sequential depositional basins on lake response to urban and agricultural pollution: A palaeoecological analysis of the Qu'Appelle Valley, Saskatchewan, Canada. *Freshwater Biology* 43(3):319-337.

Dolan, D.M., 1993. Point source loadings of phosphorus to Lake Erie: 1986–1990. J. Great Lakes Res. 19, 212–223. http://dx.doi.org/10.1016/S0380-1330(93)71212-5.

Dolan, D. M., A. K. Yui, and R. D. Geist. 1981. Evaluation of river load estimation methods for total phosphorus. *Journal of Great Lakes Research* 7(3): 207–214.

Driver, N. E. and B. M. Troutman. 1989. Regression models for estimating urban storm-runoff quality and quantity in the United States. *Journal of Hydrology* 109(3-4): 221-236.

El-Shaarawi, A. H., K. W. Kuntz, and A. Sylvestre. 1986. Estimation of loading by numerical integration. *Developments in Water Science* 27.

EPA Science Advisory Board. 2008. Hypoxia in the Northern Gulf of Mexico: An update by the EPA Science Advisory Board." Washington DC, EPA Science Advisory Board, EPA SAB-08-003.

Ferguson, R. I. 1987. Accuracy and precision of methods for estimating river loads. *Earth Surface Processes and Landforms* 12(1):95–104.

Ficklin, D. L., Y. Luo, E. Luedeling, and M. Zhang. 2009. "Climate Change Sensitivity Assessment of a Highly Agricultural Watershed using SWAT." Journal of Hydrology 374 (1-2): 16-29.

Fontaine, T. A., J. F. Klassen, T. S. Cruickshank, and R. H. Hotchkiss. 2001. "Hydrological Response to Climate Change in the Black Hills of South Dakota, USA." Hydrological Sciences Journal 46 (1):27-40.

Gassman, P. W., M. R. Reyes, C. H. Green, and J. G. Arnold. 2007. The Soil and Water Assessment Tool: Historical development, applications, and future research directions. *Transactions of the ASABE* 50(4):1211-1250.

Gentry, L. E., M. B. David, F. E. Below, T. V. Royer, and G. F. McIsaac. 2009. Nitrogen mass balance of a tile-drained agricultural watershed in east-central Illinois. *Journal of Environmental Quality* 38(5):1841-1847.

GLWQA.1978.Great Lakes Water Quality Agreement. http://www.epa.gov/greatlakes/glwqa/1978/index.html (accessed June 6, 2013).

Goolsby, D. A., W. A. Battaglin, B. T. Aulenbach, and R. P. Hooper. 2001. Nitrogen input to the Gulf of Mexico. *Journal of Environmental Quality* 30(2):329-336.

Green, C. H., M. D. Tomer, M. Di Luzio, and J. G. Arnold. 2006. Hydrologic evaluation of the Soil and Water Assessment Tool for a large tile-drained watershed in Iowa. *Transactions of the ASABE* 49(2):413-422.

Grimvall, A., P. Stålnacke, and A. Tonderski. 2000. Time scales of nutrient losses from land to sea - A European perspective. *Ecological Engineering* 14(4):363-371.

Groffman, P. M., J. M. Tiedje, D. L. Mokma, and S. Simkins. 1992. Regional scale analysis of denitrification in north temperate forest soils. *Landscape Ecology* 7(1):45-53.

Guo, Y., M. Markus, and M. Demissie. 2002. Uncertainty of nitrate load computations for agricultural watersheds. *Water Resources Research* 38(10): 31-312.

Hall M., E. Frank, G. Holmes, B. Pfahringer, P. Reutemann, and I. H. Witten. The WEKA Data Mining software: An update. *SIGKDD Explorations* 11(1).

Hawley, N., T. H. Johengen, Y. R. Rao, S. A. Ruberg, D. Beletsky, S. A. Ludsin, B. J. Eadie, D. J. Schwab, T. E. Croley, and S. B. Brandt. 2006. Lake Erie hypoxia prompts Canada-U.S. study. *Eos* 87(32):313-315.

Hayhoe, K. A. 2010. A standardized framework for evaluating the skill of regional climate downscaled techniques. Ph.D. diss, University of Illinois, Urbana-Champaign, Illinois.

Helsel, D. R., and Hirsh, R. M. 1995. *Statistical methods in water resources*. New York: Elsevier Science Publishing Company, Inc., 529 p.

Hirsch, R. M., L. M. Douglas, and S. A. Archfield. 2010. Weighted regressions on time, discharge, and season (WRTDS), with an application to Chesapeake Bay river inputs. *Journal of the American Water Resources Association* 46:857-880.

Hofstra, N. and A. F. Bouwman. 2005. Denitrification in agricultural soils: Summarizing published data and estimating global annual rates. *Nutrient Cycling in Agroecosystems* 72(3):267-278.

Howarth, R. W. 1998. An assessment of human influences on fluxes of nitrogen from the terrestrial landscape to the estuaries and continental shelves of the North Atlantic Ocean. *Nutrient Cycling in Agroecosystems* 52(2-3):213-223.

Illinois Environmental Protection Agency. 2007. Illinois Water Monitoring Strategy 2007-2012. Illinois EPA, Bureau of Water, Springfield, IL. http://www.epa.state.il.us/water/water-quality/index.html

Jackson, R. B., S. R. Carpenter, C. N. Dahm, D. M. McKnight, R. J. Naiman, S. L. Postel, and S. W. Running. 2001. Water in a changing world. *Ecological Applications* 11(4):1027-1045.

Johnes, P. J. 2007. Uncertainties in annual riverine phosphorus load estimation: Impact of load estimation methodology, sampling frequency, baseflow index and catchment population density. *Journal of Hydrology* 332(1-2):241-258.

Keefer, L., and M. Demissie. 2000. *Watershed monitoring for the Lake Decatur Watershed, 1998–1999*. Illinois State Water Survey Contract Report 2000-06, Champaign, IL.

Keefer, L., Bauer, E., and Markus, M. 2010. *Hydrologic and nutrient monitoring of the Lake Decatur watershed: Final report 1993–2008*. Illinois State Water Survey Contract Report 2010-07, Champaign, IL.

Kendall, M. G. 1955. *Rank correlation methods*. New York: Hafner Publishing Co.

Kling, G. W., G. W. Kipphut, M. M. Miller, and W. J. O'Brien. 2000. Integration of lakes and streams in a landscape perspective: The importance of material processing on spatial patterns and temporal coherence. *Freshwater Biology* 43(3):477-497.

Knutti, R., R. Furrer, C. Tebaldi, J. Cermak, and G. A. Meehl. 2010. Challenges in combining projections from multiple climate models. *American Meteorological Society* 23(10): 2739–2758.

Kočić, A., T. Hengl, and J. Horvatić. 2008. Water nutrient concentrations in channels in relation to occurrence of aquatic plants: A case study in Eastern Croatia. *Hydrobiologia* 603(1):253-266.

Kronvang, B., E. Jeppesen, D. J. Conley, M. Søndergaard, S. E. Larsen, N. B. Ovesen, and J. Carstensen. 2005. Nutrient pressures and ecological responses to nutrient loading reductions in Danish streams, lakes and coastal waters. *Journal of Hydrology* 304(1-4): 274-288.

Kundzewicz, Z. W., L. J. Mata, N. W. Arnell, P. Döll, P. Kabat, B. Jiménez, K. A. Miller, T. Oki, Z. Sen, and I. A.Shiklomanov. 2007. Freshwater resources and their management. Climate Change 2007: Impacts, Adaptation and Vulnerability. Contribution of Working Group II to the Fourth Assessment Report of the Intergovernmental Panel on Climate Change. Editors: Parry, M.L., Canziani, O.F., Palutikof, J.P., van der Linden P.J., Hanson, C.E. Cambridge University Press, Cambridge, UK, 173–210.

Kyoung, J. L., B. A. Engel, Z. Tang, J. Choi, K. -S Kim, S. Muthukrishnan, and D. Tripathy. 2005. Automated Web GIS based hydrograph analysis Tool, WHAT. *Journal of the American Water Resources Association* 41(6):1407-1416.

Labat, D., Y. Goddéris, J. L. Probst, and J. L. Guyot. 2004. Evidence for global runoff increase related to climate warming. *Advances in Water Resources* 27(6):631-642.

Lampman, G. G., N. F. Caraco, and J. J. Cole. 1999. Spatial and temporal patterns of nutrient concentration and export in the tidal Hudson River. *Estuaries* 22(2 A): 285-296.

Lewis, J. 1996. Turbidity-controlled suspended sediment sampling for runoff-event load estimation. Water Resources Research 32(7):2299-2310.

Lian, Y., Chan, I.-C., Xie, H., and Demissie, M. 2010. Improving HSPF modeling accuracy from FTABLES: Case study for the Illinois River basin. *Journal of Hydrologic Engineering* 15(8): 642–650.

Lucey, K. J., Goolsby, D. A, 1993. Effects of climatic variations over 11 years on NO3-Nitrogen concentrations in the Raccoon River, Iowa. *Journal of Environmental Quality* 22(1):38–46.

Markus, M. and M. Demissie. 2006. Predictability of annual sediment loads based on flood events. *Journal of Hydrologic Engineering* 11(4):354-361.

Markus, M., M. Demissie, M. Short, S. Verma, and A. R. Cooke. 2014. A sensitivity analysis of annual nitrate loads and the corresponding trends in the Lower Illinois River, *J. Hydrol. Eng*. pp. -doi: 10.1061/(ASCE)HE.1943-5584.0000831

Markus, M., D. J. Wuebbles, X. -Z Liang, K. Hayhoe, and D. A. R. Kristovich. 2012. Diagnostic analysis of future climate scenarios applied to urban flooding in the Chicago metropolitan area. *Climatic Change* 111(3): 879-902.

Maski, D., K. R. Mankin, K. A. Janssen, P. Tuppad, and G. M. Pierzynski. 2008. Modeling runoff and sediment yields from combined in-field crop practices using the Soil and Water Assessment Tool. *Journal of Soil and Water Conservation* 63(4):193-203.

McIsaac, G. F., and Libra, R. D., 2003, Revisiting nitrate concentrations in the Des Moines River 1945 and 1976–2001, J. Environ. Qual., 32:2280–2289.

Meehl, G. A., T. F. Stocker, W. D. Collins, P. Friedlingstein, A. T.Gaye, J. M. Gregory, A. Kitoh, R. Knutti, J. M. Murphy, A. Noda, S. C. B. Raper, I. G. Watterson, A. J. Weaver, and Z. -C. Zhao. 2007. Global climate projections. In *Climate change 2007: The physical science basis*. Contribution of Working Group I to the Fourth Assessment Report of the Intergovernmental Panel on Climate Change. Solomon, S., Qin, D., Manning, M., Chen, Z., Marquis, M., Averyt, K.B., Tignor, M., Miller, H.L., Cambridge University Press, Cambridge, United Kingdom and New York, NY, USA.

Meybeck, M. and R. Helmer. 1989. The quality of rivers: From pristine stage to global pollution. *Palaeogeography, Palaeoclimatology, Palaeoecology* 75(4):283-309.

Michalak, A. M., E. J. Anderson, D. Beletsky, S. Boland, N. S. Bosch, T. B. Bridgeman, J. D. Chaffin, et al. 2013. Record-setting algal bloom in Lake Erie caused by agricultural and meteorological trends consistent with expected future conditions. *Proceedings of the National Academy of Sciences of the United States of America* 110(16):6448-6452.

Mierzejewski. C., M. Markus, and G. Czapar. 2013. Effects of drought on nutrient concentrations and loads in rivers. Illinois State Water Survey project report submitted to National Great Rivers Research and Education Center. Illinois State Water Survey, Champaign, IL.

Milly, P. C. D., K. A. Dunne, and A. V. Vecchia. 2005. Global pattern of trends in streamflow and water availability in a changing climate. *Nature* 438(7066):347-350.

Moriasi, D. N., J. G. Arnold, M. W. Van Liew, R. L. Bingner, R. D. Harmel, and T. L. Veith. 2007. Model evaluation guidelines for systematic quantification of accuracy in watershed simulations. *Transactions of the ASABE* 50(3):885-900.

Mourad, D. S. J. and M. van der Perk. 2009. Spatio-temporal patterns of nutrient concentrations and export in a north-eastern European lowland catchment. *Hydrological Processes* 23(13):1821-1833.

Mu, Q., M. Zhao, and S. W. Running. 2011. Evolution of hydrological and carbon cycles under a changing climate. Part III: Global change impacts on landscape scale evapotranspiration. *Hydrological Processes* 25(26):4093-4102.

Myers, D. N., K. D. Metzker, and S. Davis. 2000. Status and trends in suspended-sediment discharges, soil erosion, and conservation tillage in the Maumee River Basin—Ohio, Michigan, and Indiana. Water Resources Investigations Report: 2000-4091. USGS Information Service, Denver, CO.

Nash, J., J. Sutcliffe, 1970. River flow forecasting through conceptual models; part I-A discussion of principles. J. Hydrol. 10 (3), 282–290.

Natural Resources Conservation Service. 1983. National engineering handbook, Section 3 sedimentation. U.S. Department of Agriculture.

Natural Resources Conservation Service. 2005. “Western Lake Erie basin water resources protection plan: Ohio, Indiana and Michigan. Natural Resources Conservation Service”. Retrieved Oct 8, 2012. ftp://ftp-fc.sc.egov.usda.gov/OH/pub/Programs/Lake_Erie/erie_basin_plan.pdf.

Neitsch, S. L., J. G. Arnold, J. R. Kiniry, J. R. Williams, and K. W. King. 2005. Soil and Water Assessment Tool Theoretical Documentation Version 2005. Soil and Water Assessment Tool Theoretical Documentation, Version 2005.

Neumann, D. W., B. Rajagopalan, and E. A. Zagona. 2003. Regression model for daily maximum stream temperature. *J. Environ. Engrg* 129(7): 667–674.

Panno, S. V., W. R. Kelly, K. C. Hackley, H. –H. Hwang,and A. Martinsek. 2008. Sources and fate of nitrate in the Illinois River Basin, Illinois. *Journal of Hydrology* 359(1-2):174–188.

Park, J. -Y, M. -J Park, M. -J H. -K Joh, H. -J Shin, H. -J Kwon, R. Srinivasan, and S. -J Kim. 2011. Assessment of MIROC3.2 hires climate and Clue-s land use change impacts on watershed hydrology using Swat. *Transactions of the ASABE* 54(5):1713-1724.

Parry, M.L., O.F. Canziani, J.P. Palutikof, P.J. van der Linden, and C.E. Hanson. 2007. “Climate change 2007: Impacts, adaptation and vulnerability. Contribution of Working Group II to the Fourth Assessment Report of the Intergovernmental Panel on Climate Change. Cambridge University Press, Cambridge.

Phomcha, P., P. Wirojanagud, T. Vangpaisal, and T. Thaveevouthti. 2011. Predicting sediment discharge in an agricultural watershed: A sase study of the Lam Sonthi Watershed, Thailand. *ScienceAsia* 37(1):43-50.

Postel, S. 2013. Water – and Us – in the “Anthropocene.” National Geographic Freshwater Initiative in Water Currents.

Praskievicz, S. and H. Chang. 2009. A review of hydrological modelling of basin-scale climate change and urban development impacts. *Progress in Physical Geography* 33(5): 650-671.

Preston, S. D., V. J. Bierman Jr, and S. E. Silliman. 1989. An evaluation of methods for the estimation of tributary mass loads. *Water Resources Research* 25(6):1379-1389.

Pruski, F. F. and M. A. Nearing. 2002. Runoff and soil-loss responses to changes in precipitation: A computer simulation study. *Journal of Soil and Water Conservation* 57 (1): 7-16.

Rabalais, N. N., R. E. Turner, and D. Scavia. 2002. Beyond science into policy: Gulf of Mexico hypoxia and the Mississippi River. *Bioscience* 52(2):129-142.

Randall, G. W. and D. J. Mulla. 2001. Nitrate nitrogen in surface waters as influenced by climatic conditions and agricultural practices. *Journal of Environmental Quality* 30 (2):337-344.

Raupach, M. R., G. Marland, P. Ciais, C. Le Quéré, J. G. Canadell, G. Klepper, and C. B. Field. 2007. Global and regional drivers of accelerating CO2 emissions. *Proceedings of the National Academy of Sciences of the United States of America* 104(24):10288-10293.

Raymond, P. A., M. B. David, and J. E. Saiers. 2012. The impact of fertilization and hydrology on nitrate fluxes from Mississippi watersheds. *Current Opinion in Environmental Sustainability* 4(2):212-218.

Richards, R. P. and D. B. Baker. 1993. Trends in nutrient and suspended sediment concentrations in Lake Erie tributaries, 1975-1990. *Journal of Great Lakes Research* 19(2):200-211.

Richards, R. P. and D. B. Baker. 1993. Pesticide concentration patterns in agricultural drainage networks in the Lake Erie basin. *Environmental Toxicology and Chemistry* 12(1): 13-26.

Richards, R. P. and J. Holloway. 1987. Monte Carlo studies of sampling strategies for estimating tributary loads. Water Resources Research 23(10):1939-1948.

Richards, R. P., D. B. Baker, and D. J. Eckert. 2002. Trends in agriculture in the LEASEQ watersheds, 1975-1995. *Journal of Environmental Quality* 31(1):17-24.

Richards, R. P., D. B. Baker, J. W. Kramer, D. E. Ewing, B. J. Merryfield, and N. L. Miller. 2001. Storm discharge, loads, and average concentrations in northwest Ohio Rivers, 1975-1995. *Journal of the American Water Resources Association* 37(2):423-438.

Richards, R.P. 1985. Estimating the extent of reduction needed to statistically demonstrate reduced non-point phosphorus loading to Lake Erie. *J. Great Lakes Res*. 11:110–116.

Robertson, D. M. 2003. Influence of different temporal sampling strategies on estimating total phosphorus and suspended sediment concentration and transport in small streams. *Journal of the American Water Resources Association* 39(5):1281-1308.

Robertson, D. M. and E. D. Roerish. 1999. Influence of various water quality sampling strategies on load estimates for small streams. *Water Resources Research* 35(12):3747-3759.

Royer, T. V., M. B. David, and L. E. Gentry. 2006. Timing of riverine export of nitrate and phosphorus from agricultural watersheds in Illinois: Implications for reducing nutrient loading to the Mississippi River. *Environmental Science and Technology* 40(13): 4126-4131.

Rozemeijer, J. C., Y. Van Der Velde, F. C. Van Geer, G. H. De Rooij, P. J. J. F. Torfs, and H. P. Broers. 2010. Improving load estimates for NO3 and P in surface waters by characterizing the concentration response to rainfall events. *Environmental Science and Technology* 44(16):6305-6312.

Ruddy, B. C., D. L. Lorenz, and D. K. Mueller. 2006. County-level estimates of nutrient inputs to the land surface of the conterminous United States, 1982–2001. National Water Quality Assessment Program, U.S. Geological Survey.

Salles, C., M. G. Tournoud, and Y. Chu. 2008. Estimating nutrient and sediment flood loads in a small Mediterranean river. *Hydrological Processes* 22(2):242-253.

Schilling, K. and Y.–K. Zhang. 2004. Baseflow contribution to NO3-Nitrogen export from a large, agricultural watershed, USA. *Journal of Hydrology* 295 (1-4): 305-316.

Schilling, K. E., and J. Spooner. 2006. Effects of watershed-scale land use change on stream nitrate concentrations. *J. Environ. Qual*. 35:2132–2145.

Short, M. B. 1999. Baseline loadings of nitrogen, phosphorus, and sediments from Illinois Watersheds. Illinois Environmental Protection Agency, IEPA/BOW/99-020, Springfield, IL.

Schuur, E. A. G., J. Bockheim, J. G. Canadell, E. Euskirchen, C. B. Field, S. V. Goryachkin, S. Hagemann, et al. 2008. Vulnerability of permafrost carbon to climate change: Implications for the global carbon cycle. Bioscience 58(8):701-714.

Şen, Zekâi. 2012. An innovative trend analysis methodology. *Journal of Hydrologic Engineering*, doi:http://dx.doi.org/10.1061/(ASCE)HE.1943-5584.0000556.

Smith, D. R., S. J. Livingston, B. W. Zuercher, M. Larose, G. C. Heathman, and C. Huang. 2008. Nutrient losses from row crop agriculture in Indiana. *Journal of Soil and Water Conservation* 63(6):396-409.

Smith, R. A., G. E. Schwarz, and R. B. Alexander. 1997. Regional interpretation of water-quality monitoring data. *Water Resources Research* 33(12):2781-2798.

Snedecor, G. W. and W. G. Cochran. 1980. *Statistical methods* 7th ed., The Iowa State University Press, Ames, Iowa.

Sprague, L. A., R. M. Hirsch, and B. T. Aulenbach. 2011. Nitrate in the Mississippi River and its tributaries, 1980 to 2008: Are we making progress?" *Environmental Science and Technology* 45(17):7209–7216.

Stanley, E. H. and M. W. Doyle. 2002. A geomorphic perspective on nutrient retention following dam removal. *Bioscience* 52(8):693-701.

Thiessen, A. H. 1911. Precipitation averages for large areas. *Mon Weather Rev* 39(7):1082–1084.

Toor, G. S., R. D. Harmel, B. E. Haggard, and G. Schmidt. 2008. Evaluation of regression methodology with low-frequency water quality sampling to estimate constituent loads for ephemeral watersheds in Texas. *Journal of Environmental Quality* 37(5):1847-1854.

Trenberth, K. E. 1999. Conceptual framework for changes of extremes of the hydrological cycle with climate change. *Climatic Change* 42(1):327-339.

Trenberth, K. E., L. Smith, T. Qian, A. Dai, and J. Fasullo. 2007. Estimates of the global water budget and its annual cycle using observational and model data. *Journal of Hydrometeorology* 8(4):758-769.

Troutman, B. M. 1985. Errors and parameter estimation in precipitation-runoff modeling 1. theory. *Water Resources Research* 21(8):1195-1213.

Turner, R. E., N. N. Rabalais,and D. Justic. 2006. Predicting summer hypoxia in the northern Gulf of Mexico: Riverine N, P, and Si loading. *Mar. Pollut. Bull*. 52(139–148) USEPA, 2011, http://www.epa.gov/storet/legacy/gateway.htm.

United States Environmental Protection Agency (USEPA). 2001. PLOAD version 3.0: An ArcView GIS Tool to Calculate Nonpoint Sources of Pollution in Watershed and Stormwater Projects, User's Manual. Developed for USEPA by CH2M HILL.

United States Environmental Protection Agency (USEPA). 2006. User's Guide. Spreadsheet Tool for the Estimation of Pollutant Load (STEPL), Version 4.0. Developed for USEPA by Tetra Tech, Inc. Fairfax, VA.

Verhoff, F. H., S. M. Yaksich, and D. A. Melfi. 1980. River nutrient and chemical transport estimation. *Journal of the Environmental Engineering Division*, ASCE, EE3, 591–608.

Verma, S., M. Markus, and R. A. Cooke. 2012. Development of error correction techniques for nitrate load estimation methods. *Journal of Hydrology* 432-433:12-25.

Vörösmarty, C. J., M. Meybeck, B. Fekete, K. Sharma, P. Green, and J. P. M. Syvitski. 2003. Anthropogenic sediment retention: Major global impact from registered river impoundments. *Global and Planetary Change* 39(1-2):169-190.

Walker W. W., and J. Kuhner. 1978. An empirical analysis of factors controlling eutrophication in midwestern impoundments. In International Symposium on the Environmental Effects of Hydraulic Engineering Works, University of Tennessee, Knoxville, TN.

Walker, W. W. 1996. Simplified procedures for eutrophication assessment and prediction: User manual. U.S. Army Corps of Engineers, Waterways Experiment Station Instruction Report W-96-2.

Walker, W. W. 2003. Consideration of variability and uncertainty in phosphorus total maximum daily loads for lakes. *Journal of Water Resources Planning and Management* 129(4): 337–344.

Wallin, T. R. and D. J. Schaeffer. 1979. Illinois redesigns its ambient water quality monitoring network. *Env. Mng*. 3(4): 313–319.

WSTB (Water Science and Technology Board), 2009, Nutrient control actions for improving water Quality in the Mississippi River basin and northern Gulf of Mexico. National Research Council of the National Academies, National Academies Press, Washington, D.C.

Wu, Y., S. Liu, and O. I. Abdul-Aziz. 2012. Hydrological effects of the increased CO2 and climate change in the Upper Mississippi River Basin using a Modified SWAT. *Climatic Change* 110(3-4):977-1003.

Yaksich, S. M. and F. H. Verhoff. 1983. Sampling strategy for river pollutant transport. *Journal of Environmental Engineering* 109(1):219-231.

Yu, C., W. J. Northcott, and G. F. McIsaac. 2004. Development of AN artificial neural network for hydrologic and water quality modeling of agricultural watersheds, *Transactions of the ASAE*, 47(1),:285–290.

Zahabiyoun, B., M. R. Goodarzi, A. R. M. Bavani, and H. M. Azamathulla. 2013. Assessment of climate change impact on the Gharesou River Basin using SWAT Hydrological Model." Clean - Soil, Air, Water.

Zhang, J., Y. Ju, and Z. Zai-Feng. 1995. Nationwide river chemistry trends in China: Huanghe and Changjiang. *Ambio* 24(5):275-279.

Zhang, S., Z. Wang, B. Zhang, K. Song, D. Liu, and C. Ren. 2010. Characteristics of nonpoint source pollution from an agricultural watershed during rainfall events. International Conference on Mechanic Automation and Control Engineering, MACE2010, Wuhan, 26-28th June 2010.

Zhu, Q., J. P. Schmidt, A. R. Buda, R. B. Bryant, and G. J. Folmar. 2011. "Nitrogen Loss from a Mixed Land use Watershed as Influenced by Hydrology and Seasons." Journal of Hydrology 405 (3-4): 307-315.